

POLITECNICO DI TORINO

College of Engineering



Master's Degree Course in Biomedical Engineering

MASTER'S DEGREE THESIS

**Wireless power transfer to extremely-miniaturized
diagnostic devices**

Supervisors:

Prof. Danilo DEMARCHI

Prof. Sandro CARRARA

Candidate:

BORETTO Luca

October 2019

Abstract

Recent advancements in electronics and microfabrication techniques have increased attention to the use of implantable miniaturized biosensors. In vivo biosensing is going to radically change healthcare by allowing personalized medicine. By continuous monitoring, the basic health of an individual could be well understood, making possible to detect upcoming pathologies. A further option is the continuous monitoring of a therapeutic drug that could eliminate dosage intakes by providing an individualized pharmacokinetic report of a drug. These devices could also be used in vitro to monitor cell cultures that are useful for various purposes, such as understanding and modelling certain biomechanisms, developing novel medicinal products and treatments or in the area of regenerative medicine. These devices need a power supply and must be miniaturized at the same time, so it is necessary to use wireless power transfer. For this purpose, in this work, the wireless power transfer via electromagnetic waves is examined. This thesis focus on analysing the physical limits of this technique when the receiving antenna is implanted in the human body and try to quantitatively provide values of maximum transferable power in relation to the size of the implanted antenna, depth in tissue and working frequency. Finally, through Ansys HFSS, a commercial finite element method solver, extremely miniaturized antennas (with a size of $1 \times 1 \times 1 \text{ mm}^3$ and $2 \times 2 \times 2 \text{ mm}^3$) are designed and simulated implanted in the human body and inserted in a petri dish, in order to provide practical examples in vivo and in vitro, to demonstrate that a sufficient amount of power to power a small biosensor can be transferred in both scenarios without exceeding the legal limits of transmitted power.

Acknowledgments

Vorrei ringraziare tutte le persone che hanno contribuito in qualche modo al lavoro descritto in questa tesi.

Voglio ringraziare i miei relatori: il Professor Danilo Demarchi per il suo sostegno e la sua disponibilità ed il Professor Sandro Carrara per avermi accolto a Neuchâtel nell'ICLAB dell'EPFL ed avermi incoraggiato durante i mesi lì trascorsi. Grazie ad entrambi per avermi dato utili consigli e la possibilità di ampliare le mie conoscenze attraverso questo progetto di tesi e vivere quest'esperienza.

Ringrazio la Professoressa Anja Skrivervik, docente all'EPFL, persona disponibile ed estremamente competente che ha saputo togliermi ogni dubbio aiutandomi in questo progetto.

Ringrazio la Professoressa Catherine Dehollain, docente all'EPFL, per i suoi utili consigli.

Ringrazio i colleghi conosciuti all'EPFL, David, Gian Luca, Mehdi, Martina e Mahshid con cui ho condiviso questo percorso finale.

Ringrazio tutti i Professori del corso di laurea in ingegneria biomedica del Politecnico di Torino per la loro professionalità, per avermi trasmesso la loro passione, per aver reso il mio percorso universitario interessante e stimolante ed avermi fatto sviluppare un modo di pensare che oltre ad essere stato indispensabile all'università, sarà utile per tutto il resto della mia vita.

Ringrazio tutti i compagni di corso ed amici con cui ho affrontato questi anni di studio.

Un grazie speciale a Eleonora che ha sempre creduto in me, sopportandomi e gioendo accanto a me in ogni traguardo raggiunto.

Tutto questo non sarebbe stato possibile senza il supporto della mia splendida famiglia, i miei genitori, mia sorella ed i miei nonni che mi hanno sempre appoggiato nelle mie scelte. In particolare, ringrazio di cuore i miei genitori che mi hanno permesso di studiare e con il loro esempio mi hanno insegnato dei valori importanti quali il sacrificio, la tenacia e la perseveranza. Per questo gli sarò eternamente grato!

Contents

1. Introduction	1
1.1. From traditional implantable medical devices to miniaturized diagnostic biosensors	1
1.2. Power supply options	3
1.3. Wireless power transfer	5
1.3.1. Fields regions of an antenna	5
1.3.2. Inductive coupling	8
1.3.3. Ultrasonic power transfer	9
1.3.4. Far-field power transfer	10
2. Dielectric properties of human tissues	13
2.1. Complex relative electrical permittivity	13
2.2. Gabriel model	15
2.3. Derived properties	18
3. Electrically small antennas	20
3.1. Definition	20
3.2. Parameters of antennas and characteristics of ESAs	20
3.2.1. Radiation pattern	21
3.2.2. Quality factor and bandwidth	22
3.2.3. Directivity	23
3.2.4. Gain	24
3.2.5. Radiation efficiency	25
3.2.6. Input impedance	26
3.2.7. Return loss	27
3.2.8. Effective aperture	28
3.2.9. Polarization	28
3.3. Figures of merit of implanted antennas	29
4. Power budget analysis	31
4.1. Regulatory limits	33
4.2. Losses due to reflections	36
4.3. Propagating field absorption losses	38
4.4. Losses in the reactive near field	39
4.5. Results	42

5. ESA design	46
5.1. State of art of antennas for medical devices.....	46
5.2. Design of multi-turn loop antennas	47
5.2.1. A 1x1x1 mm³ multi-turns loop antenna.....	51
5.2.2. A 2x2x2 mm³ antenna self-resonating at 5.8 GHz.....	55
5.3. Phantoms.....	57
5.3.1. Human abdomen phantom	57
5.3.2. Petri dish phantom	58
5.4. Behaviour of antennas inside the phantoms	59
5.4.1. 1x1x1 mm³ antenna subcutaneous implant.....	60
5.4.2. 2x2x2 mm³ antenna subcutaneous implant.....	63
5.4.3. 1x1x1 mm³ antenna in petri dish.....	65
5.4.4. 2x2x2 mm³ antenna in petri dish.....	67
5.5. Circuit for wireless power transfer.....	69
6. Conclusion.....	72
APPENDIX.....	73
I. Gabriel model – Matlab code	73
II. Power budget analysis – Matlab code.....	74
III. Antenna design – Visual basic script for ANSYS HFSS	79
Referencies.....	86

1. Introduction

1.1. From traditional implantable medical devices to miniaturized diagnostic biosensors

The market for implantable medical devices is constantly growing and in recent decades has reached hundreds of billions of dollars. This growth is driven by the fact that the average age of the world population has increased and with it the percentage of chronic degenerative diseases such as cardiovascular diseases, neurodegeneration, tumours and diabetes.

An important challenge of active implantable devices is to carry out their function and allow the transfer of information from inside to outside of the human body or vice versa, without however interfering negatively with people's lifestyle but improving it. At the same time, they should have small dimensions in order to facilitate their implant.

Examples of commercially available active implantable devices (Figure 1) are pacemakers, implantable cardioverter defibrillators, CRT devices (devices for cardiac resynchronization therapy), insertable cardiac monitors, drug delivery systems, deep brain stimulators, analgesic stimulators, neuromuscular stimulators, intestinal stimulators, gastric stimulators, cochlear implants, retinal prostheses.

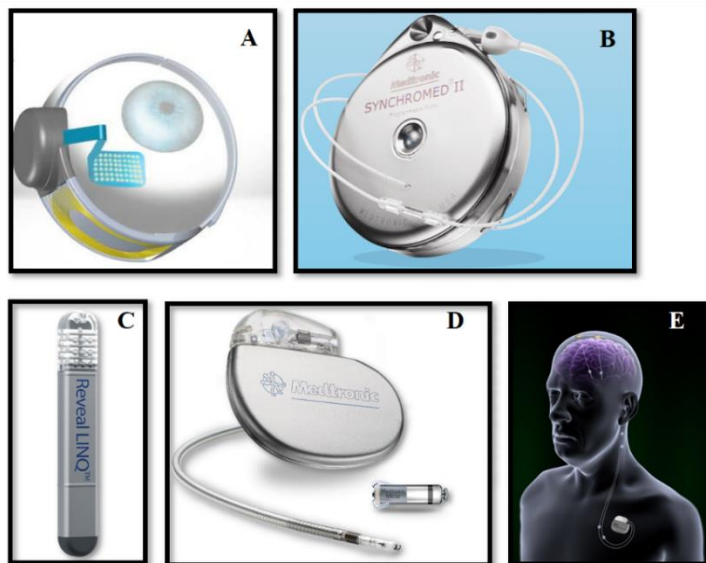


Figure 1 – Examples of commercially available active implantable devices. A) Angus II retinal prosthesis [1]. B) Medtronic Synchromed II Drug Infusion System [2]. C) Medtronic Reveal LINQ insertable cardiac monitor [3]. D) Comparison between Medtronic Micra, the smallest pacemaker in the world, and a traditional Medtronic pacemaker [4]. E) An implanted deep brain stimulator.

Recent advancements in electronics and microfabrication techniques have increased attention to the use of implantable biosensors in precision medicine. Precision medicine can be referred to as the diagnosis, monitoring and treatment of diseases, taking into consideration the variability of the individual [5]. The research seeks to design and develop miniaturized biosensors for the continuous monitoring of different human metabolites both in vivo and in vitro.

In vivo biosensing is going to radically change healthcare by allowing personalized medicine. Think about a biosensor implanted in a patient who can transmit clinically relevant health information continuously. By continuous monitoring, the basic health of an individual could be well understood, making possible to render small variations with respect to normal conditions significant markers of upcoming pathologies. A further option is the continuous monitoring of a therapeutic drug that could eliminate dosage intakes by providing an individualized pharmacokinetic report of a drug [6].

For example, by means of implantable biosensors, implanted subcutaneously, it is possible to record and transmit to a remote device, like a smartphone, the level of glucose in the blood (glycaemia) thus avoiding periodic blood withdrawals and facilitating the diagnosis and care of diabetic subjects [7] [8] [9]. An example is Eversense CGM, the first FDA-approved continuous glucose monitoring system with a totally implantable glucose sensor and a compatible mobile application for adult diabetics [10].

An additional metabolite that may be controlled using subcutaneous biosensors is lactate, a product of anaerobic muscular activities. [11]. It is possible to record the concentration of lactate in the blood (lactatemia) to monitor the muscular effort in people in rehabilitation or in sportsmen.

Other parameters that can be measured for example are temperature [12], cholesterol, pH and blood alcohol concentration [13], useful for alcoholism prevention and monitoring. Metabolic monitoring may also be of interest for cellular analysis.

In vitro instead, cells can be cultivated for various purposes, such as understanding and modelling certain biomechanisms, developing novel medicinal products and treatments, or in the area of regenerative medicine [14]. A continuous monitoring of them could enable the discovery of innovative solutions.

It is estimated that the biosensor market will reach \$ 47.40 billion by 2020 with an annual growth of 6% between 2016 and 2020 [15].



Figure 2 – Eversense CGM system [16]

1.2. Power supply options

Bioelectronic devices require an energy source to function. Let's see how it is possible to provide the power needed for these devices. Basically, there are three supply options:

- **Battery:** the use of a battery is the most widespread solution today for active implantable devices. This is the approach used for example in pacemakers, cardioverter defibrillators, in most stimulators, infusion pumps, etc. The life of the device ends with the life of the battery. When the battery is exhausted, the device is explanted and must be completely replaced.
- **Wireless power transfer:** it means transferring the energy needed to operate the device remotely. For instance, in the case of an implantable device, from outside to inside the human body. In this case there is no energy source inside the device, and when there is a need to make it work, energy is transferred from the outside. This approach probably represents the future for categories of devices such as miniaturized biosensors that will become more and more frequent in the coming years.
- **Rechargeable batteries and wireless power transfer:** it is the middle way between the two previous ones. The idea is to make a device equipped with an internal energy source, which however is not able to guarantee a particularly long

autonomy. When the internal energy source is discharged, it is recharged by wireless power transfer.

A first criterion for deciding which method to use is whether the device is life support, that is a device that if not working would put the patient at risk of life or in the condition of leading a life with extremely limited quality. Wireless power transfer is good for non-life support devices that can be implanted once and last for a lifetime because having a battery the life of the device regarding its power supply is unlimited.

Consider, for example, that it is intended to measure the temperature of a human being. It could be used a temperature sensor inserted under the skin that could be interrogated from the outside with an interrogation system that supplies the device only when needed. This is an example of an implantable device that could work only based on wireless power transfer, as well as other implantable biosensors for measuring glucose, blood pressure, pH, alcohol, lactate or implantable identification microchips.

Often, in active implantable devices, the battery takes over 50% of its volume as shown in Figure 3. This datum is sufficient to say that in order to obtain a miniaturization of bioelectronic devices in some cases it could be considered to adopt wireless power transfer techniques. A smaller size of the devices results in a simpler implant or even, if the device is small enough, in an injection as shown in [12]. Furthermore, as the batteries have a limited life, in the case of an implantable device, at the end of their life it is necessary to re-operate the subject to remove the implanted device, which results in substantial financial and sanitary expenses.

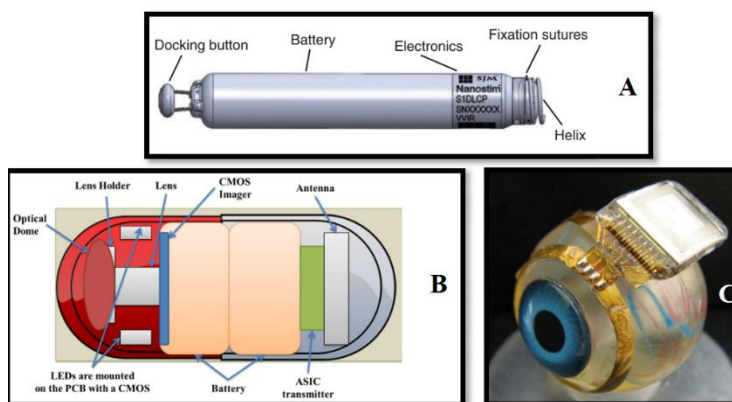


Figure 3 – Batteries of commercially available medical devices. A) St. Jude Medical's Nanostim, the first leadless pacemaker. Its battery occupies about 80 % of its volume [17]. B) Structure of a typical wireless endoscopic capsule [18]. C) Retinal prosthesis with a bulky battery [19].

1.3. Wireless power transfer

Implantable electronic devices have evolved at a surprising pace, thanks to the advancement of manufacturing technologies and the resulting miniaturisation and greater efficiency of sensors, actuators, processors and packaging. Devices with detection, communication, actuation and wireless power transfer are in great demand, paving the path for novel applications and treatments. The reliable, long-term supply of these devices has been a challenging task since their first introduction.

Over the years a lot of progress has been achieved in battery technology, however their life is still restricted and strongly dependent on their volume [20], [21]. Tries to expand battery life using energy harvesting through alternative energy sources such as thermoelectric [22], piezoelectric [23], [24], [25], biopotential [26] and fuel cells [27], [28] harvesting have been investigated, but, these techniques are anatomically specific and the power density is too weak to power a tiny bioelectronic device.

Thus, in this section the main wireless power transfer techniques such as near-field inductive coupling, far-field and ultrasonic wireless power transfer will be explained. The advantages and disadvantages of each of them will then be highlighted.

First, however, to better understand the various methods of wireless power transfer, it is necessary to understand the fields regions of an antenna so a section will be dedicated to their description.

1.3.1. Fields regions of an antenna

The space surrounding an antenna is usually divided into three regions: reactive near-field region, radiating near-field (Fresnel) region and far-field (Fraunhofer) region as shown in Figure 4.

The fields in these regions are different but there are no abrupt changes so the borders dividing these regions are not unique, but criteria have been defined to distinguish these regions and are those commonly used [29].

- Reactive near-field region: it is defined as “that portion of the near-field region immediately surrounding the antenna wherein the reactive field predominates”. The external limit of this region is commonly considered to be at distance

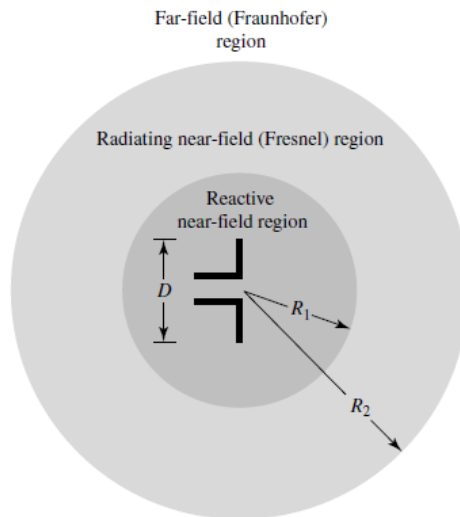


Figure 4 - Field regions of an antenna [29]

$R_1 = 0.62 \sqrt{\frac{D^3}{\lambda}}$ from the surface of the antenna. Where D is the largest dimension of the antenna and λ is the wavelength at the operating frequency. “For a very short dipole, or equivalent radiator, the outer boundary is commonly taken to exist at a distance $\frac{\lambda}{2\pi}$ from the antenna surface”. In this region electric and magnetic fields are not in phase over time and the ratio between their amplitudes is not a constant quantity.

- Radiating near-field (Fresnel) region: it is defined as “that region of the field of an antenna between the reactive near-field region and the far-field region wherein radiation fields predominate and wherein the angular field distribution is dependent upon the distance from the antenna”. In the case of an antenna having the largest size, which is large compared to the wavelength, $D > \lambda$, then this region is normally described as $0.62 \sqrt{\frac{D^3}{\lambda}} < r < \frac{2D^2}{\lambda}$. If the largest dimension of the antenna is much smaller than the wavelength, $D \ll \lambda$, then this region may not exist. The energy in this region is all radiant energy, but the combination of magnetic and electrical components is still different from the far-field. Further away in the radiative near-field, the relationship between the fields is more predictable, but still complex.

- Far-field (Fraunhofer) region: it is defined as “that region of the field of an antenna where the angular field distribution is essentially independent of the distance from the antenna. If the antenna has a maximum overall dimension D , the far-field region is commonly taken to exist at distances greater than $\frac{2D^2}{\lambda}$ ”. This distance is valid if $D > \lambda$. Moreover, to be in this region, it is necessary that $r \gg \lambda$ and $r \gg D$. In the far-field, amplitudes of the fields fall off as $\frac{1}{r}$.

In the far-field region the field propagates like a spherical wave that locally can be well approximated by a plane wave, so the field must have the typical characteristics of uniform plane waves. The electric field E and the magnetic field H are in temporal phase, their ratio is η (intrinsic impedance of the medium), and they are orthogonal to each other and with respect to the direction of propagation. This is because the radiated electromagnetic field in far-field region is always tangent to a sphere centred at antenna centre:

$$E_r \ll E_\varphi, E_\theta \qquad H_r \ll H_\varphi, H_\theta$$

Therefore:

$$\vec{E}(\vec{P}) \cong E_\varphi \hat{\varphi} + E_\theta \hat{\theta} \qquad (1)$$

$$\vec{E}(\vec{P}) \cdot \hat{r} \cong 0 \qquad (2)$$

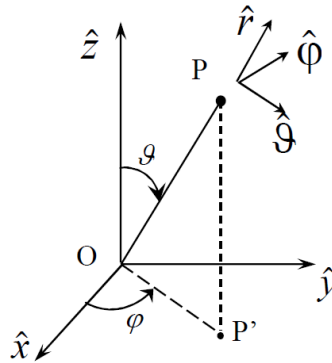


Figure 5 – Spherical coordinates

The general expression of the radiated field simplifies to the approximations in the following:

$$\vec{E}(\vec{P}) \cong -\eta \hat{r}(\vec{P}) \times \vec{H}(\vec{P}) \qquad (3)$$

$$\vec{H}(\vec{P}) \cong \frac{1}{\eta} \hat{r}(\vec{P}) \times \vec{E}(\vec{P}) \quad (4)$$

As it is possible to see from equations (3) and (4) electric and magnetic field are linearly dependent so it is enough to know one of them to know the other one too. The far-field radiated power density or Poynting vector can be expressed as:

$$\vec{S}(\vec{P}) = \frac{1}{2} \vec{E}(\vec{P}) \times \vec{H}^*(\vec{P}) \cong \frac{1}{2\eta} (\vec{E}(\vec{P}) \cdot \vec{E}^*(\vec{P})) \hat{r} \quad (5)$$

1.3.2. Inductive coupling

In inductive coupling, an alternating current flowing in a transmitting coil generates an alternating magnetic field which, passing through a secondary coil, induces an electromotive force in the receiving coil which can be used to feed a load.

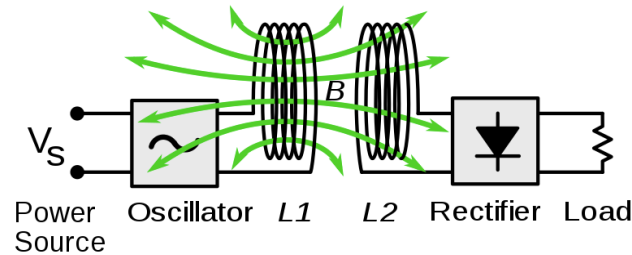


Figure 6 – Scheme of inductive coupling

In this way it is possible to transfer data and power over short distances. Basically, the receiver coil must be in the near-field of the transmitting coil.

This method has so far been the preferred one for energy transfer when dealing with implantable medical devices [30].

Since the inductive coupling mainly exploits the low frequencies, typically between hundreds of kHz and a few MHz, it is practical to power the IMD due to the low attenuation of the signal in human tissues in that range of frequencies.

However, despite its popularity, power transfer in the near-field also presents challenges. This method is not very compatible with a moving subject because, for example, obtaining a good alignment between coils is difficult to achieve [31]. Coil misalignment

generally causes low power transfer efficiency and low data transfers [32], [33]. Furthermore, since a near-field phenomenon is exploited, the external coil must be in close proximity to the system, which, by imagining a continuous transfer of data and power, restricts comfort and freedom to carry out daily tasks for the subject carrying the device.

1.3.3. Ultrasonic power transfer

In this technique, an ultrasonic oscillator is electrically excited to generate surface vibrations resulting in acoustic pressure waves typically in the 200 kHz to 1.2 MHz frequency range. A piezoelectric energy harvester implanted within the body within the main lobe of the transmitter radiation converts acoustic energy into electrical energy [34].

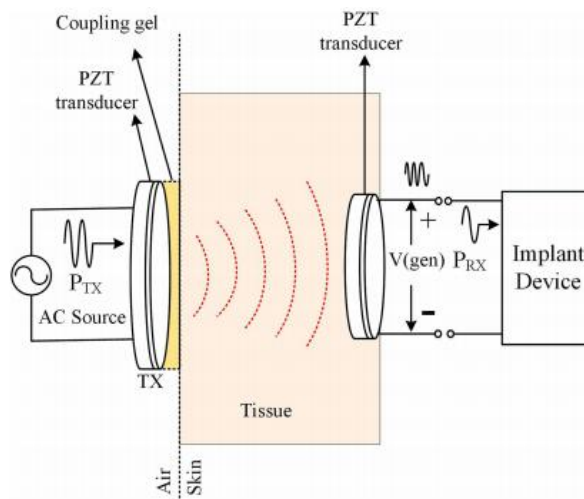


Figure 7 – Scheme of ultrasonic energy transfer method [35]

Ultrasonic links have demonstrated to be the most efficient of all the methods investigated, as evidenced in [36]. On the negative side, ultrasounds are not efficient in front of tissue interfaces with different impedances, such as different organs and muscles. In addition, their application and efficiency can be limited by high attenuation in liquids and bones. Finally, the transmitting ultrasound transducer must be put in direct contact with the subject's skin, due to the mismatch of air-skin impedance, which gives rise to the same mobility and freedom problems as inductive coupling.

1.3.4. Far-field power transfer

Far-field wireless power transfer works on the principle of electromagnetic radiation, in which a receiving antenna is positioned at a large separation from a transmitting antenna. The power received by the receiving antenna is rectified and transferred to a load.

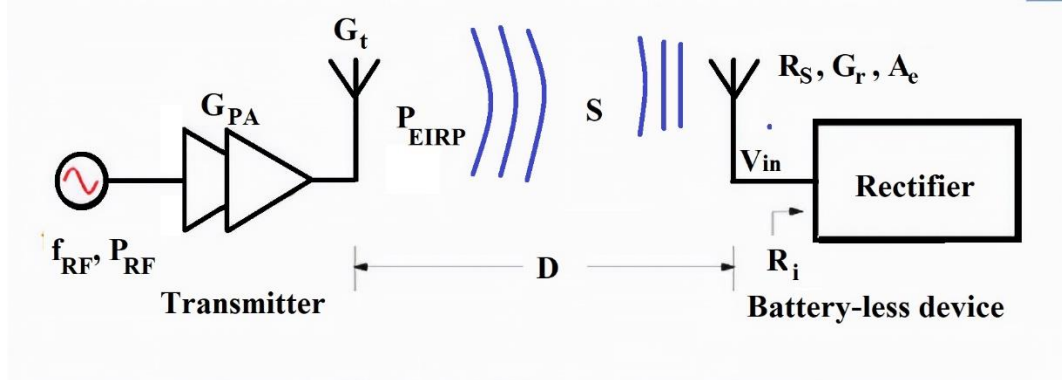


Figure 8 – Scheme of far-field power transfer

If an omnidirectional transmitting antenna radiates a power P_t , then the power density S at distance D from it is given by:

$$S = \frac{P_t}{4\pi D^2} \quad (6)$$

If the transmitting antenna has an antenna gain G_t (parameters of antennas will be explained deeply in section 3.2) in the direction of the receiving antenna, then equation (6) becomes:

$$S = \frac{P_t}{4\pi D^2} G_t = \frac{EIRP}{4\pi D^2} \quad (7)$$

The effective aperture of the receiving antenna is given by:

$$A_e = G_r \frac{\lambda^2}{4\pi} \quad (8)$$

Where G_r is the antenna gain of the receiving antenna and λ is the wavelength at the operating frequency. Therefore, ideally, the power received by the receiving antenna in the free space is given by:

$$P_r = \frac{P_t}{4\pi D^2} G_t A_e \quad (9)$$

The equation (9) is well known as Friis Transmission Formula and it can be rewritten as:

$$P_r = P_t G_t G_r \left(\frac{\lambda}{4\pi D} \right)^2 \quad (10)$$

Considering a more realistic case, it is necessary to take into account the impedance mismatch of each antenna and the polarization mismatch between the two antennas, equation (10) becomes:

$$P_r = P_t G_t G_r \left(\frac{\lambda}{4\pi D} \right)^2 (1 - |S_{11}|^2) (1 - |S_{22}|^2) X_{pol} \quad (11)$$

Since it is imagined that future implantable devices are completely compatible with the patient's lifestyle, it is necessary to proceed developing solutions that do not need carriers of implantable medical devices to have a power source attached to the skin, as in inductive coupling systems. Therefore, it is essential to extend the distance at which implantable devices can communicate and be powered wirelessly. This can be achieved with antennas that take advantage of the radiative transfer, in which wireless communication and power are performed using the propagation of electromagnetic waves. With this method it is possible to transmit power and information without the obligation of an external energy source attached to the skin.

On the negative side, the propagating electromagnetic waves suffers the absorption in human tissues, since frequencies in the microwave range as usually used, making difficult to power a deeply implanted device.

On the positive side, unlike near-field inductive coupling and ultrasonic power transfer, the far-field power transfer, is not strictly limited to alignment problems and short distance between receiving antenna and transmitter. In addition, the transmitting antenna can transmit power to several receiving antennas at the same time.

For these positive aspects of far-field wireless power transfer, this thesis will focus on analysing the physical limits of this technique when the receiving antenna is implanted in

the human body and will try to quantitatively provide values of maximum transferable power in relation to the size of the implanted antenna, depth in tissue and working frequency. Finally, through HFSS 2019 R1 (Ansys, U.S.A.), a commercial finite element method solver, antennas implanted in the human body and inserted in a petri dish will be simulated, in order to provide practical examples in vivo and in vitro, to demonstrate that a sufficient amount of power to power a small biosensor can be transferred in both scenarios without exceeding the legal limits of transmitted power.

2. Dielectric properties of human tissues

2.1. Complex relative electrical permittivity

The study of the interaction of electromagnetic fields with an organism requires that the dielectric properties of all the tissues involved are known, which consist in the value of the complex relative dielectric constant $\hat{\epsilon}$ at the working frequency.

The definition of the complex relative electrical permittivity can be derived from the Ampere-Maxwell equation:

$$\vec{\nabla} \times \vec{H} = \vec{J} + \frac{\partial \vec{D}}{\partial t} \quad (12)$$

Where \vec{H} is the magnetic field, \vec{J} is the current density of free charges and \vec{D} the electric flux density.

In the absence of impressed electric currents and in sinusoidal harmonic mode, if the material to be handled is a dielectric (possibly) with losses (condition verified by all biological tissues), the current density of free charges \vec{J} can be expressed as a function of the electric field \vec{E} through the electric conductivity σ_f :

$$\vec{J} = \sigma_f \vec{E} \quad (13)$$

The electric flux density \vec{D} is related to the electric field \vec{E} and to the electric polarization vector \vec{P} :

$$\vec{D} = \epsilon_0 \vec{E} + \vec{P} \quad (14)$$

Where $\epsilon_0 \approx 8.854187817 \cdot 10^{-12}$ F/m is the dielectric constant of the vacuum.

Equation (12) can therefore be rewritten as:

$$\vec{\nabla} \times \vec{H} = \sigma_f \vec{E} + j\omega(\epsilon_0 \vec{E} + \vec{P}) \quad (15)$$

or rather:

$$\vec{\nabla} \times \vec{H} = \sigma_f \vec{E} + j\omega\epsilon_0(\epsilon - j\epsilon^*)\vec{E} \quad (16)$$

Where $\omega=2\pi f$ is the angular pulsation.

Defining:

$$\hat{\epsilon} = \epsilon - j\left(\epsilon^* + \frac{\sigma_f}{\omega\epsilon_0}\right) \quad (17)$$

It can be seen that from a phenomenological and therefore experimental point of view, it is not in fact possible to distinguish between dielectric and ohmic losses.

Equation (28) can therefore be rewritten as:

$$\vec{\nabla} \times \vec{H} = j\omega\epsilon_0\hat{\epsilon}\vec{E} \quad (18)$$

By highlighting the dielectric character of the leaks, it is possible to write:

$$\vec{\nabla} \times \vec{H} = \vec{J}_{TOT} \quad (19)$$

$$\vec{J}_{TOT} = j\omega\epsilon_0(\epsilon' - j\epsilon'')\vec{E} \quad (20)$$

With $\epsilon' = \text{Re}\{\hat{\epsilon}\}$ e $\epsilon'' = -\text{Im}\{\hat{\epsilon}\}$.

By highlighting the ohmic character of the leaks, on the other hand, one can write:

$$\vec{J}_{TOT} = (\sigma - j\omega\epsilon_0\epsilon')\vec{E} \quad (21)$$

With ϵ' real part of the complex dielectric constant:

$$\epsilon' = \text{Re}\{\hat{\epsilon}\} \quad (22)$$

while σ is total electrical conductivity:

$$\sigma = -\omega\epsilon_0\text{Im}\{\hat{\epsilon}\} \quad (23)$$

We can therefore finally consider the complex relative dielectric constant as:

$$\hat{\epsilon} = \epsilon' - j\epsilon'' = \epsilon - j\frac{\sigma}{\omega\epsilon_0} \quad (24)$$

As it is possible to see from the last equation, the complex dielectric constant depends on the frequency. In the following of this chapter we will see how the dielectric properties of human body tissues vary with frequency.

2.2. Gabriel model

C. Gabriel and his collaborators [37], from a considerable amount of experimental data, proposed a parametric model for the evaluation of the dielectric properties of a large number of human tissues in the frequency range from 10 Hz to 100 GHz.

This model is based on the superimposition of four Cole-Cole dispersion relationships. The Cole-Cole dispersion relationship is in turn based on Debye's relaxation theory.

According to the Debye's model the complex dielectric relative constant is written as [38]:

$$\hat{\epsilon} = \epsilon_{\infty} + \frac{\epsilon_s - \epsilon_{\infty}}{1 + j\omega\tau} - j \frac{\sigma_s}{\omega\epsilon_0} \quad (25)$$

Where ϵ_{∞} is the relative permittivity for $\omega \rightarrow \infty$, ϵ_s is the relative permittivity for $\omega \rightarrow 0$, τ relaxation time for the material and σ_s the electrical conductivity for $\omega \rightarrow 0$.

At frequency whereby $\omega\tau = 1$, relaxation frequency, half the molecules can align to external electric field while the remainder does not.

The imaginary part described by using the Debye model, is represented by two parts: the relative permittivity and the conductivity.

Biological tissue exhibits losses as there are polarization and conduction phenomena. These losses are for:

- Conduction: due to the motion of free charges (Joule effect)
- Polarization: dipoles rotate trying to align to the applied electric field. These rotations generate collisions that dissipate energy.

Debye's equation is accurate for dielectrics whose relaxation phenomena is characterized by a single (characteristic) relaxation time.

This is often not the case for biological tissues, that include different molecules, and it is necessary to take into account more than one different relaxation times for each tissue.

Cole-Cole model [39] instead is more general than Debye model. It considers a wider relaxation time by using a parameter α in $[0,1]$.

$$\hat{\epsilon} = \epsilon_{\infty} + \frac{\epsilon_s - \epsilon_{\infty}}{1 + (j\omega\tau)^{(1-\alpha)}} \quad (26)$$

The Gabriel model is based on the Cole-Cole one and it considers the inhomogeneity of the structure. The dielectric constant is represented as sum of four Cole-Cole terms plus a conductivity term.

According to Gabriel model the dielectric constant is represented by:

$$\hat{\epsilon} = \epsilon_{\infty} + \sum_{n=1}^4 \frac{\Delta\epsilon_n}{1 + (j\omega\tau_n)^{(1-\alpha_n)}} + \frac{\sigma_i}{j\omega\epsilon_0} \quad (27)$$

Where $\Delta\epsilon = \epsilon_s - \epsilon_{\infty}$ and σ_i the ionic conductivity for $\omega \rightarrow 0$.

From measured experiments it has been possible individuate all parameters whose allow to accurately predict the complex permittivity by using Gabriel model.

Tissue type	ϵ_{∞}	$\Delta\epsilon_1$	τ_1 (ps)	α_1	$\Delta\epsilon_2$	τ_2 (ns)	α_2	$\Delta\epsilon_3$	τ_3 (μ s)	α_3	$\Delta\epsilon_4$	τ_4 (ms)	α_4	σ
Blood	4.0	56.0	8.38	0.10	5200	132.63	0.10	0.0			0.0			0.7000
Bone (cancellous)	2.5	18.0	13.26	0.22	300	79.58	0.25	2.0×10^4	159.15	0.20	2.0×10^7	15.915	0.00	0.0700
Bone (cortical)	2.5	10.0	13.26	0.20	180	79.58	0.20	5.0×10^3	159.15	0.20	1.0×10^5	15.915	0.00	0.0200
Brain (grey matter)	4.0	45.0	7.96	0.10	400	15.92	0.15	2.0×10^5	106.10	0.22	4.5×10^7	5.305	0.00	0.0200
Brain (white matter)	4.0	32.0	7.96	0.10	100	7.96	0.10	4.0×10^4	53.05	0.30	3.5×10^7	7.958	0.02	0.0200
Fat (infiltrated)	2.5	9.0	7.96	0.20	35	15.92	0.10	3.3×10^4	159.15	0.05	1.0×10^7	15.915	0.01	0.0350
Fat (not infiltrated)	2.5	3.0	7.96	0.20	15	15.92	0.10	3.3×10^4	159.15	0.05	1.0×10^7	7.958	0.01	0.0100
Heart	4.0	50.0	7.96	0.10	1200	159.15	0.05	4.5×10^5	72.34	0.22	2.5×10^7	4.547	0.00	0.0500
Kidney	4.0	47.0	7.96	0.10	3500	198.94	0.22	2.5×10^5	79.58	0.22	3.0×10^7	4.547	0.00	0.0500
Lens cortex	4.0	42.0	7.96	0.10	1500	79.58	0.10	2.0×10^5	159.15	0.10	4.0×10^7	15.915	0.00	0.3000
Liver	4.0	39.0	8.84	0.10	6000	530.52	0.20	5.0×10^4	22.74	0.20	3.0×10^7	15.915	0.05	0.0200
Lung (inflated)	2.5	18.0	7.96	0.10	500	63.66	0.10	2.5×10^5	159.15	0.20	4.0×10^7	7.958	0.00	0.0300
Muscle	4.0	50.0	7.23	0.10	7000	353.68	0.10	1.2×10^6	318.31	0.10	2.5×10^7	2.274	0.00	0.2000
Skin (dry)	4.0	32.0	7.23	0.00	1100	32.48	0.20	0.0			0.0			0.0002
Skin (wet)	4.0	39.0	7.96	0.10	280	79.58	0.00	3.0×10^4	1.59	0.16	3.0×10^4	1.592	0.20	0.0004
Spleen	4.0	48.0	7.96	0.10	2500	63.66	0.15	2.0×10^5	265.26	0.25	5.0×10^7	6.366	0.00	0.0300
Tendon	4.0	42.0	12.24	0.10	60	6.37	0.10	6.0×10^4	318.31	0.22	2.0×10^7	1.326	0.00	0.2500

Figure 9 - Parameters of equation (36) used to predict the dielectric properties of tissues [37].

Using Gabriel's model and its parameters, a Matlab code (see Appendix I) has been implemented to make easier to have available the complex relative permittivity and consequently the values of relative permittivity and electrical conductivity of all the tissues listed in Figure 13. The values obtained are in accordance with those reported in [40] and in [41].

It can be observed that these vary with frequency and in particular the relative permittivity of human tissues decreases with increasing frequency, as shown in Figure 14, while

conductivity increases with frequency, as shown in Figure 15. Some values are also tabulated in Table 1.

Figure 10 - Relative permittivity of human tissues from 100 MHz to 100 GHz

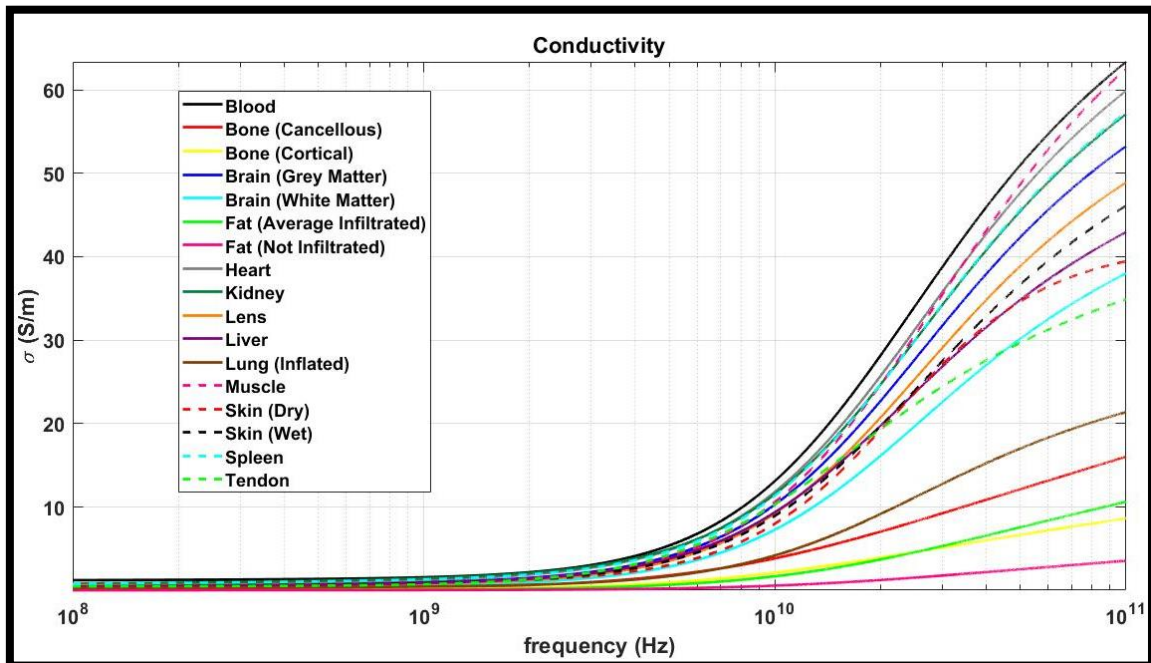
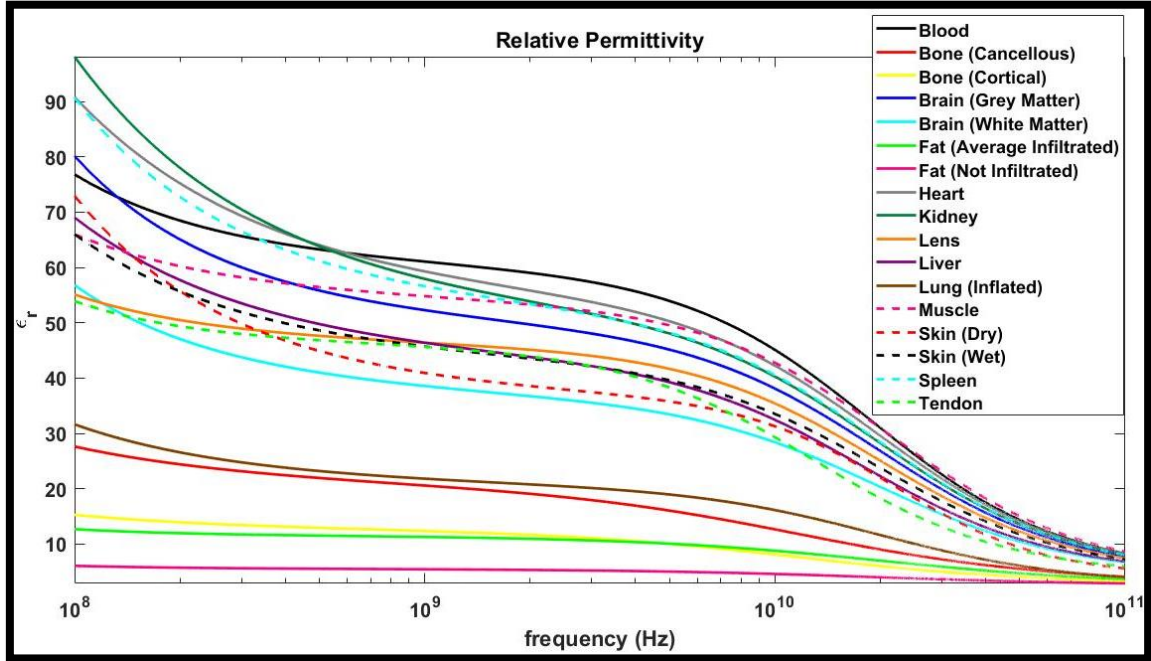


Figure 11 - Conductivity of human tissues from 100 MHz to 100 GHz

Table 1 – Relative permittivity and conductivity of human tissues: fat, muscle, skin.

Tissue	1 GHz		10 GHz		100 GHz	
	ϵ	σ (S/m)	ϵ	σ (S/m)	ϵ	σ (S/m)
Fat	5.4470	0.0535	4.6021	0.5853	2.8890	3.5620
Muscle	54.8115	0.9781	42.7709	10.6235	8.6340	62.5255
Skin	40.9363	0.8998	31.2952	8.0116	5.6003	39.4525

2.3. Derived properties

Since the complex relative dielectric constant of a tissue is known, it is then possible to derive various other quantities from it.

Dielectric loss

Loss tangent quantifies a dielectric material's inherent dissipation of electromagnetic energy. It can be expressed as:

$$\tan \delta = \frac{|\text{Im}\{\hat{\epsilon}\}|}{|\text{Re}\{\hat{\epsilon}\}|} \quad (28)$$

Table 2 – Loss tangent of human tissues: fat, muscle, skin.

Tissue	1 GHz	10 GHz	100 GHz
	$\tan \delta$	$\tan \delta$	$\tan \delta$
Fat	0.1766	0.2286	0.2216
Muscle	0.3208	0.4465	1.3017
Skin	0.3951	0.4602	1.2663

Wave number

Considering an electromagnetic wave that propagates in tissues, this is described by means of a wave vector $\vec{k} = k\hat{k}$.

The wave vector module is called the wave number and in the case of a lossy medium ($\epsilon'' > 0$) like human tissues, it is a complex number:

$$k = k' + jk'' = \beta - j\alpha. \quad (29)$$

It is possible to obtain the wave number through the dispersion equation with the assumption that the relative magnetic permeability of human tissues can be considered $\mu_r = 1$ being the human body weakly magnetic and therefore $\mu = \mu_0 \approx 1.256637 \cdot 10^{-6}$ H/m:

$$k^2 = \omega^2 \hat{\epsilon} \mu \quad (30)$$

The latter equation has 4 solutions, but the solution for which $\alpha, \beta \geq 0$ must be taken.

It can therefore be obtained:

$$k = \omega \sqrt{\hat{\epsilon} \mu} = \beta - j\alpha \quad (31)$$

Penetration depth

Penetration depth is a measure of how deep light or any electromagnetic radiation can penetrate a material. It is defined as the depth at which the intensity of the radiation inside the material falls to 1/e of its original value at the surface.

Knowing the wave number, it is possible to obtain the penetration depth as:

$$\frac{1}{\alpha} = -\frac{1}{\text{Im}\{k\}} \quad (32)$$

Wavelength

In human tissues the wavelength can be defined as:

$$\lambda = \frac{2\pi}{\beta} = \frac{2\pi}{\text{Re}\{k\}} \quad (33)$$

3. Electrically small antennas

3.1. Definition

When talking about antennas for implantable bioelectronic devices, it is important to try to make them as small as possible. When the largest size of the antenna is much smaller than the wavelength at the working frequency then it is referred to as electrically small antennas (ESA). According to Best [42] an ESA is an antenna for which $ka < 0.5$, where $k = 2\pi/\lambda$ is the wave number and a is the radius of the smallest sphere that can contain the antenna.

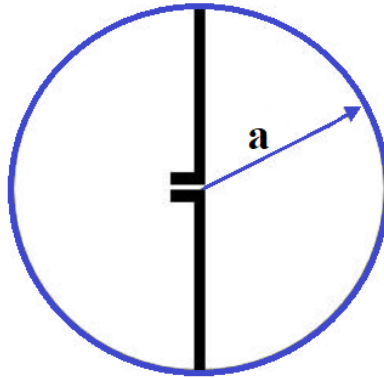


Figure 12 – Scheme of an antenna inscribed in a sphere of radius a .

3.2. Parameters of antennas and characteristics of ESAs

In this section the main parameters of the antennas will be described, and it will be shown how these are in the electrically small antennas.

A fundamental principle of electromagnetism, called the "principle of reciprocity", also ensures that any antenna can function indifferently, in theory, both as a transmitting and receiving antenna (if connected respectively to a transmitter and a receiver). Reciprocity is one of the most advantageous features of antennas. The principle of reciprocity, that is a consequence of Maxwell's, equations affirms that the reception and transmission properties of an antenna are identical. Therefore, antennas do not have distinct radiation patterns of transmission and reception, so knowing the radiation pattern in the

transmission mode then the radiation pattern in reception mode is also known. This allows to simplify the analysis of the parameters of the antennas allowing to quantify them regardless of the mode of use.

3.2.1. Radiation pattern

The radiation pattern is a diagram able to show in a clear and immediate way which are the most privileged radiation directions, and which are the least privileged of a given antenna.

Since one is interested in behaviour at reasonably large distances from the antenna, the radiation pattern is evaluated in far-field conditions.

Electrically small antennas are “omnidirectional”, which means that their radiation pattern is isotropic in a single plane. In particular, the radiation pattern of every ESA is the same of a dipole antenna. As example in Figure 13.A the radiation pattern of a loop antenna with diameter 9.5 mm resonating at 11.2 GHz is shown. Figure 13.B shows that a loop antenna with diameter 1 mm, at the same frequency is an electrically small antenna and its radiation pattern becomes the same of a dipole antenna.

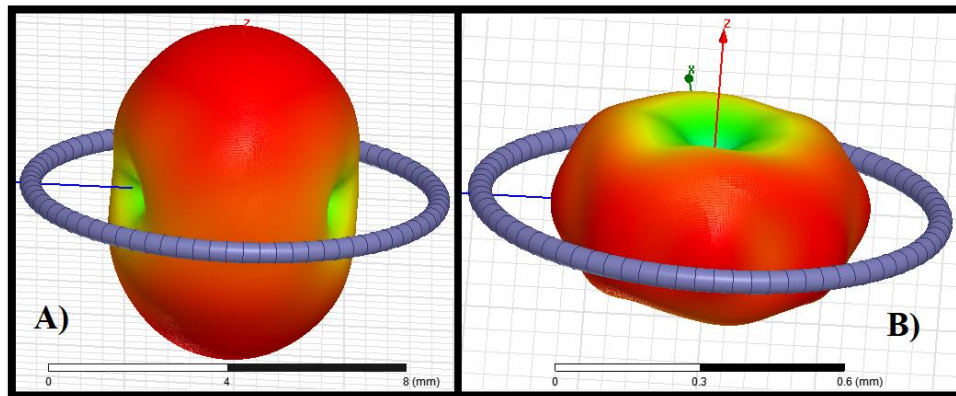


Figure 13 – Radiation pattern of a loop antenna: A) Radiation pattern of a 9.5 mm diameter loop at its resonance frequency (11.2 GHz). B) Radiation pattern of a 1 mm diameter loop at 11.2 GHz.

3.2.2. Quality factor and bandwidth

The quality factor of an antenna, Q , is the ratio between the energy stored around the antenna and the radiated power and it is generally defined as [43]:

$$Q = \begin{cases} \frac{2\omega W_e}{P_{rad}}, & W_e > W_m \\ \frac{2\omega W_m}{P_{rad}}, & W_m > W_e \end{cases} \quad (34)$$

where W_e and W_m are the respectively electrical and magnetic energy stored around the antenna and P_{rad} is the radiated power. This means that low Q imply higher radiation losses while high Q imply higher stored energy.

The radiative properties of ESAs have been studied for the first time by Wheeler [44]. Subsequently, a complete theory was presented by Chu [45] in which the minimum quality factor of a linear polarized antenna, which fits into a sphere of a given radius, was derived. The lower bound on Q , often referred to as the Chu-limit, is given by [43]:

$$Q_{lb} = \frac{1}{(ka)^3} + \frac{1}{ka} \quad (35)$$

This shows that for very small ka , Q takes on enormous values. This results in the fact that electrically small antennas are not good radiators.

Bandwidth, on the other hand, describes the frequency range over which the antenna can properly radiate or receive power. Bandwidth is often specified in terms of fractional bandwidth, which is defined as the normalized spread between the half-power frequencies is:

$$BW = \frac{f_{upper} - f_{lower}}{f_{center}} \cong \frac{1}{Q} \quad (36)$$

As the bandwidth is inversely proportional to the quality factor, electrically small antennas have very narrow bandwidths. Figure 14 shows how the minimum quality factor and the maximum bandwidth in free space change according to equations (13) and (14).

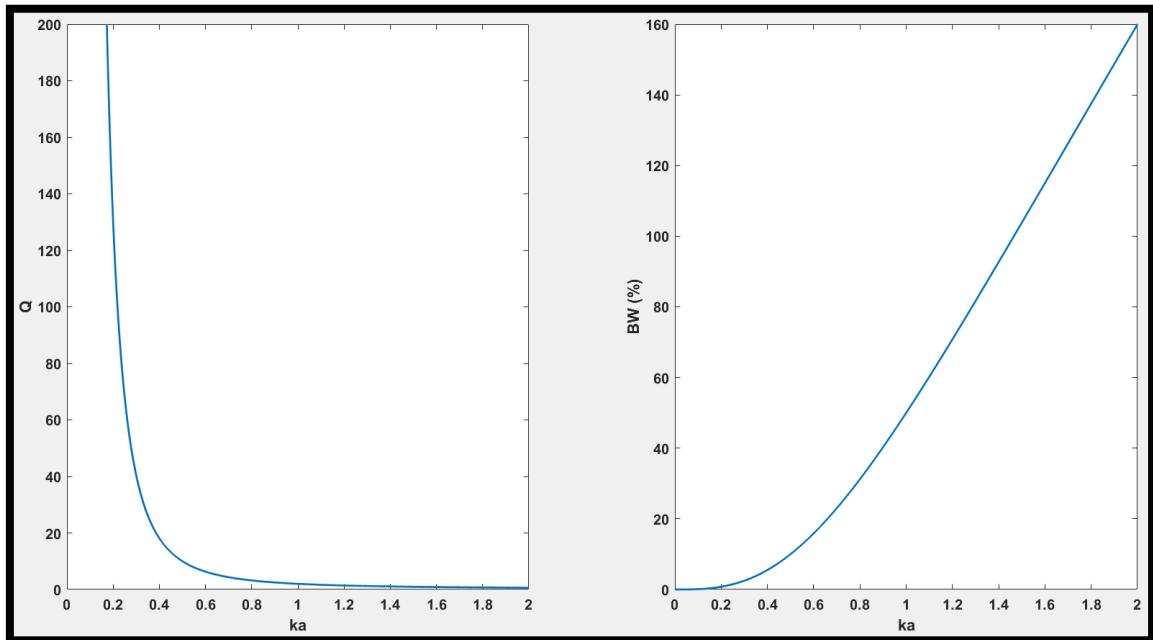


Figure 14 – Minimum quality factor vs ka on the left and maximum half-power bandwidth on the right in free space.

3.2.3. Directivity

Directivity is the measurement of the portion of radiated power in a specific direction. One is often interested in maximum directivity, which therefore represents the portion of radiated power in the direction of maximum antenna pointing.

To define the directivity, it is necessary to introduce some concepts:

- The steradian is the solid angle relative to a sphere of radius 'r'. Since the surface of a sphere of radius r is $4\pi r^2$, there are 4π steradians in a sphere.
- The radiation intensity U is defined as the power radiated by an antenna per unit of solid angle, then for steradian.

Directivity, D, is defined as the ratio between the intensity of radiation in a certain direction and the intensity of radiation averaged in all directions:

$$D(\theta, \varphi) = \frac{U(\theta, \varphi)}{U(\theta, \varphi)_{avg}} = \frac{4\pi U(\theta, \varphi)}{P_{rad}} \quad (37)$$

If the direction is not specified, the direction of maximum radiation intensity (maximum directivity) is implied:

$$D_{max} = \frac{U_{max}}{U_{avg}} = \frac{4\pi U_{max}}{P_{rad}} \quad (38)$$

3.2.4. Gain

Antenna gain is closely related to directivity and is a measure that considers the efficiency of the antenna and its directional capabilities.

Gain of an antenna, in a given direction, is defined as “the ratio of the intensity, in a given direction, to the radiation intensity that would be obtained if the power accepted by the antenna were radiated isotropically. The radiation intensity corresponding to the isotropically radiated power is equal to the power accepted by the antenna divided by 4π ”. It can be expressed as:

$$G(\theta, \varphi) = \frac{4\pi U(\theta, \varphi)}{P_{acc}} \quad (39)$$

Therefore, the peak gain of an antenna is expressed as:

$$G_{max} = \frac{4\pi U_{max}}{P_{acc}} \quad (40)$$

The power accepted by the antenna is related to the power radiated by a coefficient called radiation efficiency, e_{rad} :

$$P_{rad} = e_{rad} P_{acc} \quad (41)$$

Therefore, the gain of an antenna is related to its directivity as follows:

$$G(\theta, \varphi) = e_{rad}D(\theta, \varphi) \quad (42)$$

In 1948, Chu, using the expansion of the spherical wave function outside the smallest sphere enclosing the antenna, was the first to derive the minimum possible antenna quality factor, the maximum gain and the maximum possible G/Q ratio for an omnidirectional linearly polarized antenna concluding that the maximum gain is independent of the antenna polarization and for an electrically small antenna, in free space, it is 1.5 [45]. In a subsequent analysis, according to Geyi [46], the maximum possible G/Q ratio, respectively for small omnidirectional and directional antennas, can be expressed as:

$$\max \frac{G}{Q} \Big|_{omn}^{small} \approx \frac{3(ka)^3}{2(ka)^2 + 1} \quad (43)$$

$$\max \frac{G}{Q} \Big|_{dir}^{small} \approx \frac{6(ka)^3}{2(ka)^2 + 1} \quad (44)$$

3.2.5. Radiation efficiency

The radiation efficiency of an antenna, e_{rad} is the ratio of the power accepted by the antenna to the power radiated by the antenna. A high-efficiency antenna is capable of radiating most of the accepted power. The radiation efficiency is a number between 0 and 1.

For an ideal loss-less antenna the radiation efficiency is 1 (0 dB) or, in percentage, 100%. Since real antennas are made of real materials with finite conductivity and therefore with conduction losses, part of the power accepted by the antenna is absorbed by it without being radiated. As a result, the radiation efficiency is less than 1.

The radiation efficiency is commonly expressed as:

$$e_{rad} = \frac{P_{rad}}{P_{acc}} = \frac{R_{rad}}{R_{rad} + R_{loss}} = \frac{R_{rad}}{R_A} \quad (45)$$

Where R_{rad} is the radiation resistance, caused by the radiation reaction of the conduction electrons in the antenna; R_{loss} is the ohmic resistance of the conductors of the antenna; R_A is the input resistance of the antenna.

The energy consumed by the ohmic resistance is converted into heat radiation while the energy consumed by the radiation resistance is converted into electromagnetic waves.

For a real ESA, R_{loss} tends to be much larger than R_{rad} making the radiation efficiency very low (very high quality factors) and consequently its gain.

3.2.6. Input impedance

The input impedance of an antenna can be defined as the impedance presented by an antenna to its terminals, or as the ratio between the voltage and the current between its terminals. It can be expressed as:

$$Z_A = R_A + jX_A = R_{rad} + R_{loss} + jX_A \quad (46)$$

Where R_A and X_A are respectively the input resistance and the input reactance of the antenna. An antenna is self-resonant when $X_A=0$ and so $Z_A=R_A$.

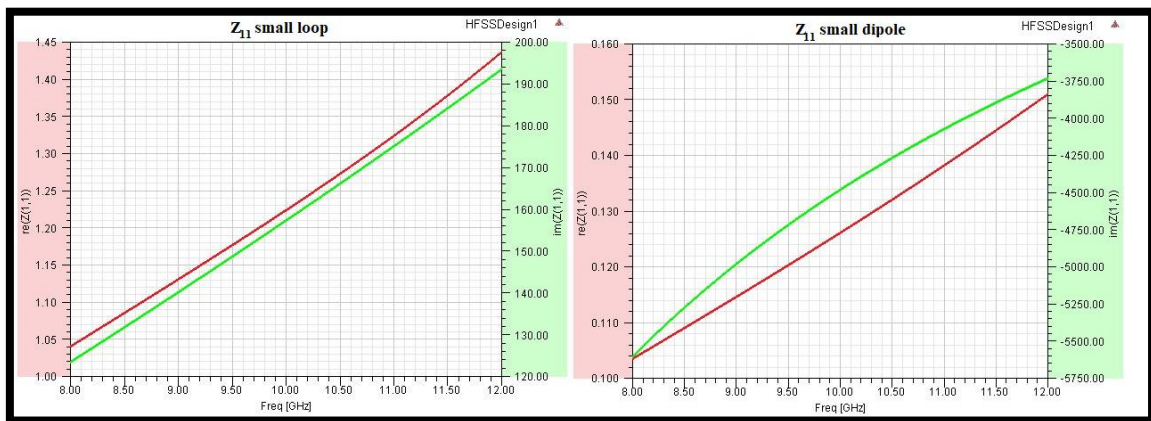


Figure 15 – Input impedance of an electrically small loop and of an electrically small dipole.

Normally, the input impedance of an electrically small antenna presents a low resistance and a high absolute value of reactance, $|X_A|$. Electric ESAs present high capacitive reactance while magnetic ESAs present high inductive reactance as shown in Figure 15.

As a result, a matching circuit may be required to minimize losses for impedance mismatch to the transmission line. Moreover, if the input resistance is close to 0 it is practically impossible to have impedance matching.

For example, the reactance of an electrically small linear electric dipole can be estimated by [47]:

$$X_{small_dipole} = -\frac{\eta_0}{\pi^2} \frac{\lambda}{2h} \ln\left(\frac{h}{b}\right) \quad (47)$$

Where h is the length of each arm of the dipole, b is the radius of the wire and η_0 is the wave impedance of the medium ($\eta_0 \approx 377 \Omega$ in free space).

While for an electrically small loop, the reactance can be estimated as [47]:

$$X_{small_loop} = \eta_0 \frac{2\pi r}{\lambda} \ln\left(\frac{r}{b}\right) \quad (48)$$

With r radius of the loop and b radius of the wire.

3.2.7. Return loss

The return loss or reflection coefficient, S_{11} , represents how much power is reflected from the antenna. Power is reflected from the antenna if there is an impedance mismatch between the antenna and the transmission line. The maximum power transmission is obtained when the antenna input impedance and the transmission line impedance are conjugated to each other, so when $Z_A = Z_0^*$. For instance, in the case of wireless power transfer Z_A should be equal to the complex conjugated of the impedance of the rectifier.

Therefore, the frequencies for which S_{11} assumes the lowest values correspond to the antenna band.

The return loss defines the ratio between the power accepted by the antenna and the input power to the antenna as:

$$P_{acc} = P_{in}(1 - |S_{11}|^2) \quad (49)$$

3.2.8. Effective aperture

In a given direction the effective aperture of an antenna is defined as “the ratio of the available power at the terminals of a receiving antenna to the power flux density of a plane wave incident on the antenna from that direction, the wave being polarization-matched to the antenna”.

$$A_e = \frac{P_R}{S} \quad (50)$$

Being an area, it is expressed in m².

It is linked to antenna gain and wavelength by the following expression:

$$A_e = G \frac{\lambda^2}{4\pi} \quad (51)$$

3.2.9. Polarization

Polarization of an antenna is the polarization of the field radiated by the antenna. Consider a receiving antenna and an incoming plane wave. If the polarization of the antenna is different from the polarization of the wave, then there is a polarization mismatch that can be expressed as:

$$X_{pol} = \cos^2 \phi \quad (52)$$

Where ϕ is the angle between the electric field of the plane wave and the electric field that the antenna would generate if it were radiating.

For example, the polarization mismatch from linear to circular polarization is 0.5 (-3 dB).

3.3. Figures of merit of implanted antennas

When considering ESAs radiating in lossy media, such as implantable or wearable antennas, everything changes dramatically.

In fact, if in free space the key performance indicators of an ESA are the quality factor (which can be linked to bandwidth) and the directivity ratio quality factor, in a lossy medium it is difficult to define key performance indicators. This is because, first, it is difficult to define the quality factor in this scenario. Also other characteristics of antennas such as the radiation pattern no longer exist for an implanted antenna that radiates in the human body because for them it is no longer possible to define a far field region because the radiated electromagnetic field is absorbed by the medium with losses in which the antenna is located [48].

So, while for ESAs in free space fundamental limits and key performance indicators, thanks to the work of Wheeler, Chu, Harrington and other ESA pioneers have been defined, for ESAs in lossy media research on fundamental limits is still at the beginning.

According to Skrivervik and her collaborators [49], the figures of merit, for example in the case of an implanted antenna, could be connected to the total power reaching the outside of the host lossy body or to the power density outside the lossy body in the direction of maximum radiation. They have carried out preliminary work based on the study of elementary sources in a spherical multilayer phantom representing a multilayer medium with losses [50]. According to this study, these key performance indicators depend mainly on the type of source (electrical, magnetic or combination of the two), the dielectric and conductive properties of the materials that make up the phantom at the selected frequency, the size of the plant (represented by a lossless encapsulation) and certainly the depth of the implant. From the point of view of the type of source it emerges that the power density that reaches the free space is much higher in the case of a magnetic dipole as shown in Figure 16. This is because the losses in the reactive near-field of a magnetic source are less than those of an electric source.

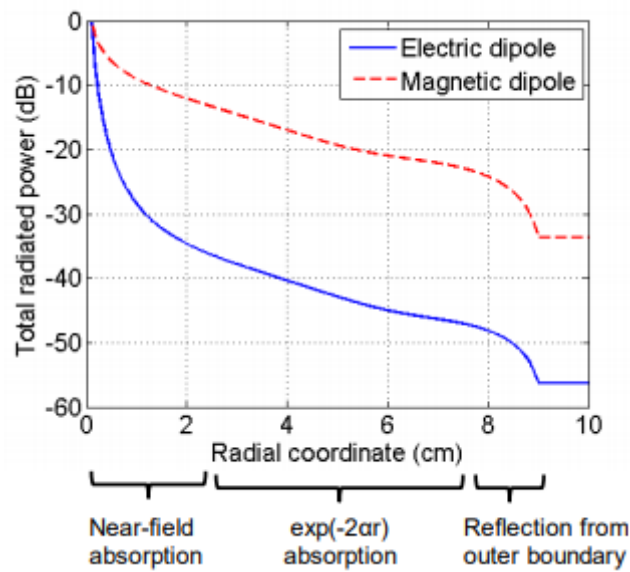


Figure 16 - Total radiated power as a function of the radial coordinate, for an elementary source implanted in the centre of a lossy host medium [49].

The theoretical aspects of this study will be taken as a reference in the next chapter in the attempt to obtain an estimation of the maximum power that could be transferred to an antenna implanted under the skin while remaining within the limits of the regulators.

4. Power budget analysis

In order to understand whether sufficient power can be transferred to a miniaturized diagnostic biosensor, an analysis of the available power budget is required. The efficiency of power transfer will be very low, this is because in the path between the transmitting antenna and the receiving antenna miniaturized in order to be compatible with a miniaturized biosensor, there are several causes of loss. In addition, the regulatory limits impose limitations on the maximum electric field strength, magnetic field and power density of the incident electromagnetic wave and the maximum specific absorption rate in the tissues (SAR), which contribute to making even lower the maximum power available at the location of the receiving antenna.

In this analysis, only the receiving antenna and the equivalent plane wave incident on the human body will be considered. The dielectric properties of tissues at various frequencies will be used and three types of loss will be considered: losses by reflection due to the mismatch impedance between air and tissue; losses due to absorption during propagation of electromagnetic waves in tissues; losses in the near field reactive of the receiving antenna due to the coupling between antenna and tissue.

In this analysis, the transmitting antenna, the impedance mismatch between receiving antenna and rectifier will not be considered. Moreover, in the absence of further analysis criteria, the receiving antenna will be considered ideal and its gain will be considered to be the maximum for an ESA that is 1.5.

In general, the maximum receivable power will be estimated as a function of frequency, dielectric properties of the tissues and size of the implant as:

$$P_R = S \cdot A_e \cdot e_{reflections} \cdot e_{propagation} \cdot e_{near-field} \quad (53)$$

Where S is the maximum power density of the equivalent plane wave incident on the human body, given by the Regulators, A_e is the maximum effective aperture of the receiving antenna and the remaining terms are the efficiencies related to the three types of loss listed above.

Before getting to the heart of the analysis, however, it is necessary to understand what is the state of the art in terms of consumption for miniaturized biosensors for diagnostics in order to identify what can be the minimum size of the receiving antenna and the frequency range that can be used to obtain values of received power sufficient to power these devices.

Currently, in the literature it is possible to find an implantable biosensor capable of monitoring pH and blood alcohol concentration requiring a power lower than $1 \mu\text{W}$ [13], an ADPLL-based implantable amperometric biosensor in 65nm CMOS requiring $4 \mu\text{W}$ [51], a wirelessly powered CMOS glucose sensor for an active contact lens requiring $3 \mu\text{W}$ [7] and a fully-monolithic wireless bio-sensing system requiring 63 nW [9].

We will consider the case of a subcutaneous implant, because as we have already said in the introduction chapter, this is a useful place for example for the continuous monitoring of different metabolites of the human body and, moreover, if the size of the implant is not too large, we could think of making an injectable device making the implant less invasive.

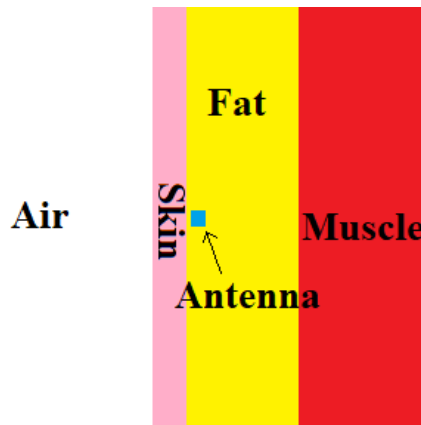


Figure 17 – Scheme of an antenna implanted subcutaneously.

First of all, it is necessary to have an idea of the thickness of human skin. In a studio [52], it was observed that the mean skin thickness for the anterior abdomen is 2.3 mm. This value will then be used as a reference for skin thickness in this analysis. An overall implant depth of 2.5 mm will also be considered considering that the antenna is in the subcutaneous adipose tissue as shown in Figure 17.

4.1. Regulatory limits

The Regulators that define the limits of exposure to electromagnetic fields vary in different parts of the world.

In the United States of America, there are two government agencies: the FCC (Federal Communication Commission) and the FDA (Food and Drug Administration).

In the European Union there is a non-governmental body, the ICNIRP (International Commission on Non-Ionizing Radiation Protection), which defines exposure limits to time-varying electric, magnetic and electromagnetic fields [53].

In Switzerland, the Federal Office for the Environment, BAFU (Bundesamt für Umweltschutz) has published the Ordinance on Non-Ionizing Radiation (ONIR).

ICNIRP defines exposure limits by differentiating first of all between exposure limits for the general population and for workers. Afterwards, it prepares basic restrictions and reference levels.

Basic restrictions

The basic restrictions are based directly on established health effects and biological considerations. Parameters that are limited are magnetic flux density (B), current density (J), specific absorption rate (SAR) and power density (S), depending on the frequency range used.

SAR is a measure of the percentage of electromagnetic energy absorbed by the human body when it is exposed to the action of a radio frequency (RF) electromagnetic field. More specifically, SAR is defined as the amount of electromagnetic energy that is absorbed in the unit of time by an element of unitary mass of a biological system, so that its unit of measurement is $\text{J/s}\cdot\text{kg}=\text{W/kg}$.

The SAR can be calculated from the knowledge of the electric field strength within the tissue, as follows:

$$SAR = \frac{1}{2} \frac{\sigma |\vec{E}_{rms}|^2}{\rho} \quad (54)$$

Where ρ is the sample density, \vec{E}_{rms} is the rms value of the electric field strength and σ is the electrical conductivity.

SAR is a local (pointwise) quantity, the averaging mass (volume) is crucial in assessing the max electric field in strongly varying situations as typical in penetration in human body. Localized SAR averaging mass is any 10 g of contiguous tissue; the maximum SAR so obtained should be the value used for the estimation of exposure.

$$\overline{SAR} = \frac{1}{V} \int_{sample} SAR dr \quad (55)$$

Basic restrictions for time varying electric and magnetic fields for frequencies up to 10 GHz are shown in Figure 18.

Exposure characteristics	Frequency range	Current density for head and trunk (mA m ⁻²) (rms)	Whole-body average SAR (W kg ⁻¹)	Localized SAR (head and trunk) (W kg ⁻¹)	Localized SAR (limbs) (W kg ⁻¹)
Occupational exposure	up to 1 Hz	40	—	—	—
	1–4 Hz	40/ <i>f</i>	—	—	—
	4 Hz–1 kHz	10	—	—	—
	1–100 kHz	<i>f</i> /100	—	—	—
	100 kHz–10 MHz	<i>f</i> /100	0.4	10	20
General public exposure	10 MHz–10 GHz	—	0.4	10	20
	up to 1 Hz	8	—	—	—
	1–4 Hz	8/ <i>f</i>	—	—	—
	4 Hz–1 kHz	2	—	—	—
	1–100 kHz	<i>f</i> /500	—	—	—
	100 kHz–10 MHz	<i>f</i> /500	0.08	2	4
	10 MHz–10 GHz	—	0.08	2	4

^a Note:

1. *f* is the frequency in hertz.
2. Because of electrical inhomogeneity of the body, current densities should be averaged over a cross-section of 1 cm² perpendicular to the current direction.
3. For frequencies up to 100 kHz, peak current density values can be obtained by multiplying the rms value by $\sqrt{2}$ (~1.414). For pulses of duration t_p the equivalent frequency to apply in the basic restrictions should be calculated as $f = 1/(2t_p)$.
4. For frequencies up to 100 kHz and for pulsed magnetic fields, the maximum current density associated with the pulses can be calculated from the rise/fall times and the maximum rate of change of magnetic flux density. The induced current density can then be compared with the appropriate basic restriction.
5. All SAR values are to be averaged over any 6-min period.
6. Localized SAR averaging mass is any 10 g of contiguous tissue; the maximum SAR so obtained should be the value used for the estimation of exposure.
7. For pulses of duration t_p the equivalent frequency to apply in the basic restrictions should be calculated as $f = 1/(2t_p)$. Additionally, for pulsed exposures in the frequency range 0.3 to 10 GHz and for localized exposure of the head, in order to limit or avoid auditory effects caused by thermoelastic expansion, an additional basic restriction is recommended. This is that the SA should not exceed 10 mJ kg⁻¹ for workers and 2mJ kg⁻¹ for the general public, averaged over 10 g tissue.

Figure 18 - Basic restrictions for time varying electric and magnetic fields for frequencies up to 10 GHz [53].

Reference levels

Some basic restrictions quantities typically, as J and SAR, cannot be measured directly in body. For this reason, some reference levels are derived from relevant basic restrictions using measurement and/or computational techniques, and some address perception and adverse indirect effects of exposure to electromagnetic field.

The derived quantities, expressed as “unperturbed” values, are electric field strength (E), magnetic field strength (H), magnetic flux density (B) and the equivalent plane wave power density (S_{eq}). Values are shown in Figure 19.

“Compliance with the reference level will ensure compliance with the relevant basic restriction” [53].

Frequency range	E-field strength ($V\ m^{-1}$)	H-field strength ($A\ m^{-1}$)	B-field (μT)	Equivalent plane wave power density S_{eq} ($W\ m^{-2}$)
up to 1 Hz	—	3.2×10^4	4×10^4	—
1–8 Hz	10,000	$3.2 \times 10^4/f^2$	$4 \times 10^4/f^2$	—
8–25 Hz	10,000	$4,000/f$	$5,000/f$	—
0.025–0.8 kHz	$250/f$	$4/f$	$5/f$	—
0.8–3 kHz	$250/f$	5	6.25	—
3–150 kHz	87	5	6.25	—
0.15–1 MHz	87	$0.73/f$	$0.92/f$	—
1–10 MHz	$87/f^{1/2}$	$0.73/f$	$0.92/f$	—
10–400 MHz	28	0.073	0.092	2
400–2,000 MHz	$1.375f^{1/2}$	$0.0037f^{1/2}$	$0.0046f^{1/2}$	$f/200$
2–300 GHz	61	0.16	0.20	10

^a Note:

1. f as indicated in the frequency range column.
2. Provided that basic restrictions are met and adverse indirect effects can be excluded, field strength values can be exceeded.
3. For frequencies between 100 kHz and 10 GHz, S_{eq} , E^2 , H^2 , and B^2 are to averaged over any 6-min period.
4. For peak values at frequencies up to 100 kHz see Table 4, note 3.
5. For peak values at frequencies exceeding 100 kHz see Figs. 1 and 2. Between 100 kHz and 10 MHz, peak values for the field strengths are obtained by interpolation from the 1.5-fold peak at 100 kHz to the 32-fold peak at 10 MHz. For frequencies exceeding 10 MHz it is suggested that the peak equivalent plane wave power density, as averaged over the pulse width does not exceed 1,000 times the S_{eq} restrictions, or that the field strength does not exceed 32 times the field strength exposure levels given in the table.
6. For frequencies exceeding 10 GHz, S_{eq} , E^2 , H^2 , and B^2 are to be averaged over any $68/f^{1.05}$ -min period (f in GHz).
7. No E-field value is provided for frequencies < 1 Hz, which are effectively static electric fields. perception of surface electric charges will not occur at field strengths less than $25\ kVm^{-1}$. Spark discharges causing stress or annoyance should be avoided.

Figure 19 - Reference levels for general public exposure to time-varying electric and magnetic fields (unperturbed rms) [53].

Since the power budget analysis will not consider the transmitting antenna but only the receiving antenna, the reference levels will be used to be in compliance with the regulators.

4.2. Losses due to reflections

The first obstacle for wireless power transfer through electromagnetic fields is represented by losses due to reflections. These are due to the mismatch impedance between air and tissue and between the various tissues that electromagnetic waves pass through.

In the far-field region of transmitting antenna, the efficiency due to reflections at the outer boundary, air-skin, can be written as [50]:

$$e_{\text{losses due to reflections}} = \frac{Re \left\{ \frac{|T|^2}{\eta_{air}} \right\}}{Re \left\{ \frac{1}{\eta_{skin}} \right\}} \quad (56)$$

Where the wave impedance in each medium, η , can be expressed as:

$$\eta = \sqrt{\frac{j\omega\mu}{\sigma + j\omega\varepsilon}} \quad (57)$$

And:

$$T = \frac{2\eta_{air}}{\eta_{air} + \eta_{skin}} \quad (58)$$

Since the dielectric properties of the tissues vary with frequency, losses due to reflections are also frequency dependent. Figure 20 shows how air-to-skin transmission efficiencies vary at different frequencies.

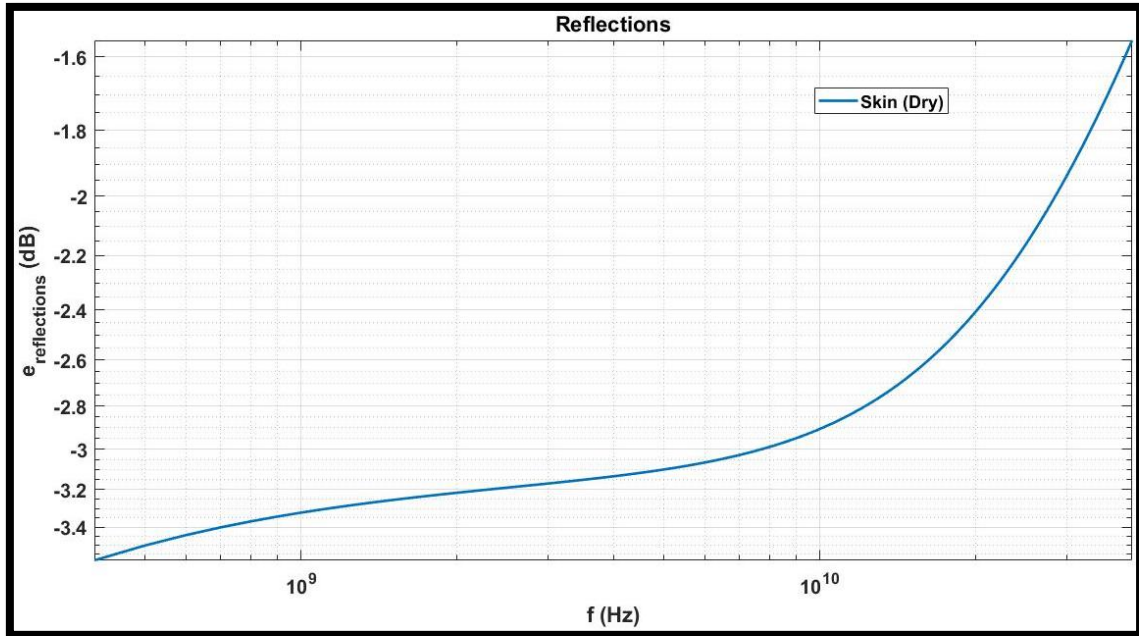


Figure 20 - Air-skin transmission efficiency

It is possible to see that the efficiency related to the losses due to reflections increases with the frequency.

Certainly, considering also the tissues following the skin, the losses by reflection increase even more. In fact, inside the human body, electromagnetic waves undergo different reflections, as shown schematically in Figure 21.

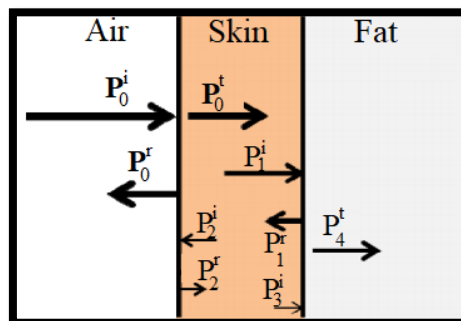


Figure 21 – Scheme of the reflection losses inside human body.

In this analysis, given the uncertainty of the interactions that actually occur within the tissues in terms of reflections, for the calculation of the efficiency correspondent to the losses due to reflections, only the losses at the air-skin interface will be considered.

4.3. Propagating field absorption losses

The second type of loss is represented by losses due to absorption during propagation of electromagnetic waves in tissues.

The efficiency corresponding to losses by absorption of the propagating field decays exponentially and can be expressed as:

$$e_{\text{propagating field}} = e^{-2\alpha z} \quad (59)$$

absorption losses

Where α is the absolute value of the imaginary part of the wave number in the medium, $k = \beta - j\alpha$, and z is the thickness of the medium.

In Figure 22 the efficiency correspondent to propagating field absorption losses in different tissues, with $z = 2.5$ mm is show.

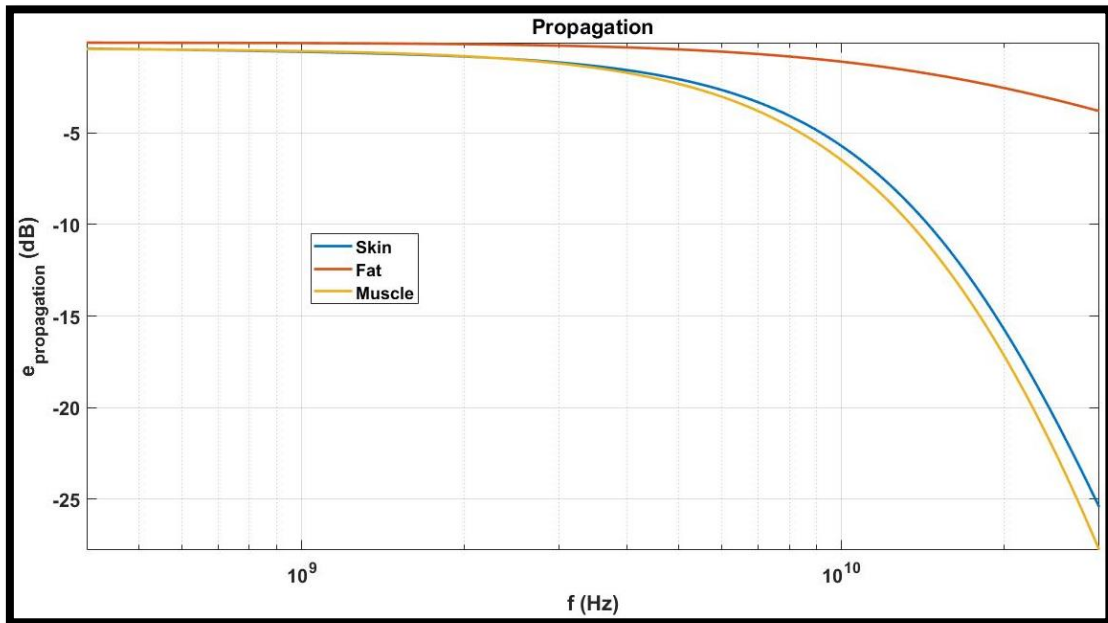


Figure 22 – Efficiency relative to propagating field absorption losses – depth = 2.5 mm

The absorption depends both on the type of tissue and on the frequency being precisely α dependent on both. In particular, the fat tissue absorbs less than the skin and muscle tissue and therefore the efficiency of propagation is greater in it. For all tissues, the absorption by the tissues increases as the frequency increases.

For the case of a subcutaneous implant, considering the previously defined implant location, at a depth of 2.3 mm of skin and 0.2 mm of fat, the efficiency corresponding to losses by absorption during propagation is shown in Figure 23.

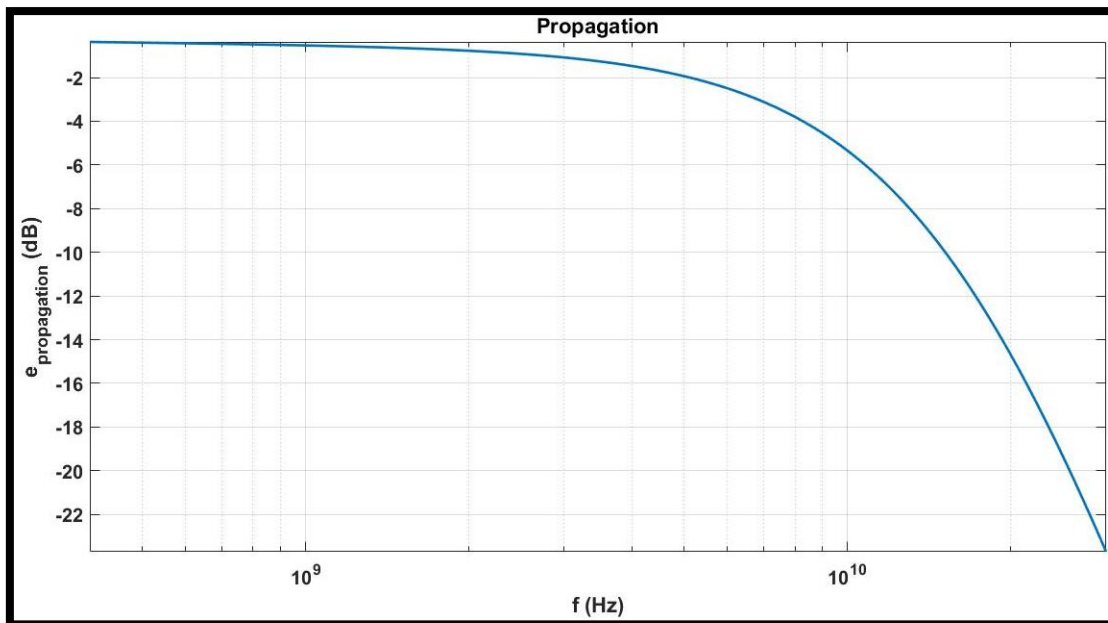


Figure 23 - Efficiency relative to propagating field absorption losses – depth = 2.3 mm skin + 0.2 mm fat tissue.

4.4. Losses in the reactive near field

The losses in the reactive near field of the receiving antenna are losses due to the coupling between the antenna and the host tissue with losses. The first two types of losses that we have seen (losses by reflection and propagation) are inevitable and depend substantially on the characteristics of the human body. The losses in the reactive near-field instead depend not only on the characteristics of the tissue in which the receiving antenna is implanted, but also on the size of the encapsulation in which it is contained. Therefore,

by increasing the size of the encapsulation without losses, these can be decreased so that most of the near field reactive of the antenna is contained in the encapsulation.

The efficiency corresponding to this type of loss can be expressed as [50]:

$$e_{\text{losses in the reactive near-field}} = \frac{e^{-2\alpha(r_{\text{far}}-r_{\text{impl}})} \text{Re}\{j\eta \hat{H}'_n{}^{(2)}(kr_{\text{far}}) \hat{H}_n{}^{(2)*}(kr_{\text{far}})\}}{\text{Re}\{j\eta \hat{H}'_n{}^{(2)}(kr_{\text{impl}}) \hat{H}_n{}^{(2)*}(kr_{\text{impl}})\}} \quad (60)$$

Where \hat{H}_n is the Hankel function (radial index n), r_{impl} is the radius of the lossless encapsulation containing the antenna and r_{far} is the " large enough " radius for which, considering the antenna implanted in transmission mode, there are practically only far-field components.

For the dominant spherical mode, the last expression can be approximated as [50]:

$$e_{\text{losses in the reactive near-field}} = \frac{|k|^2 \text{Re}\{\eta\}}{\text{Im}\left\{\frac{\eta}{(kr_{\text{impl}})^3}\right\}} \quad (61)$$

Figure 24 shows the efficiency corresponding to losses in the reactive near-field for different human tissues for $r_{\text{impl}} = 100 \mu\text{m}$. The losses are greater for fat tissue than for skin and muscle tissue. This is because a lower magnitude of permittivity (at the same loss tangent) increases the radius of the region of the reactive near field and therefore at the same r_{impl} a smaller part of the reactive near field region will be contained in the encapsulation.

Figure 25 shows how the efficiency in fat tissue varies with the radius of the implant. It can be seen that by decreasing the size of the implant to a few μm , the losses in the near-field reactive become enormous. When the size of the implant is large enough and therefore a large part of the near-field reactive is contained in the encapsulation, the efficiency tends asymptotically to 100 % (0 dB).

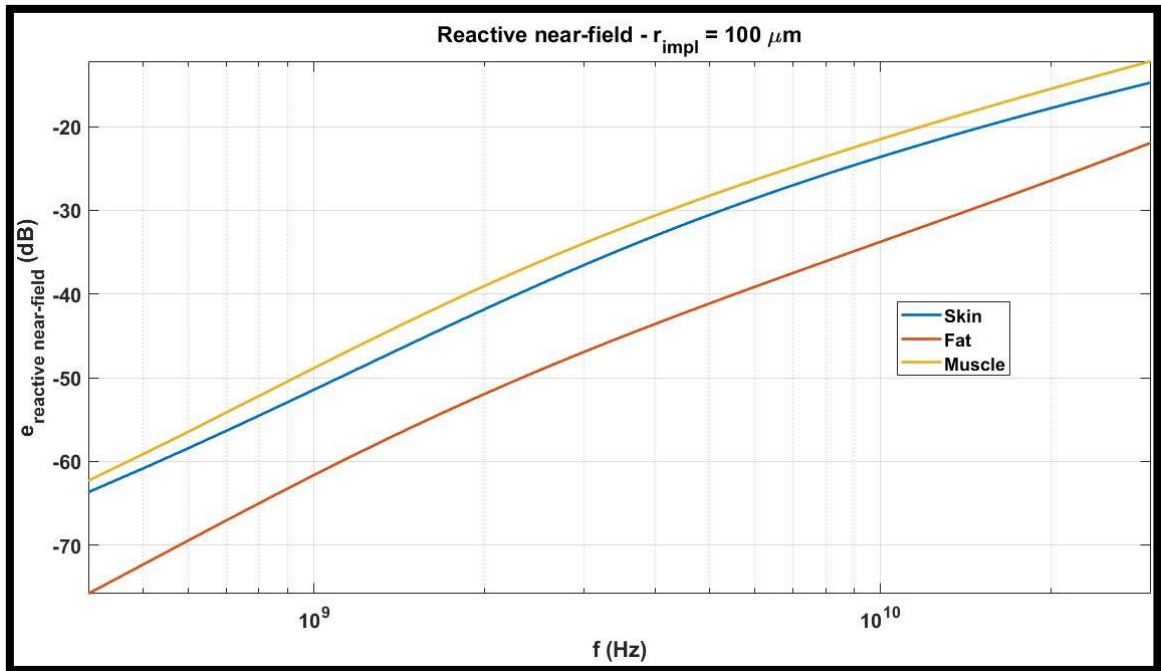


Figure 24 - Efficiency corresponding to losses in the reactive near-field - $r_{impl} = 100 \mu m$.

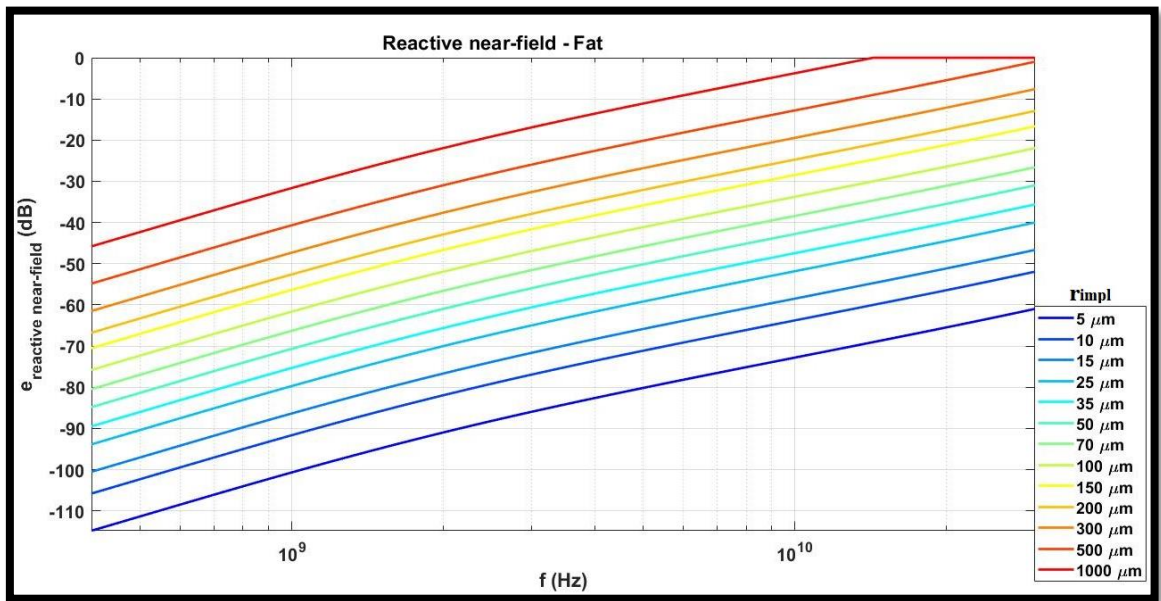


Figure 25 - Efficiency corresponding to losses in the reactive near-field in fat tissue for different values of r_{impl} .

4.5. Results

Now that we have seen what the three types of losses are and how they manifest themselves in the human body, we have all the tools to try to make a power budget analysis.

We have seen that in general the losses by reflection decrease as the frequency increases, the losses by absorption increase as the frequency increases, while the losses in the near field depend both on the size of the implant and on the frequency.

Figure 26 shows the total efficiency or the product (or sum in dB) of the efficiencies related to these three types of losses. For the case of an implant at a depth of 2.3 mm of skin and 0.2 mm of fatty tissue, the total efficiency has its maximum point above 10 GHz.

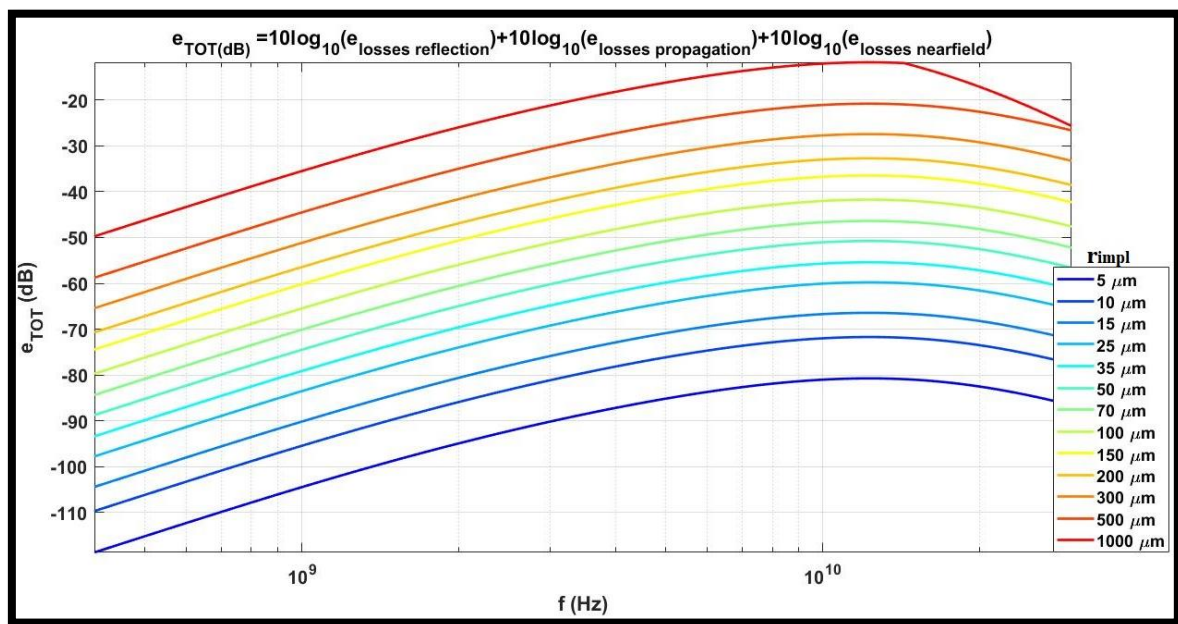


Figure 26 – Sum (dB) of the *efficiencies related to the three types of losses for different values of r_{impl} .*

Looking at the equation (53) you can see that in addition to the power density there is still a term to consider, the effective aperture of the antenna. As defined by the equation (51) the effective aperture of an antenna, considering the gain constant, is directly proportional to the square of the wavelength and therefore inversely proportional to the square of the frequency. Considering an ideal antenna without loss and with gain equal

to the maximum gain for an omnidirectional ESA that is 1.5, the maximum antenna effective aperture as a function of frequency is shown in Figure 27.

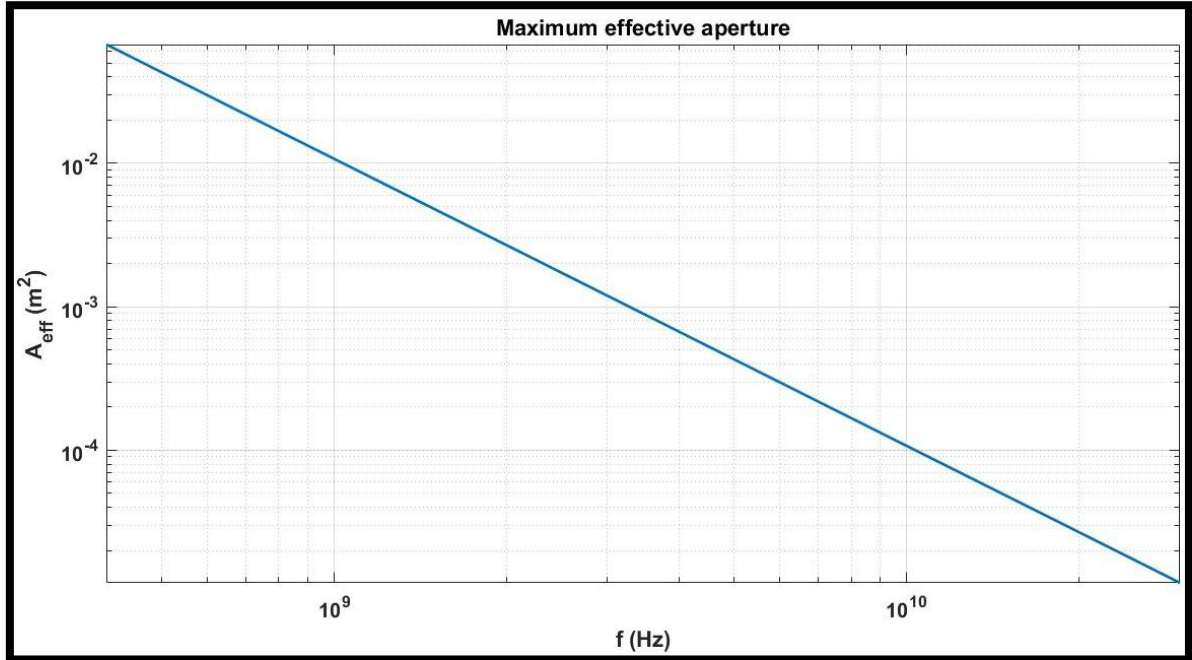


Figure 27 – Maximum effective aperture for an omnidirectional ideal ESA

By now merging all the terms and using the maximum permissible incident power density according to the table in Figure 19, we obtain an estimate of the maximum obtainable power which is shown in Figure 28 as a function of the frequency and size of the antenna.

It can be seen that there is a frequency band highlighted in grey so that substantially the power transfer efficiency is optimal. This band goes from about 2 GHz to about 12 GHz.

Of course, we have to consider that in the case of a real antenna, the radiation efficiency is not 1 (0 dB) but lower. In particular, the radiation efficiency decreases with decreasing ka , so the maximum gain of a real ESA will be smaller than 1.5 and will not be constant but dependent on frequency, size and material with antenna losses. It is therefore possible to think that the optimal frequency range will move further towards higher frequencies.

In any case, this analysis, made considering an ideal antenna without losses, can allow us to understand which the maximum transferable power is, depending on the size of the

antenna and therefore can be useful as a starting point for defining a minimum size of the antenna, to try in the next chapter to design real antennas.

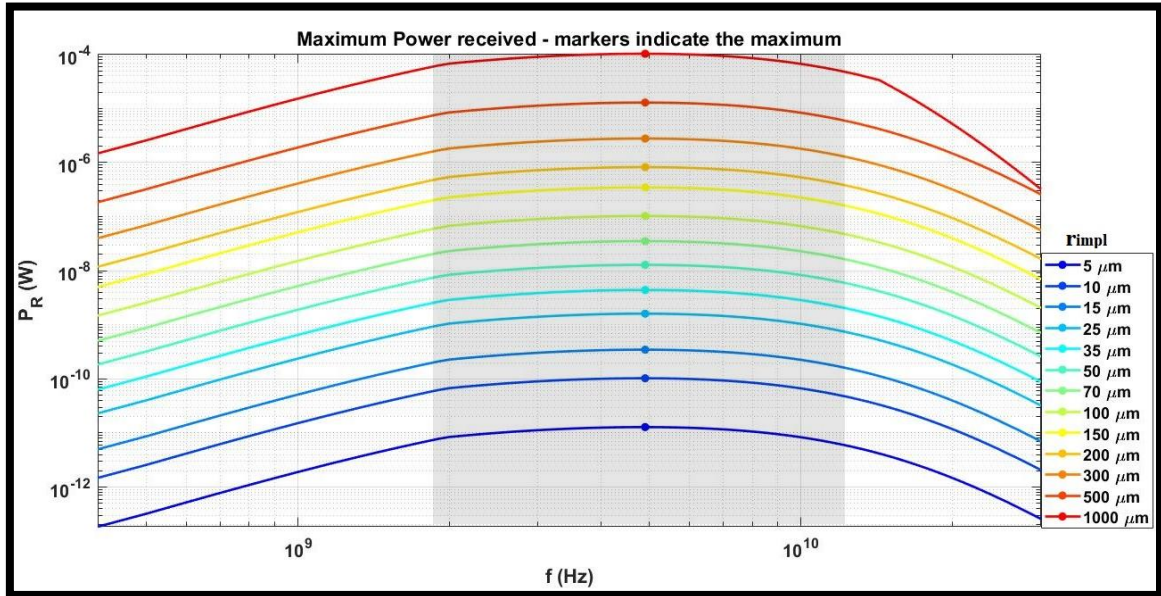


Figure 28 – Maximum power received by an ideal omnidirectional ESA considered implanted at dept 2.3 mm skin and 0.2 mm fat tissue.

The maximum received power for each r_{impl} value, as shown in Figure 27, is shown in Table 3. We can see that in order to hope to receive a sufficient amount of power to supply a miniaturized biosensor for diagnostics it is necessary to go up to r_{impl} values greater than 300 μm or an antenna with a maximum size of 600 μm . Considering that we are talking about an ideal antenna without losses and what we want to do is to make a real antenna, the size of the antenna must be greater. It may be reasonable then to proceed, designing real antennas occupying volumes of a few mm^3 .

Table 3 - Maximum power received by an ideal omnidirectional ESA considered implanted at depth 2.3 mm skin and 0.2 mm fat tissue.

Frequency (GHz)	$\epsilon_{\text{losses_reflection}}$ (dB)	$\epsilon_{\text{losses_propagation}}$ (dB)	$\epsilon_{\text{losses_reactive_nearfield}}$ (dB)	Maximum Power received (μW)	r_{impl} (μm)
4.9	-3.1036	-1.8878	-80.3598	$1.2872 \cdot 10^{-5}$	5
			-71.3289	$1.0297 \cdot 10^{-4}$	10
			-66.0462	$3.4753 \cdot 10^{-4}$	15
			-59.3907	0.0016	25
			-55.0069	0.0044	35
			-50.3598	0.0129	50
			-45.9760	0.0353	70
			-41.3289	0.1030	100
			-36.0462	0.3475	150
			-32.2980	0.8238	200
			-27.0153	2.7803	300
			-20.3598	12.8716	500
-11.3289	102.9727	1000			

5. ESA design

5.1. State of art of antennas for medical devices

Before starting to design miniaturised antennas, it is important to have an idea of the state of the art of antennas for medical devices. Table 4 shows a list of miniaturised antennas found in the literature with their working frequency and size.

Table 4 - State of the art of antennas for implantable medical devices

Type	Size	Central Frequency	Application	Reference
Meandered dipole	$29.2 \times 5 \text{ mm}^2$	1.4 GHz	Telemetry	[54]
Helix	$\pi \times 4.9^2 \times 15 \text{ mm}^3$	2.45 GHz	Telemetry Drug dosage monitoring	[55]
Spiral	$\pi \times 5^2 \times 5 \text{ mm}^3$	500 MHz	Telemetry Endoscopic capsule	[56]
Stent Antenna	$\pi \times 6^2 \times 30 \text{ mm}^3$	2.45 GHz	Telemetry/WPT Cardiovascular stent	[57]
Folded loop	$38 \times 38 \times 2.2 \text{ mm}^3$	2.45 GHz	Telemetry Cochlear	[58]
Helical folded dipole	$\pi \times 0.8^2 \times 36 \text{ mm}^3$	924 MHz	Telemetry	[59]
Microstrip patch	$9.2 \times 9.2 \times 1.27 \text{ mm}^3$	2.45 GHz	Telemetry	[60]
CSRR	$8.5 \times 8.5 \times 1.27 \text{ mm}^3$	2.45 GHz	Glucose monitoring	[61]
Patch	$10 \times 10 \times 1.27 \text{ mm}^3$	2.45 GHz	Telemetry	[62]

Folded dipole	$20.3 \times 0.8 \times 0.8 \text{ mm}^3$	924 MHz	Telemetry	[63]
PIFA	$6.5 \times 6.5 \text{ mm}^2$	2.4 GHz	Telemetry Intracranial Pressure Sensor	[64]
Fractal	$20 \times 20 \times 1.6 \text{ mm}^3$	2.4 GHz / 5.8 GHz	Energy Harvesting	[65]
Multilayered spiral	$\pi \times 5^2 \times 32 \text{ mm}^3$	2.45 GHz	Telemetry	[66]

5.2. Design of multi-turn loop antennas

From the analysis made in chapter 4 it was concluded that it could be possible to transfer a sufficient level of power to a subcutaneous system with an antenna having a volume of a few mm^3 in a frequency range from about 2 GHz to about 12 GHz.

Now we will try to develop, using the Ansys HFSS software, antennas that fall within these characteristics.

From [49], it is possible to understand that in a lossy medium, the losses in the near-field of an electric dipole are greater than those of a magnetic dipole. We could therefore in principle think that a loop antenna has less losses in the near-field than a dipole antenna.

Loop antennas are typically grouped into two classes, electrically small and electrically large:

- Electrically small loops are those whose circumference is much smaller than a wavelength ($C \ll \lambda$).
- Electrically large loops are those whose circumference is about one wavelength in free space ($C \sim \lambda$) [29].

If we consider the frequency range identified in chapter 4, the wavelengths range from about 150 mm to about 25 mm. Considering an electrically large loop, it should have a radius equal to approximately:

$$r = \frac{C}{2\pi} \approx \frac{\lambda}{2\pi} \quad (62)$$

Therefore, in the above-mentioned frequency range, the radii range from about 24 mm to about 4 mm, corresponding to diameters of 48 mm and 8 mm respectively.

Let's consider, for example, the objective of designing an antenna with a diameter of 1 mm. The resonance frequency of a loop of that size is about 48 GHz, which is obviously too high to transmit power inside the human body.

At 12 GHz, a loop of that size is electrically small and, as a consequence, the radiation efficiency is very low because its radiation resistance will be much lower than its ohmic resistance. Moreover, as we have seen in Chapter 3.2.6., its input impedance will be almost completely reactive, in particular it will have a real part slightly greater than 0 and an imaginary part much greater than 0.

In particular, its inductance, as already mentioned, can be estimated using equation (48) while its most radiation resistance can be expressed as:

$$R_{rad} = 20\pi^2 \left(\frac{C}{\lambda}\right)^4 \quad (63)$$

We see that the radiation resistance is directly proportional to the circumference and frequency both elevated to the fourth, so at the same frequency we can guess that a loop with a smaller radius will have lower radiation resistance.

As an example, through the Ansys HFSS software, a copper loop antenna with major radius $a = 0.5$ mm and a minor radius $b = a/20 = 25$ μm has been simulated (Figure 29).

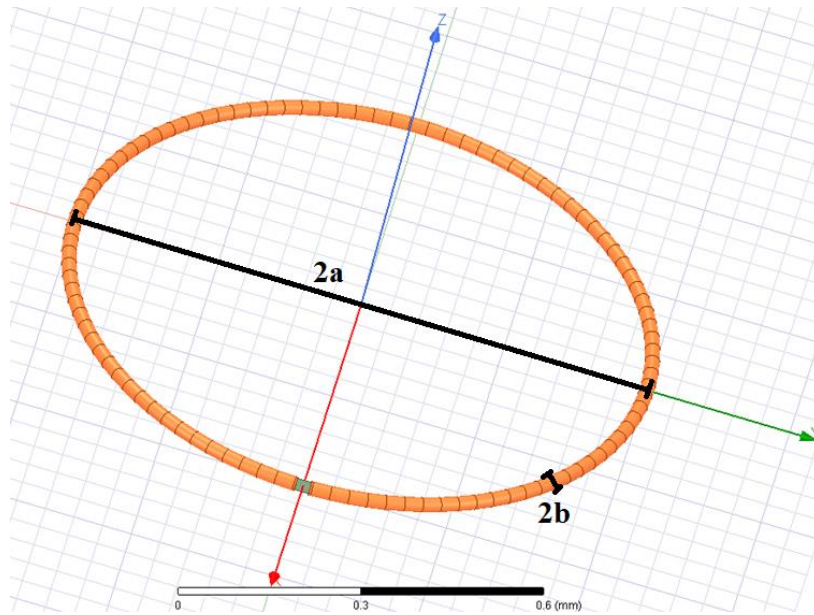


Figure 29 – Loop antenna.

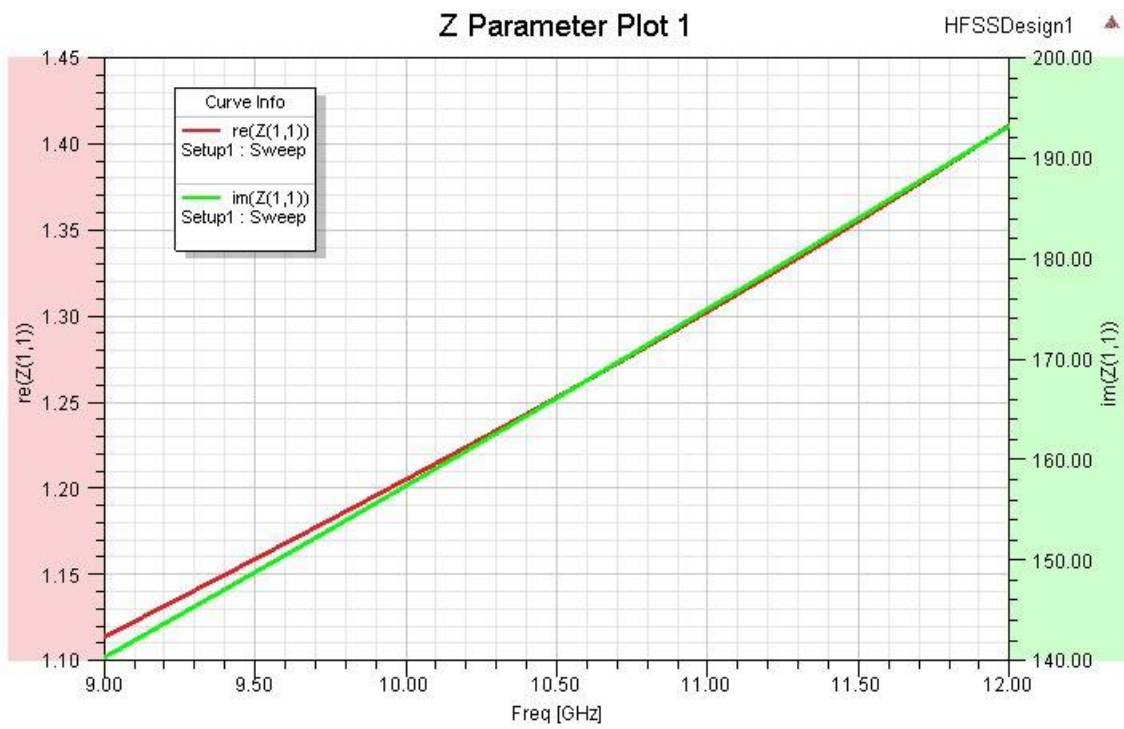


Figure 30 – Input impedance of an electrically small loop between 9 and 12 GHz.

Figure 30 shows the antenna input impedance. It can be seen that, as expected, it has a much larger imaginary part than the real part.

It also has an ohmic resistance greater than the radiation resistance as evidenced by observing the gain of the antenna (Figure 31) which has a peak of -15.2 dBi, revealing a low radiation efficiency.

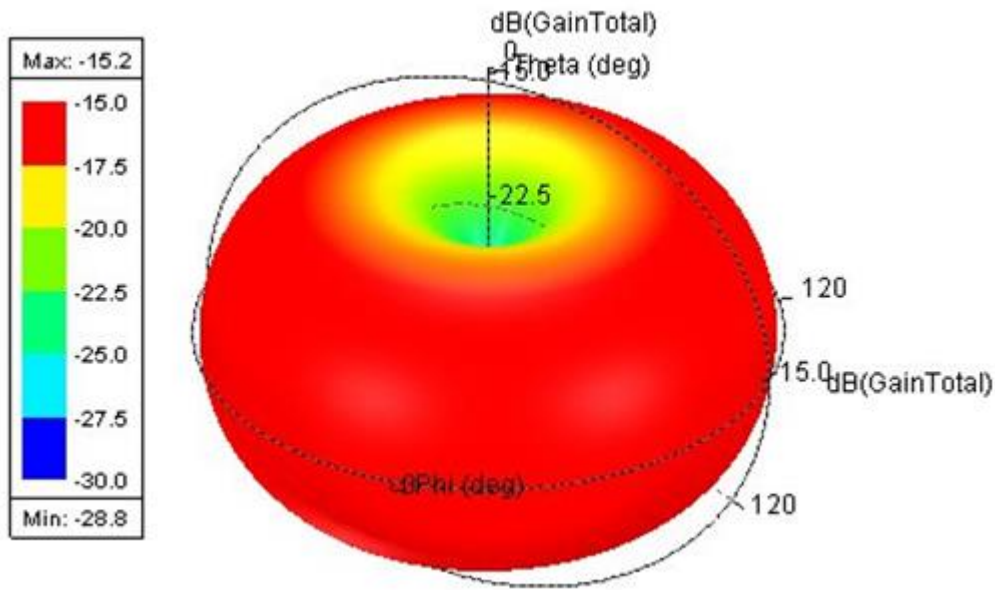


Figure 31 – Gain (dBi) of a 1 mm diameter loop antenna at 10 GHz.

For the same loop circumference, it is possible to increase the radiation resistance by switching from a loop antenna to a multi-turns loop antenna (Figure 32). In fact, the radiation resistance also depends on the number of turns, N , of the loop:

$$R_{rad} = 20\pi^2 \left(\frac{C}{\lambda}\right)^4 N^2 \quad (64)$$

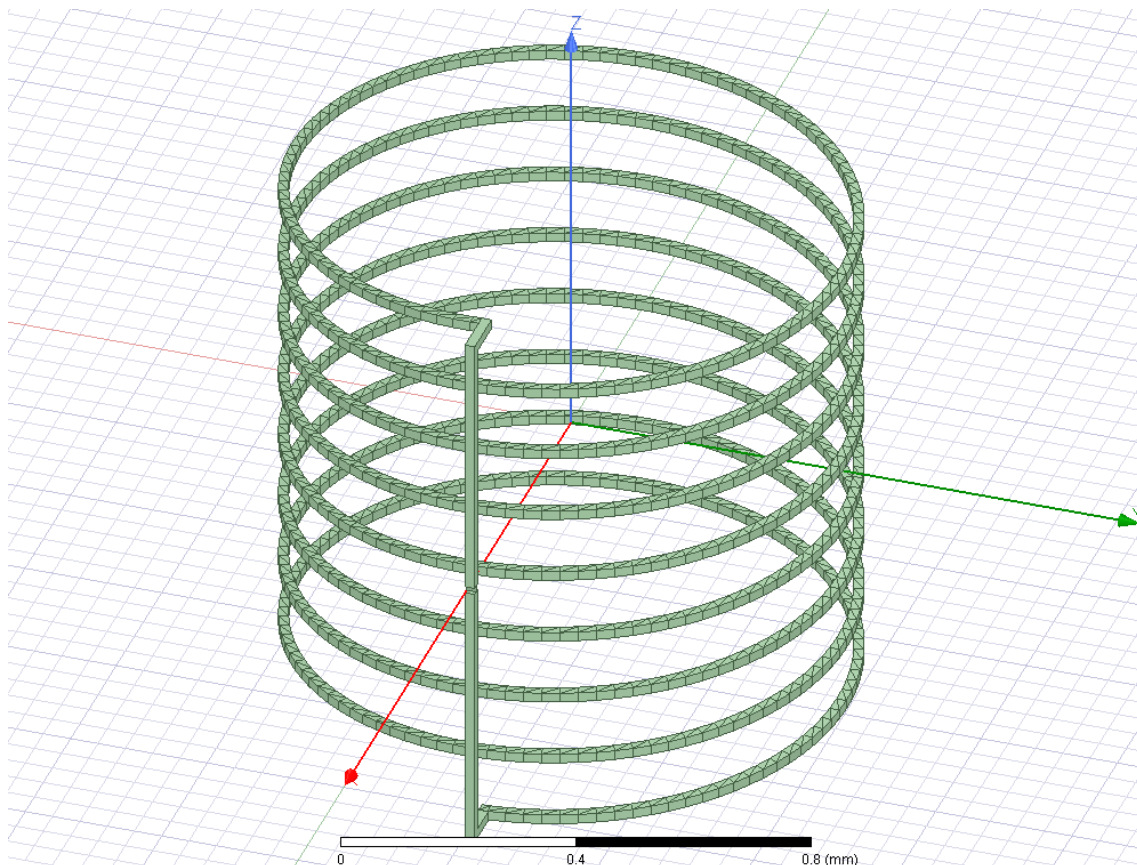


Figure 32 – Multi-turns loop antenna.

5.2.1. A $1 \times 1 \times 1 \text{ mm}^3$ multi-turns loop antenna

In this subchapter, a multi-turns loop antenna with a diameter of 1 mm and a height of 1 mm will be designed. Copper will be used as material.

An electrically small loop antenna has an imaginary part of the input impedance that is mainly inductive. When the number of turns is greater than 1, we can talk about multi-turns loop antenna. The imaginary part of the input impedance of an antenna of this type, is not always mainly inductive but the parasitic capacitance that occurs between the various turns causes a cancellation of the reactance. In fact, for certain frequencies, self-resonance frequencies, the inductive and capacitive reactance are equal in module and therefore the input impedance is completely real.

The resonance frequency occurs when the overall length of the conductor composing the antenna is equal to about λ .

Let's see some examples. Let's consider that we want to have a working frequency of the antenna (resonance frequency) that is in the frequency range identified in the analysis made in chapter 4. We have identified as the upper limit a frequency of about 12 GHz, which corresponds to a wavelength of about 25 mm. If we want to make a multi-turns loop antenna with a diameter of each loop of 1 mm, we need about 8 turns ($\lambda/(2\pi r)$).

Therefore, Figure 33 shows the reflection coefficients, S11 with respect to 50 Ω , for values of N from 8 to 11. For N=8 we can observe a self-resonance frequency at 13.8 GHz, for N=9 at 12.3 GHz, for N=10 at 11.1 GHz and for N=11 at 10.1 GHz. The overall height of each antenna is 1 mm, so the inter-coil distance varies with the variation of N.

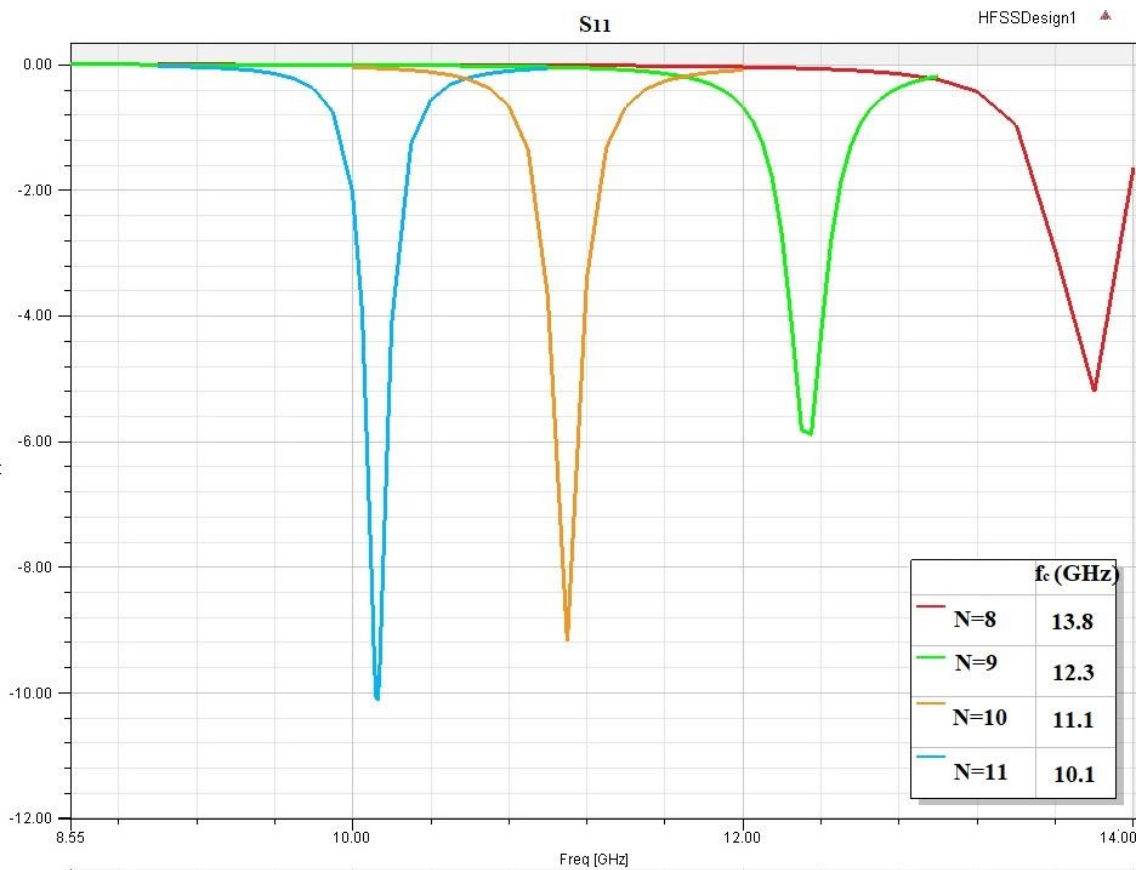


Figure 33 – Comparison of return loss (relative to 50 Ω) and resonant frequency for different N.

The antenna with $N=8$ has a too high resonance frequency, so keep on considering $N=9,10,11$.

Now let's consider the gain of these antennas. For $N=9$ the peak gain is -8.1 dBi (Figure 34), for $N=10$ it is -11.8 dBi and for $N=11$ it is -13.2 dBi. It was therefore decided to keep the antenna for $N=9$ (Figure 35).

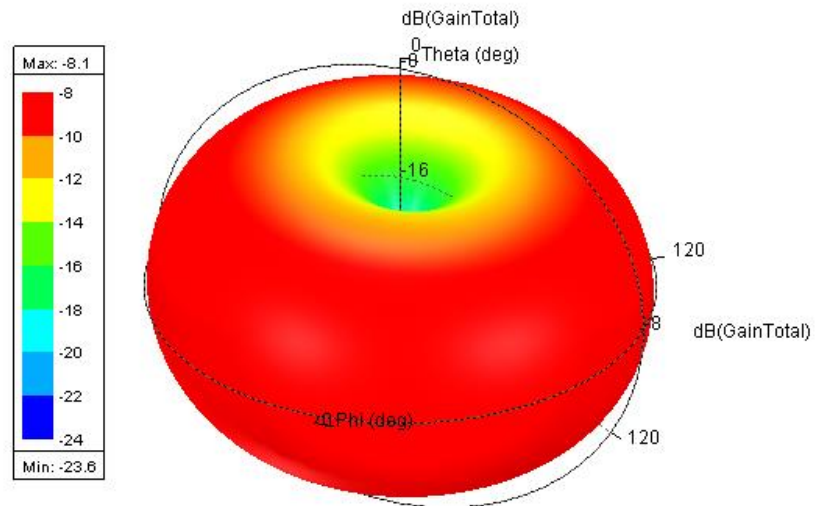


Figure 34 – Gain (dBi) of a 9-turns copper loop antenna with diameter and height 1 mm.

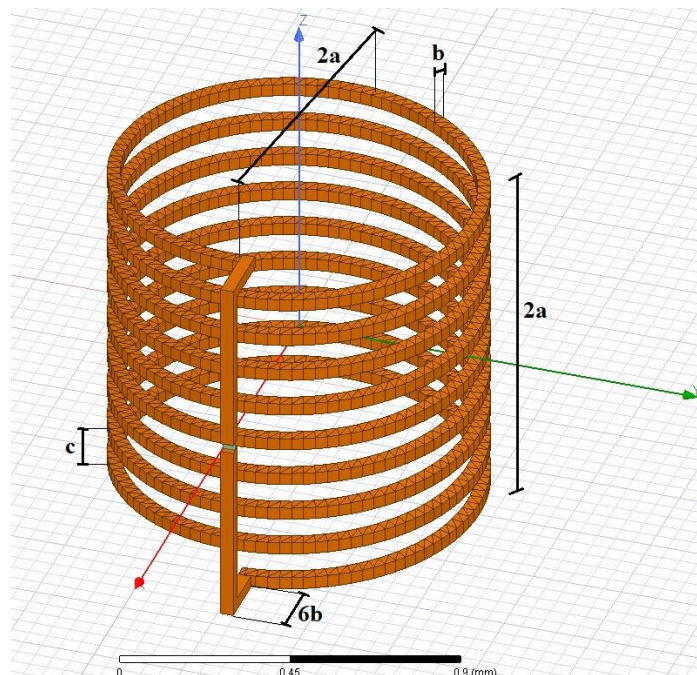


Figure 35 - 9-turns loop antenna.

Observe the antenna input impedance in Figure 36. You can see that at 12.3 GHz it has a real part equal to 16.5Ω and an imaginary part null, being precisely the resonance frequency.

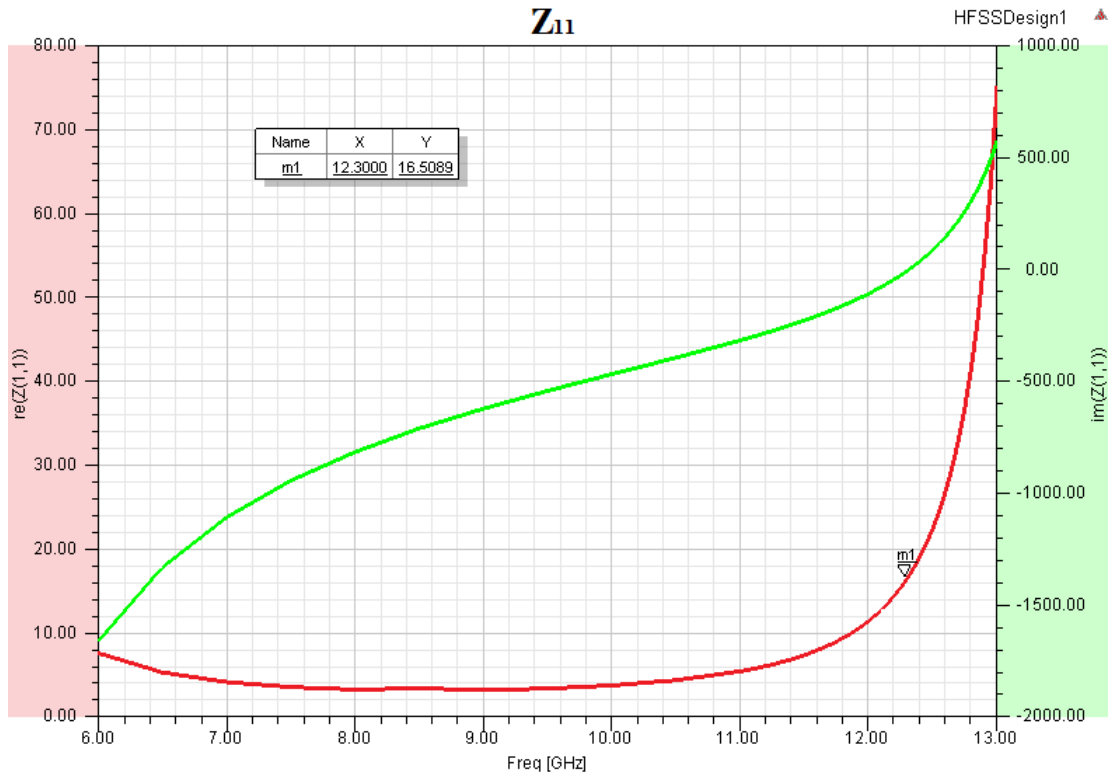


Figure 36 – Input impedance of a 9-turns copper loop antenna with diameter and height 1 mm.

In particular, the antenna parameters are summarized in Table 5.

Table 5 – Parameters for designed the 9-turns loop antenna (Reference to Figure 35).

Parameter	Value
Number of turns (N)	9
Radius (a)	0.5 mm
Height	1 mm
Edge of the square section of the wire (b)	$25\sqrt{2} \mu\text{m}$
Pitch (c)	$2a/N$

5.2.2. A 2x2x2 mm³ antenna self-resonating at 5.8 GHz

Now consider designing an antenna in the Industrial, Scientific and Medical (ISM) band. Consider having the antenna resonant at 5.8 GHz. This is possible by changing the parameters in Table 5 to those in Table 6.

Table 6 – Parameters for designed the 9-turns loop antenna self-resonating in the ISM band (Reference to Figure 35).

Parameter	Value
Number of turns (N)	9
Radius (a)	1.045 mm
Height	2a
Edge of the square section of the wire (b)	$a\sqrt{2}/39$
Pitch (c)	$2a/N$

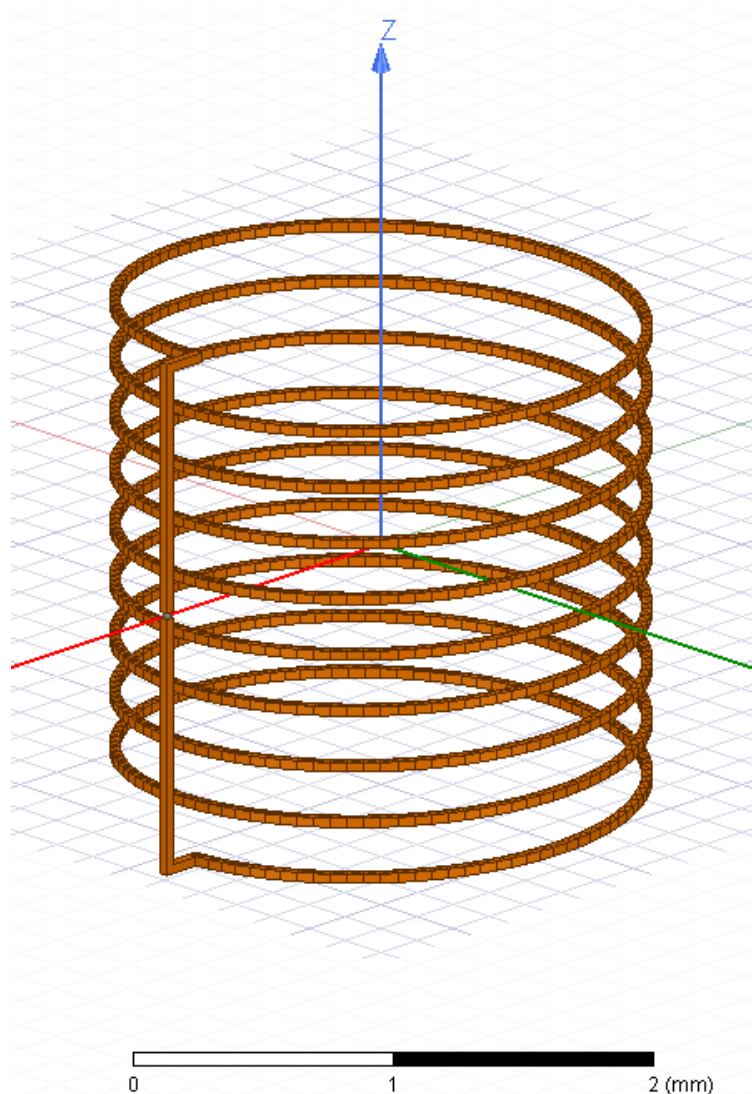


Figure 37 – 9-turns loop antenna resonating a 5.8 GHz.

In this case, the S_{11} parameter shows resonance at 5.8 GHz (Figure 38) and at that frequency the input impedance is 14.5Ω (Figure 40).

The antenna gain at the resonance frequency is -8.7 dBi (Figure 39), slightly worse than the antenna with a volume of 1 mm^3 .

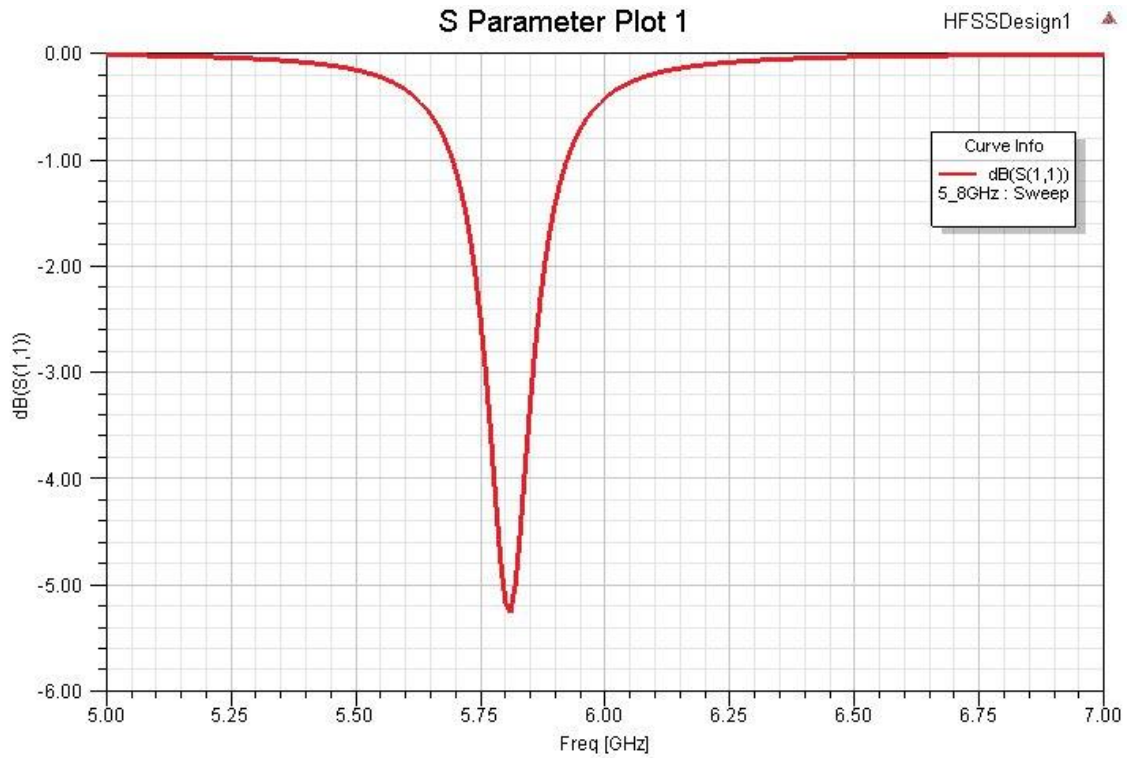


Figure 38 – S_{11} parameter of the 9-turns loop antenna resonating at 5.8 GHz.

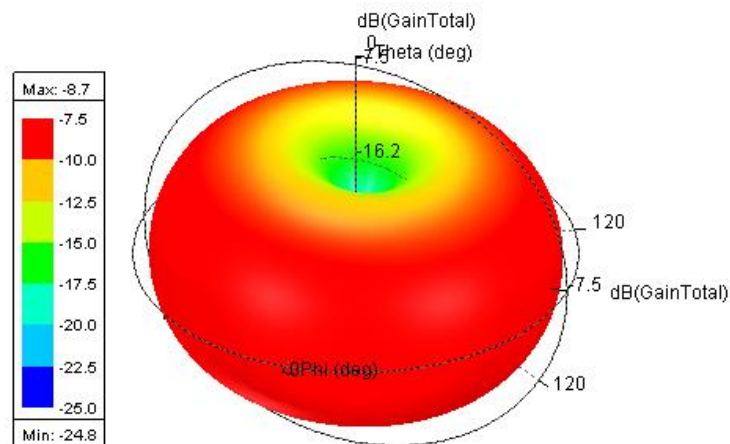


Figure 39 – Gain (dBi) of the 9-turns loop antenna at the resonant frequency (5.8 GHz).

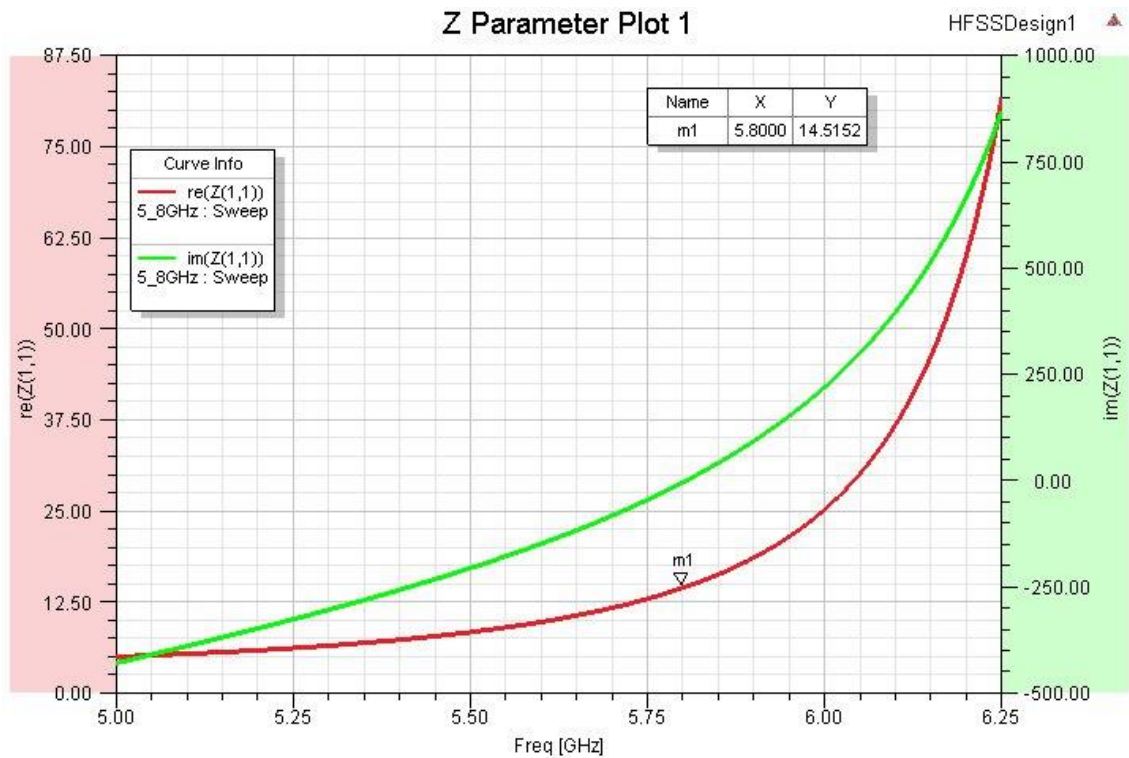


Figure 40 - Input impedance of a 9-turns copper loop antenna with diameter and height about 2 mm.

5.3. Phantoms

5.3.1. Human abdomen phantom

In order to simulate the behaviour of antennas when implanted under the skin it is necessary to create a phantom with the dielectric properties of human tissues.

Since the use of a complete human body phantom would require computational resources too high compared to the hardware available for this project, it was necessary to simplify the simulation by creating the phantom with the appropriate dielectric properties of a single piece of the human body.

In particular, given the availability in the literature of average sizes of the "layers" of the human anterior abdomen in this study [52], this part has been modelled.

The characteristics of the fabrics have been reproduced using the code in APPENDIX I which exploits the model of Gabriel.

The phantom consists, moving on the z axis, of a multilayer structure composed of air, 2.3 mm of skin, 1.5 cm of fat tissue and 2 cm of muscle tissue as shown in Figure 41. On the XY plane instead all these layers have a square section with side 5 cm.

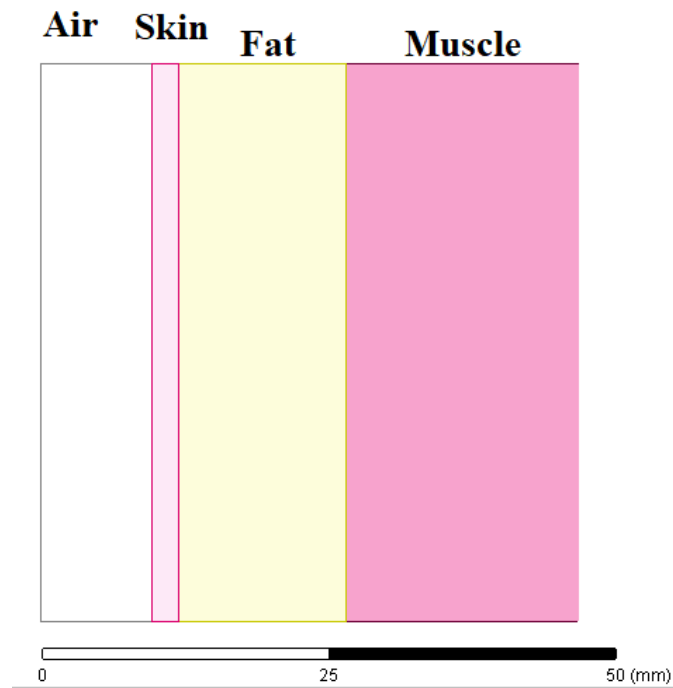


Figure 41 – Human anterior abdomen phantom.

5.3.2. Petri dish phantom

To simulate the antennas in an in vitro scenario, the phantom of a polystyrene petri dish was created, half filled with biological medium for cell cultures.

The petri dish model created has standard sizes available here [67] [68]. In particular, the petri dish used has a diameter of 60 mm and a height of 15 mm.

Half of it was filled with biological medium for cell cultures, whose dielectric properties were found in [69] and are shown in Figure 42.

The medium is composed of: 88% DMEM (Dulbecco's Modified Eagle Medium (1X))

- 10% FBS (Fetal Bovine Serum)

- 1% Antibiotic mix (Penicillin - Streptomycin)
- 1% Non-Essential Amino Acids

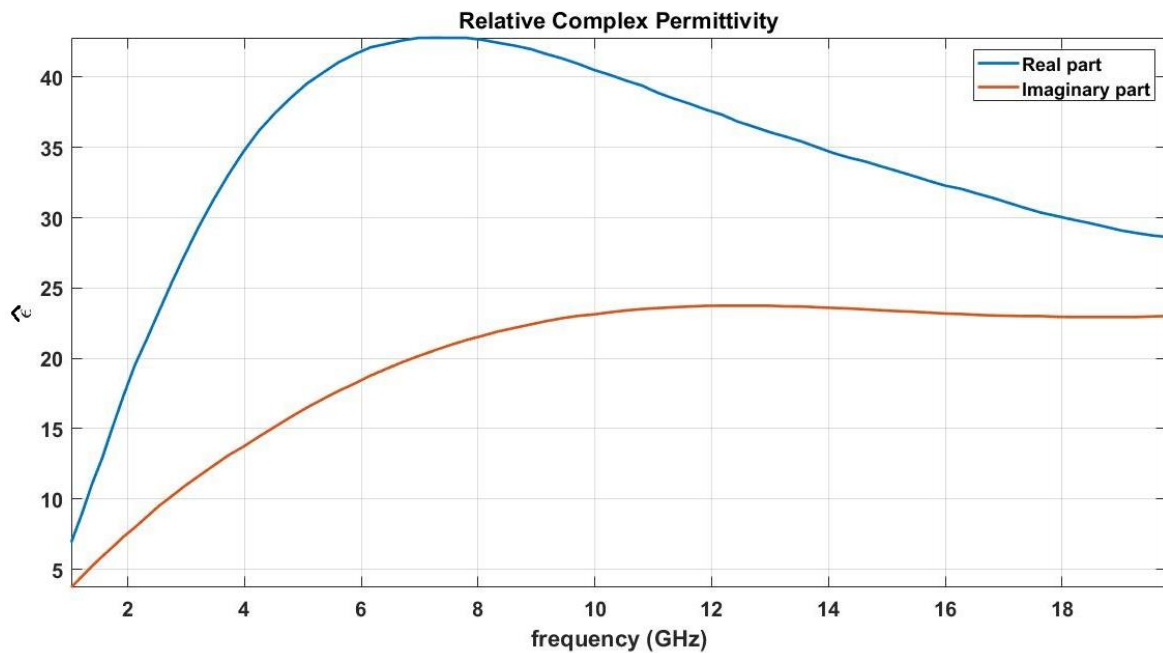


Figure 42 – Relative complex permittivity of Stem cell culture medium.

5.4. Behaviour of antennas inside the phantoms

As we anticipated in Chapter 3.3, when an antenna is in a lossy medium, such as the human body or cell culture medium, its characteristics are strongly dependent on the shape and composition of the host object and the position of the antenna in it.

In fact, the resonance frequency when it is in a medium other than air changes according to the relative permittivity of the host medium. Bandwidth normally increases. “But at this point, the importance of this bandwidth should be questioned, as it is more related to the power lost in the surrounding medium than to the useful bandwidth relative to the power radiated by the body phantom” [70].

The radiation pattern depends on the phantom and the position of the antenna in it, so it loses its meaning. "The diagram of antenna in a conducting medium is strongly dependent upon the origin of coordinates" [48].

As concerns radiation efficiency, in a medium with losses the radiated power depends on the distance from the antenna, so it is difficult to define it. If we consider that the medium has a finite size, as in the case of an implantable antenna or an antenna in a petri dish, we can define the radiated power using the classic definition in free space (outside the host body) at far-field distance. Therefore, as we have already said, the real figure of merit of an implanted antenna is the maximum radiated power or the power density reaching the free space in the direction of maximum radiation (towards the outside of the host body).

It is therefore permissible to simulate the antennas in the two phantoms and assess the gain in the direction of maximum radiation. By the time the host medium is with losses, the calculated gain will already take into account the losses in the host body.

Let's now see in the next paragraphs the behaviour of the two designed antennas in the two defined phantoms.

Since the copper antennas are not biocompatible, it is necessary to consider biocompatible isolation. Moreover, beyond biocompatibility, it is important that the antenna is not in direct contact with the tissues to avoid short circuits and not to have too much coupling between antenna and host body.

In [71], it is identified as the optimal biocompatible insulating material for implantable antennas, zirconia ($\epsilon_r = 29$ and $\tan\delta=0.00175$ at 10 GHz). This ceramic material has a very low loss tangent and has a high dielectric constant, making it also an excellent candidate for reducing losses in the near field of the implanted antenna.

For both antennas and for both applications considered, a zirconia insulation will be used. The isolation consists of a cube with a side of 2.6 mm for the resonant antenna at 5.8 GHz and a cube with a side of 1.6 mm for the resonant antenna at 12.3 GHz. The insulation thickness for both cases is 50 μm .

5.4.1. 1x1x1 mm³ antenna subcutaneous implant

Figure 43 shows the smallest antenna implanted in the subcutaneous adipose tissue.

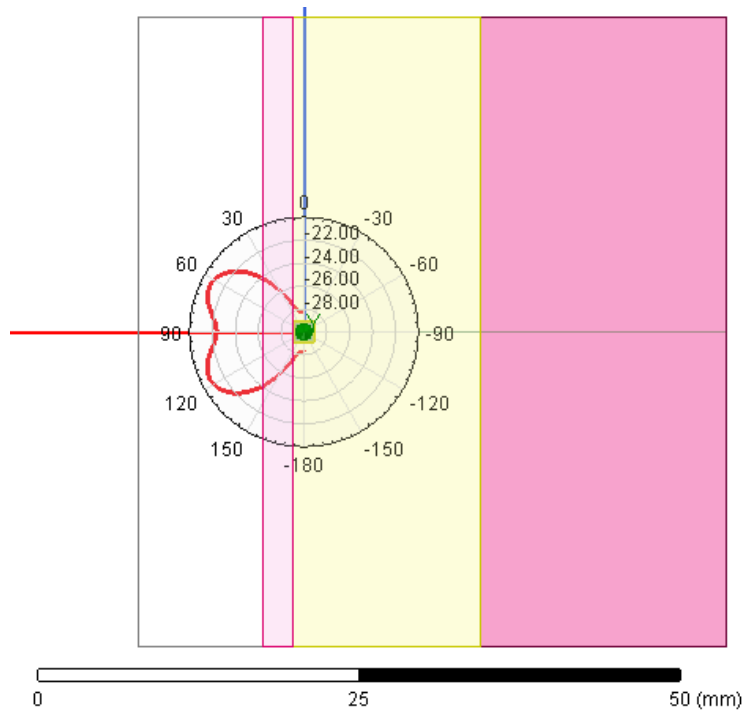


Figure 43 – Subcutaneous implant of 1 mm³ 9-turns loop antenna.

In the direction of maximum radiation, the peak gain is -20.79 dBi at the resonance frequency of the antenna, which drops from 12.3 GHz to 12 GHz (Figure 44).

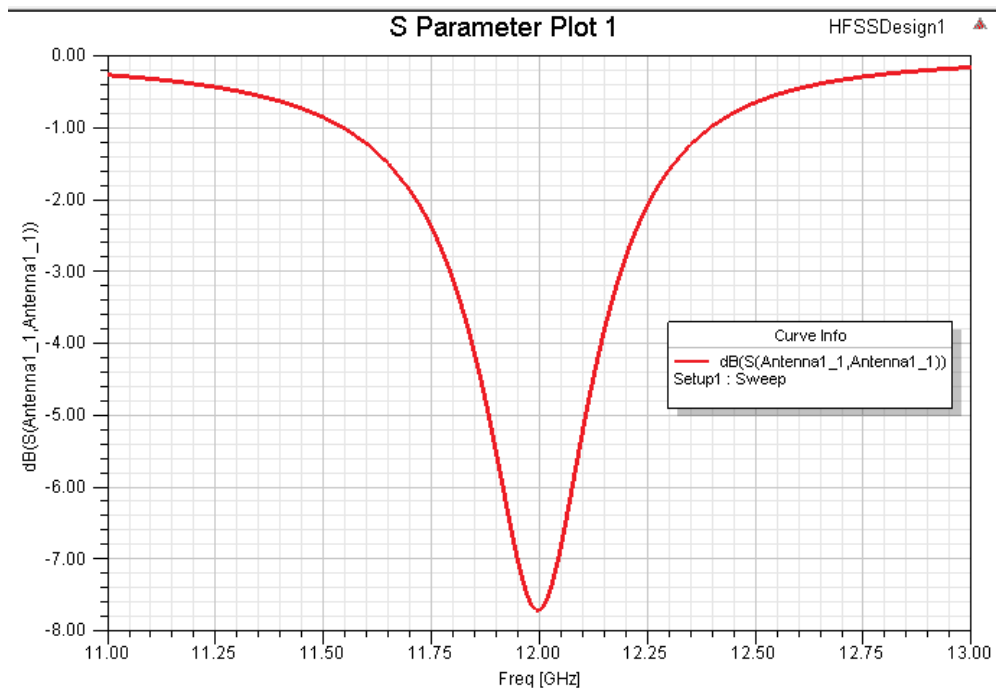


Figure 44 - Return loss (dB) (referred to 50 Ω) of the 9-turns copper loop antenna with diameter and height 1 mm, while subcutaneously implanted.

The input impedance also changes compared to the free space situation. In particular, at the resonance frequency the input impedance changes from 16.5 Ω to about 21 Ω (Figure 45).

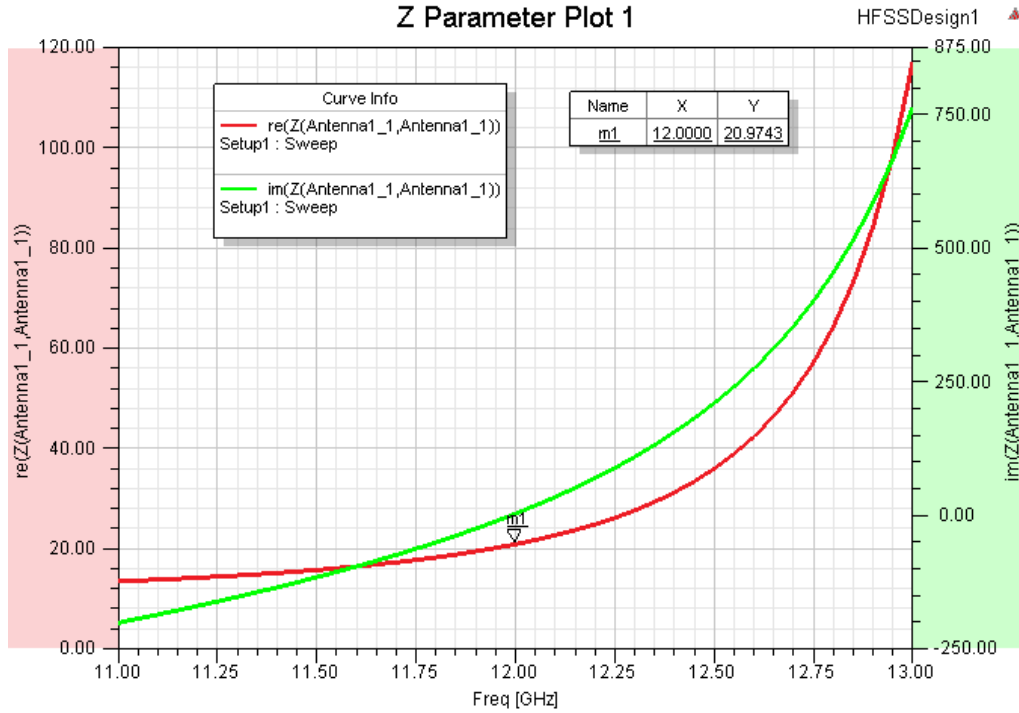


Figure 45 – Input impedance of the smallest antenna while subcutaneously implanted.

At 12 GHz the limit on the power density imposed by the ICNIRP is 10 W/m². The wavelength in free space is 24.9827 mm. The gain of -20.79 dBi linearly equals 0.00834. Considering a polarization mismatch loss between transmitting and receiving antenna of -3 dB (0.5) and in the hypothesis of impedance matching between antenna and rectifier, the received power is:

$$P_R = S \cdot A_{eff} \cdot Xp = S \cdot G \cdot \frac{\lambda^2}{4\pi} \cdot Xp \cong 2.1 \mu W$$

5.4.2. 2x2x2 mm³ antenna subcutaneous implant

Figure 46 shows the largest antenna implanted in the subcutaneous adipose tissue.

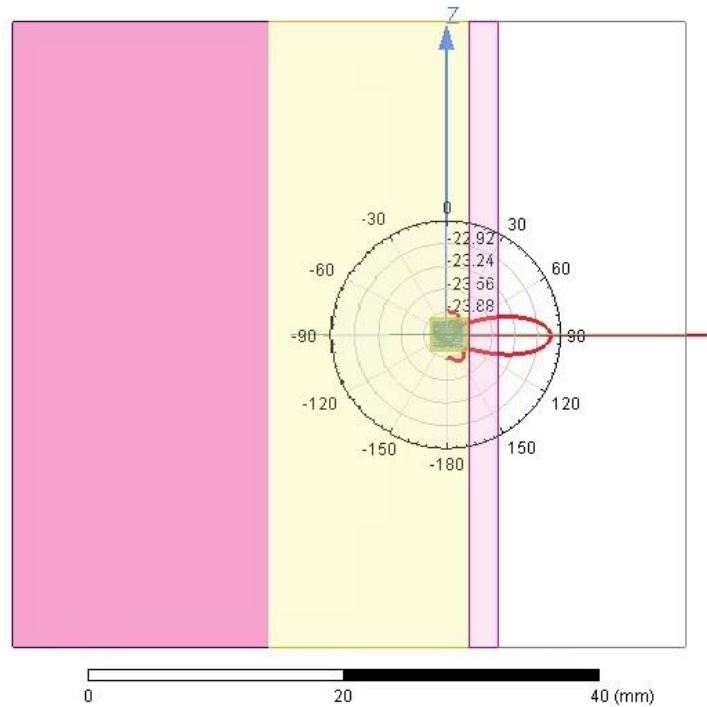


Figure 46 – 8 mm³ antenna subcutaneously implanted.

In the direction of maximum radiation, the peak gain is -20.6 dBi at the resonance frequency of the antenna, which drops from 5.8 GHz to 5.35 GHz (Figure 47).

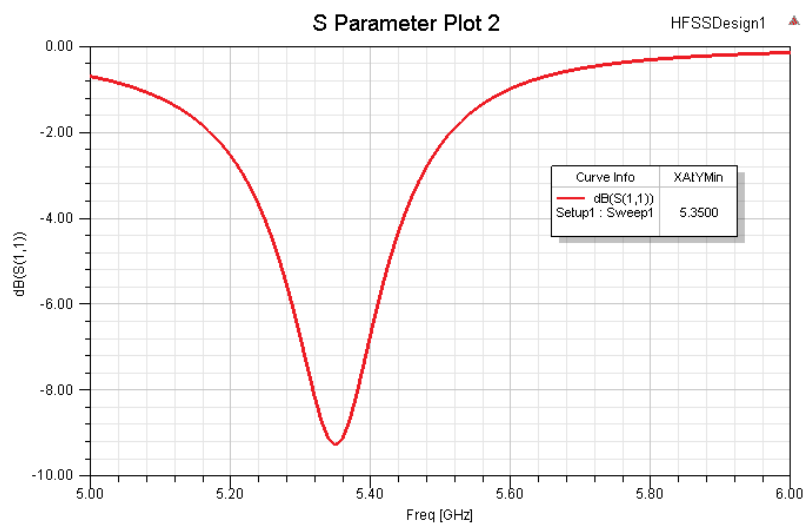


Figure 47 - Return loss (dB) (referred to 50 Ω) of the 9-turns copper loop antenna with diameter and height 2 mm, while subcutaneously implanted.

The input impedance also changes compared to the free space situation. In particular, at the resonance frequency the input impedance changes from 14.5 Ω to about 24.5 Ω (Figure 48).

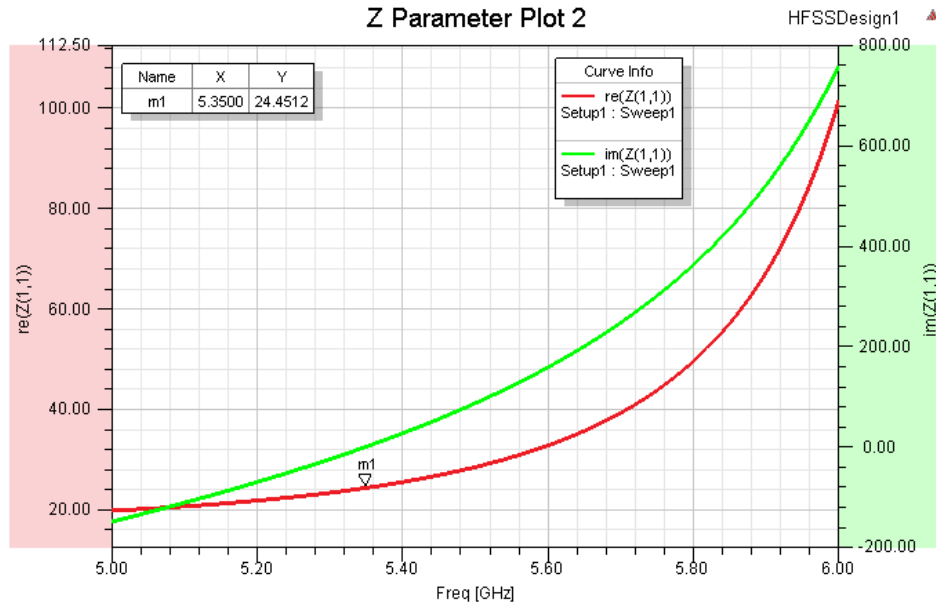


Figure 48 – Input impedance of the biggest antenna while subcutaneously implanted.

At 5.35 GHz the limit on the power density imposed by the ICNIRP reference levels is 10 W/m². The free space wavelength is 56 mm. The gain of -20.6 dBi linearly applies to 0.00871. Considering a polarization mismatch loss between transmitting and receiving antenna of -3 dB (0.5) and in the hypothesis of impedance matching between antenna and rectifier, the received power is:

$$P_R = S \cdot A_{eff} \cdot Xp = S \cdot G \cdot \frac{\lambda^2}{4\pi} \cdot Xp \cong 11 \mu W$$

5.4.3. 1x1x1 mm³ antenna in petri dish

Figure 49 shows the smallest antenna inserted at the bottom of a petri dish containing the cell culture medium.

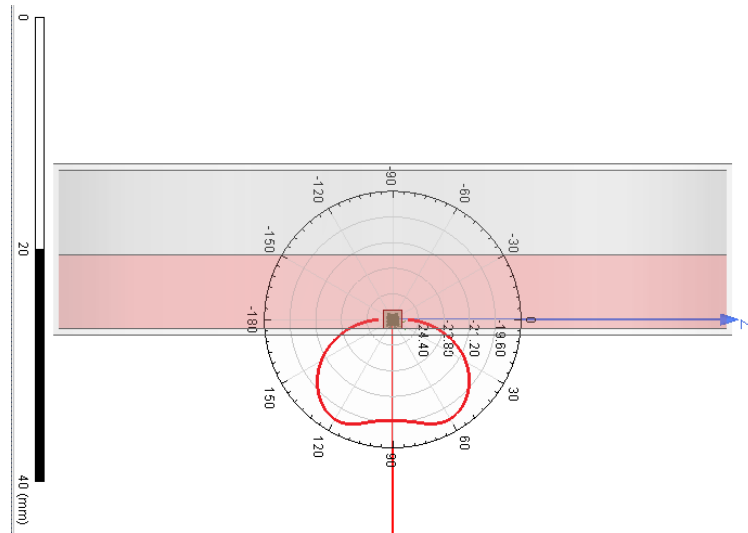


Figure 49 – The smallest antenna inside the petri dish.

In the direction of maximum radiation, the peak gain is -18.4 dBi at the resonance frequency of the antenna, which drops from 12.3 GHz to 11.9 GHz (Figure 50).

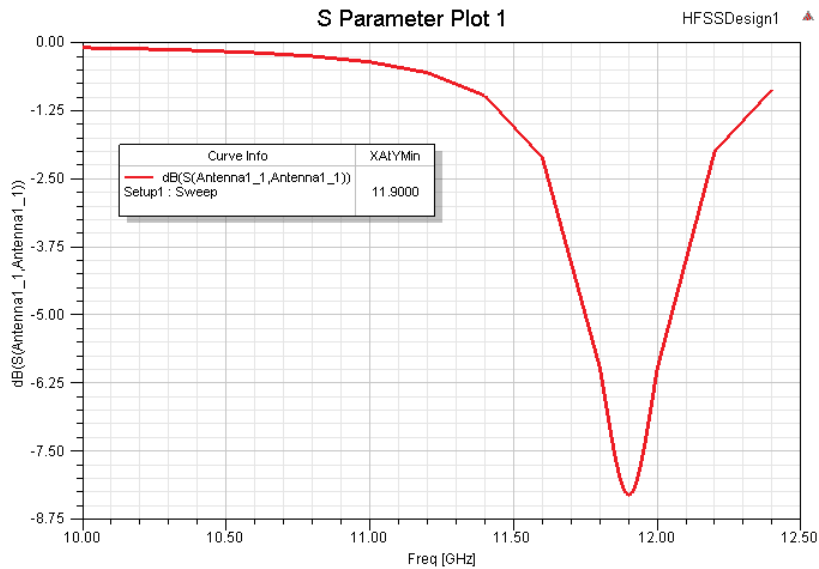


Figure 50 - Return loss (dB) (referred to 50 Ω) of the 9-turns copper loop antenna with diameter and height 1 mm, while inside the petri dish.

The input impedance also changes compared to the free space situation. In particular, at the resonance frequency the input impedance changes from 16.5 Ω to about 22.3 Ω (Figure 51).

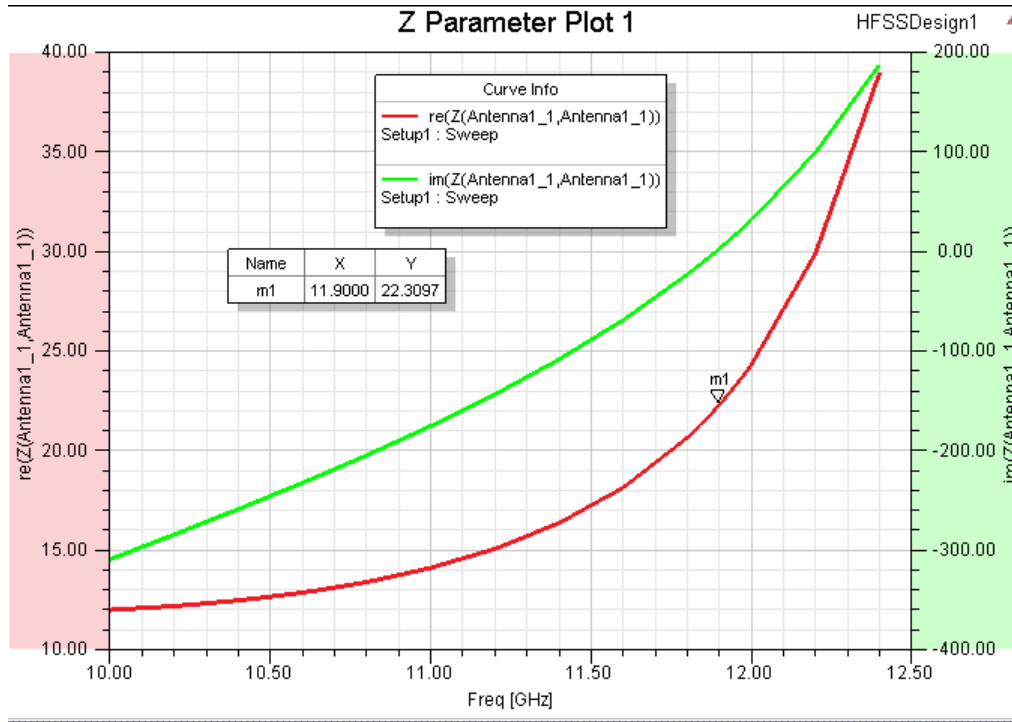


Figure 51 – Input impedance of the smallest antenna inside the petri dish.

At 11.9 GHz the power density limit imposed by the ICNIRP is 10 W/m². The wavelength in free space is 25,192 mm. The gain of -18.4 dBi linearly applies to 0.01445. Considering a polarization mismatch loss between transmitting and receiving antenna of -3 dB (0.5) and in the hypothesis of impedance matching between antenna and rectifier, the received power is:

$$P_R = S \cdot A_{eff} \cdot Xp = S \cdot G \cdot \frac{\lambda^2}{4\pi} \cdot Xp \cong 3.65 \mu W$$

5.4.4. 2x2x2 mm³ antenna in petri dish

Figure 52 shows the largest antenna inserted at the bottom of a petri dish containing the cell culture medium.

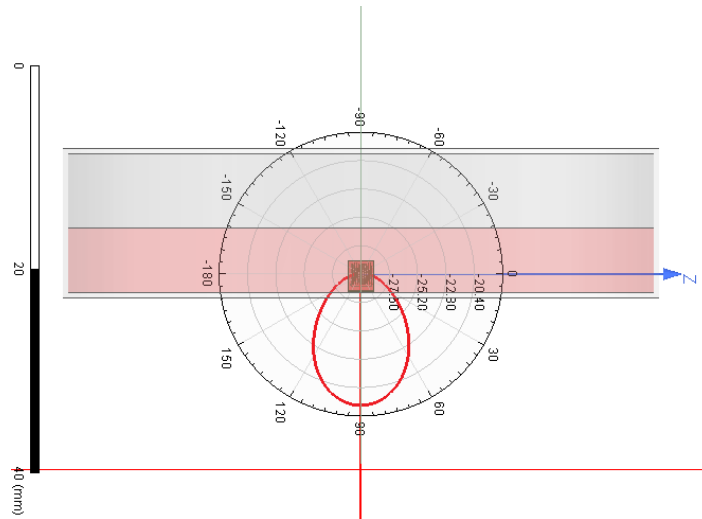


Figure 52 - The biggest antenna inside the petri dish.

In the direction of maximum radiation, the peak gain is -18.9 dBi at the resonance frequency of the antenna, which drops from 5.8 GHz to 5.2 GHz (Figure 53).

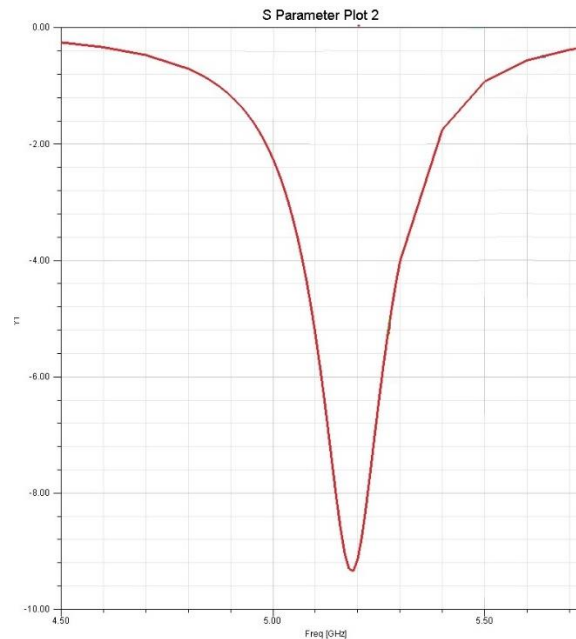


Figure 53 - Return loss (dB) (referred to 50 Ω) of the 9-turns copper loop antenna with diameter and height 2 mm, while inside the petri dish.

The input impedance also changes compared to the free space situation. In particular, at the resonance frequency the input impedance increases from 14.5 Ω to about 25 Ω (Figure 54).

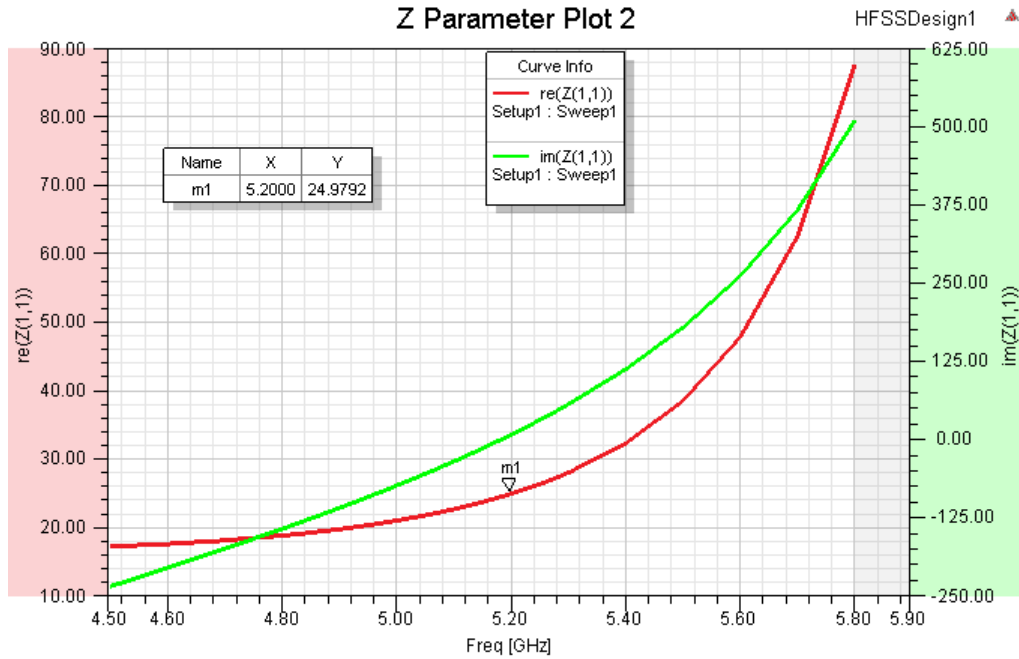


Figure 54 – Input impedance of the smallest antenna inside the petri dish.

At 5.2 GHz the power density limit imposed by the ICNIRP is 10 W/m². The wavelength in free space is 57.652 mm. The gain of -18.9 dBi linearly applies to 0.01288. Considering a polarization mismatch loss between transmitting and receiving antenna of -3 dB (0.5) and in the hypothesis of impedance matching between antenna and rectifier, the received power is:

$$P_R = S \cdot A_{eff} \cdot Xp = S \cdot G \cdot \frac{\lambda^2}{4\pi} \cdot Xp \cong 17 \mu W$$

5.5. Circuit for wireless power transfer

In order to be used effectively to power the device, the RF power received must be rectified. The component that allows this operation is called the rectifier. It is a device used to rectify an alternating signal into a unidirectional signal.

Figure 55 shows the block diagram of a possible ultra-low-power RFID tag where we can see the presence of a rectifier.

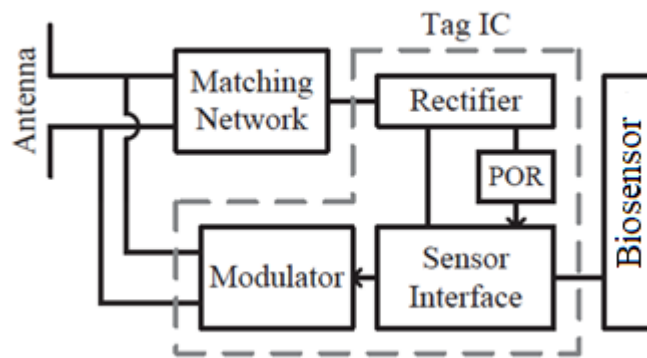


Figure 55 – Example of an ultra-low-power RFID tag [72]

For maximum power transfer, the antenna impedance must be equal to the complex conjugate of the rectifier impedance. If this is not the case, part of the received power will be reflected by the rectifier. To better understand this concept, we can observe the transmission coefficient between antenna and rectifier.

The transmission coefficient between antenna and rectifier τ can be expressed as:

$$\tau = 1 - |S_{11}|^2 = 1 - \left| \frac{Z_C - Z_A^*}{Z_C + Z_A} \right|^2 \quad (65)$$

Where Z_A is the input impedance of the antenna while Z_C is the impedance of the chip connected to the antenna.

The expression (65) is linked to the power budget by the equation (11) that we remember as:

$$P_r = P_t G_t G_r \left(\frac{\lambda}{4\pi D} \right)^2 (1 - |S_{11}|^2) (1 - |S_{22}|^2) X_{pol} = P_t G_t G_r \left(\frac{\lambda}{4\pi D} \right)^2 \tau_1^2 \tau_2^2 X_{pol}$$

Where τ_1 , τ_2 are the coefficients of transmission between the transmitting antenna and its transmission line and between the receiving antenna and the rectifier.

A rectifier is by nature a high nonlinear circuit, so it is not easy to predict his input impedance. Therefore, the equivalent input impedance depends on the architecture of the rectifier, on the input power and on the frequency.

In literature we can find different rectifiers, for example in [73], a rectifier having a typical input impedance of $33 - j260 \Omega$ at the frequency of 2.45 GHz shall be presented.

We could, for example, hypothesize that the real part of the input impedance of the rectifier is substantially constant while the imaginary part varies with the frequency. The imaginary part is capacitive because negative, $X_C = -260 \Omega$ at 2.45 GHz. We could hypothesize to be able to estimate the value that it would assume to other frequencies using the following relation that binds the capacitive reactance to the frequency:

$$X_C = -\frac{1}{\omega C} = -\frac{1}{2\pi f C} \quad (66)$$

Hence:

$$C = -\frac{1}{2\pi f X_C} = -\frac{1}{2\pi \cdot 2.45 \cdot 10^9 \cdot (-260) \cdot \text{Hz} \cdot \Omega} \cong 0.25 \text{ pF}$$

Consider, for example, the case of an antenna with a diameter of 2 mm inserted in a petri dish (Chapter 5.4.4). Looking at the antenna input impedance (Figure 54), we see that the real part is approximately equal to the real part of the rectifier impedance, $\text{Re}\{Z_A\} \approx \text{Re}\{Z_C\}$, at the frequency of 5.4 GHz.

By inserting 5.4 GHz in the expression (66) we obtain:

$$X_C(5.4 \text{ GHz}) \cong -118 \Omega$$

Looking again at Figure 54 we see that the imaginary part of the antenna input impedance is about 125Ω . So, we can conclude that at 5.4 GHz, $Z_A \approx Z_C^*$, so impedance matching occurs.

Considering the same antenna, however, implanted subcutaneously (Chapter 5.4.2), looking at Figure 48, we see that at 5.6 GHz, $\text{Re}\{Z_A\} \cong \text{Re}\{Z_C\}$ while $\text{Im}\{Z_A\} \approx 160 \Omega$. It can be assumed that at that frequency $\text{Im}\{Z_C\} \cong -114 \Omega$, then a matching circuit is required to compensate for a 46Ω reactance. A capacitor of about 620 fF could be used.

Considering instead the case of Chapter 5.4.3, of the antenna with a diameter of 1 mm in the petri dish, looking at Figure 51 we can see that at 12.3 GHz the real part of the antenna input impedance is about equal to the typical resistance of the rectifier. At 12.3 GHz we can assume that the reactance of the rectifier is about -50Ω . At the same frequency the antenna reactance is about 140Ω . In this case, it is advisable to insert a matching circuit as there is a 90Ω reactance to be compensated. At that frequency it corresponds to a capacitor of about 140 fF. Also, in the case of the same antenna but implanted subcutaneously (Chapter 5.4.1) the situation is very similar (Figure 45). A tuneable matching circuit like the one shown in Figure 56 could be considered.

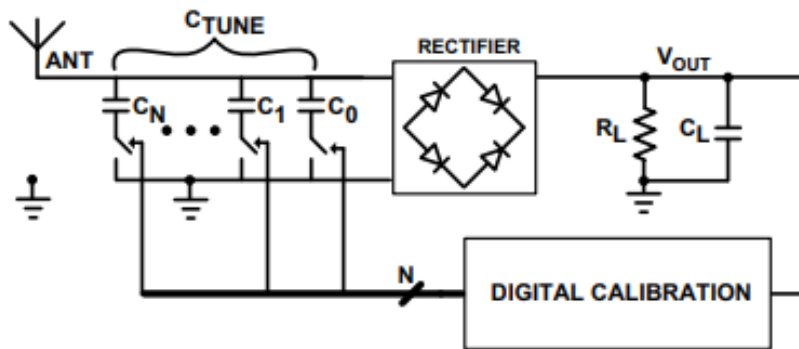


Figure 56 - Impedance tuning scheme with parallel programmable tuning capacitor bank with N-Bits [74].

6. Conclusion

In the coming years, the development of miniaturised diagnostic devices will become increasingly frequent. It is therefore important to understand which are the limits if one wants to power these devices via wireless power transfer.

In this thesis, it was first made a theoretical analysis that led to the result that remaining in compliance with the limits of the law on exposure to electromagnetic fields, to transmit enough power to power a miniaturized device for diagnostics implanted subcutaneously, through electromagnetic coupling, it is necessary to use receiving antennas with a size of at least a few mm^3 and the optimal frequency range goes from about 2 to about 12 GHz.

Then two antennas were designed, one about $1 \times 1 \times 1 \text{ mm}^3$ and the other about $2 \times 2 \times 2 \text{ mm}^3$, self-resonant respectively at 12.3 GHz and 5.8 GHz in free space and were simulated both in vivo and in vitro by Ansys HFSS software. The results obtained confirm the theoretical analysis and show that for the smaller antenna 2.1 μW and 3.65 μW can be transferred respectively to a subcutaneous implant and to a device inserted in a petri dish; while for the larger antenna for the same two scenarios 11 μW and 17 μW can be transferred respectively.

A final analysis concerning the impedance matching between antenna and rectifier gives further confirmation on the feasibility of powering these miniaturized devices, showing that the impedance matching, in order to reach the condition of maximum power transfer, can be achieved.

In conclusion, the power levels obtained in the simulations of these designed antennas are sufficient to meet the power requirements of different biosensors available in literature. In both scenarios studied, the power received by the two antennas depends on the frequency and the corresponding ka . So, the choice of which antenna to use in your device depends on the consumption of the same. For devices with higher consumption it is necessary to opt for the larger antenna while for others with minimized consumption it is possible to use the smaller antenna, with the possibility of building an extremely miniaturized device powered by electromagnetic waves emitted by a transmitting device.

APPENDIX

I. Gabriel model – Matlab code

% This function provides dielectric properties of biological tissues
% using the Gabriel model.

% Inputs:

% - tissue (str) is the name of tissue

% - f (int/double) is the frequency range

% Output:

% - tissprop (struct) is a structure containing all the dielectric

% properties

% References:

% [1] "The dielectric properties of biological tissues: III.

% Parametric models for the dielectric spectrum of tissues", (1996),

% S Gabriel†, R W Lau and C Gabriel

function tissprop=gabriel_model(tissue,f)

load('GabrielModel_params.mat'); %#ok<LOAD> [1] % it is available here:

%https://drive.google.com/open?id=1mtPJhBAUxZ84ap8ZDucYPi_QejK_fOht

p=params.p;

tissues=params.tissues;

eps_0 = 8.854187817e-12; % Vacuum permittivity (F/m)

mu_0 = 4*pi*1e-7; % Vacuum permeability (H/m)

j=find(strcmp(tissues,tissue));

prop=zeros(length(f),6);

for u=1:length(f)

 w=2*pi*f(u);

 SUM=0;

 v=p(j,2:end-1);

 c=1e-12;

 for n=0:3

 if ~isnan(v(1+3*n)) && ~isnan(v(2+3*n)) && ~isnan(v(3+3*n))

 SUM=SUM+v(1+3*n)/(1+(1i*w*v(2+3*n)*c)^(1-v(3+3*n)));

 end

 c=c*1e3;

 end

 eps_c=p(j,1)+SUM+p(j,end)/(1i*w*eps_0); % [1]

 eps_r=real(eps_c);

 sigma=-imag(eps_c)*w*eps_0;

```

loss_tan=abs(imag(eps_c)/real(eps_c)); % loss tangent
k=w*sqrt(mu_0*eps_0*eps_c); % wavenumber
alpha=-imag(k);
beta=real(k);
pen_depth=1/alpha; % penetration dept (m)
lambda=2*pi/beta; % wavelength (m)

prop(u,1)=f(u);
prop(u,2)=sigma;
prop(u,3)=eps_r;
prop(u,4)=loss_tan;
prop(u,5)=lambda;
prop(u,6)=pen_depth;
end

tissprop=struct();
tissprop.prop=prop;
tissprop.tissue=tissue;
tissprop.columns={'frequency','conductivity','relative_permettivity'...
    'loss_tangent','wavelength','skin_dept'};

```

II. Power budget analysis – Matlab code

```

clear
close all
clc

% PARAMETERS
tissues={'Skin (Dry)','Fat (Not Infiltrated)'}; % tissues list
freq=4e8:1e8:30e9; % range of frequencies (Hz)
r_impl=[5e-6,10e-6,15e-6,25e-6,35e-6,50e-6,70e-6,100e-6,...
    150e-6,200e-6,300e-6,500e-6,1000e-6];% radius of the implant (m)
depts=[0.0023,0.0002]; % thickness of tissues (m)

%-----
%-----CODE-----
%-----

G=1.5; % Maximum gain for an ideal ESA

% initialization of vectors
P=zeros(length(freq),length(r_impl));
e_lossy_nearfield=zeros(length(freq),length(r_impl));
e_lossy_reflection=zeros(1,length(freq));
e_lossy_propagation=zeros(1,length(freq));
E=zeros(1,length(freq));

```

```

S=zeros(1,length(freq));
A_eff=zeros(1,length(freq));
results=struct();

% Constants
eps_0 = 8.854187817e-12; % Vacuum permittivity (F/m)
mu_0 = 4*pi*1e-7; % Vacuum permeability (H/m)

% DIELECTRIC PROPERTIES OF TISSUES (Gabriel model)
data=struct();
for j=1:length(tissues)
    tissprop=gabriel_model(tissues(j),freq);
    prop=tissprop.prop;
    data(j).tissue=tissues(j);
    data(j).dept=depts(j);
    data(j).sigma=prop(:,2); % Conductivity (S/m)of tissue
    data(j).eps_r=prop(:,3); % Relative permittivity of tissue
    data(j).lambda=prop(:,5); % wavelength in tissue
end

% Properties of Vacuum
eps_r=1;
sigma=0;
c=1/sqrt(eps_0*eps_r*mu_0); % Velocity of light in vacuum (m/s)

for j=1:length(freq)
    f=freq(j); % frequency (Hz)
    w=2*pi*f; % angular pulsation (rad/s)

    % WAVE NUMBER
    k_i=w*sqrt((eps_0*eps_r-1i*sigma/w)*mu_0); % Wavenumber in vacuum(1/m)
    for u=1:length(tissues)
        data(u).k(j)=w*sqrt((eps_0*data(u).eps_r(j)-1i*data(u).sigma(j)/w)*mu_0); %
Wavenumber in tissue (1/m)
    end

    %----- WAVE IMPEDENCE-----
    eta=sqrt(mu_0/eps_0); % Wave impedance in vacuum (Ohm)
    for u=1:length(tissues)
        data(u).eta(j)=sqrt(1i*w*mu_0/(data(u).sigma(j)+1i*w*eps_0*data(u).eps_r(j)));
% Wave impedance in tissue(Ohm)
    end

    %----- COMPUTE LOSSES-----

```

```

% A) Losses due to reflections
T=2*eta/(data(1).eta(j)+eta);
e_lossy_reflection(j)=real(abs(T)^2/eta)/real(1/data(1).eta(j)); %efficiency near-field

% B) Losses due to propagation field absorption
data(1).alpha(j)=-imag(data(1).k(j));
e_lossy_propagation(j)=exp(-2*data(1).alpha(j)*data(1).dept);
if length(tissues)>1 % Multilayer model
    for u=2:length(tissues)
        data(u).alpha(j)=-imag(data(u).k(j));
        e_lossy_propagation(j)=e_lossy_propagation(j)*exp(-
2*data(u).alpha(j)*data(u).dept);
    end
end

% C) Losses in the reactive near-field
for g=1:length(r_impl)

e_lossy_nearfield(j,g)=abs(data(length(tissues)).k(j))^2*real(data(length(tissues)).eta(j))
/imag(data(length(tissues)).eta(j)/(data(length(tissues)).k(j)*r_impl(g)^3));
end
% %-----
%
% Get the maximum incident E-field
E(j)=maxE_from_Table(f); % reference value ICNIRP (V/m)
S(j)=E(j)^2/eta; % power density (W/m^2)

lambda_0=c/f; % wavelength in free space (m)
A_eff(j)=G*lambda_0^2/(4*pi); %Effective aperture (m^2)

end

% Plot losses due to reflection
figure
loglog(freq, 10*log10(e_lossy_reflection),'LineWidth',2)
grid on
xlabel('f (Hz)')
ylabel('e_r_e_f_l_e_c_t_i_o_n_s (dB)')
axis tight
title('Reflections')
set(gca,'fontweight','bold','FontSize',15)

% Plot losses due to propagation
figure
plot(freq,10*log10(e_lossy_propagation), 'LineWidth',2)
grid on

```

```

xlabel('f (Hz)')
ylabel('e_p_r_o_p_a_g_a_t_i_o_n (dB)')
axis tight
set(gca, 'XScale', 'log')
title('Propagation')
set(gca,'fontweight','bold','FontSize',15)

% Plot losses in near-field
e_lossy_nearfield(e_lossy_nearfield>1)=1; % set to 1 the values > 1
cmap = jet(length(r_impl));
str=cell(1,length(r_impl));
figure
for j=1:length(r_impl)
    plot(freq,10*log10(e_lossy_nearfield(:,j)), 'LineWidth',2,'Color',cmap(j,:))
    hold on
    str{j}=strcat(num2str(r_impl(j)*1e6),' \mum');
end
grid on
set(gca, 'XScale', 'log')
xlabel('f (Hz)')
ylabel('e_r_e_a_c_t_i_v_e_n_e_a_r_f_i_e_l_d (dB)')
axis tight
legend(str)
title(strcat('Reactive near-field - ',tissues(end)))
set(gca,'fontweight','bold','FontSize',15)

% Plot sum of losses
hold off
figure
cmap = jet(length(r_impl));
for j=1:length(r_impl)

plot(freq,10*log10(e_lossy_reflection.*e_lossy_propagation.*e_lossy_nearfield(:,j)),'Li
neWidth',2,'Color',cmap(j,:));
    hold on
end
grid on
set(gca, 'XScale', 'log')
xlabel('f (Hz)')
ylabel('e_T_O_T (dB)')
legend(str)
axis tight
title('e_T_O_T (d_B)=10log_1_0(e_l_o_s_s_e_s_
_r_e_f_l_e_c_t_i_o_n)+10log_1_0(e_l_o_s_s_e_s_
_p_r_o_p_a_g_a_t_i_o_n)+10log_1_0(e_l_o_s_s_e_s_n_e_a_r_f_i_e_l_d)')
set(gca,'fontweight','bold','FontSize',15)

% Plot maximum effective aperture

```

```

figure
loglog(freq, A_eff,'LineWidth',2)
grid on
xlabel('f (Hz)')
ylabel('A_e_f_f (m^2)')
axis tight
title('Maximum effective aperture')
set(gca,'fontweight','bold','FontSize',15)

% Compute and Plot maximum Power received
figure
for j=1:length(r_impl)
    P(:,j)=S.*A_eff.*e_lossy_reflection.*e_lossy_propagation.*e_lossy_nearfield(:,j); %
Maximum power received (W)
    loglog(freq,P(:,j),'-o','MarkerIndices',
find(P(:,j)==max(P(:,j))),'MarkerSize',5,'MarkerFaceColor',cmap(j,:),'LineWidth',2,'Col
or',cmap(j,:))
    hold on
end
legend(str)
title('Maximum Power received - markers indicate the maximum')
grid on
xlabel('f (Hz)')
ylabel('P_R (W)')
axis tight
set(gca,'fontweight','bold','FontSize',15)

% Copy results in a structure
for j=1:length(r_impl)
    ind=find(P(:,j)==max(P(:,j)));
    results(j).freq=freq(ind);
    results(j).e_refl=10*log10(e_lossy_reflection(ind));
    results(j).e_prop=10*log10(e_lossy_propagation(ind));
    results(j).e_nearfield=10*log10(e_lossy_nearfield(ind,j));
    results(j).Pr=P(ind,j);
    results(j).r_impl=r_impl(j);
end

%%%%%%%%%%%%%%%%%%%%%%%%%%%%%%%%%%%%%%%%%%%%%%%%%%%%%%%%%%%%%%%%%%%%%%%%%
%-----MAXIMUM E-FIELD-----%
%%%%%%%%%%%%%%%%%%%%%%%%%%%%%%%%%%%%%%%%%%%%%%%%%%%%%%%%%%%%%%%%%%%%%%%%%

% This function provides the reference levels for general public exposure
% to time-varying electric fields (unperturbed rms values)

% References:
% "ICNIRP GUIDELINES FOR LIMITING EXPOSURE TO TIMEVARYING
ELECTRIC,

```

% MAGNETIC AND ELECTROMAGNETIC FIELDS (UP TO 300 GHZ)"(Table 7)
% PUBLISHED IN: HEALTH PHYSICS 74 (4):494-522; 1998

```
function E=maxE_from_Table(f)

if f<=25 && f>1
    E=10000;
elseif f>25 && f<=3e3
    E=250/(f/1e3);
elseif f>3e3 && f<=1e6
    E=87;
elseif f>1e6 && f<=10e6
    E=87/sqrt(f/1e6);
elseif f>10e6 && f<=400e6
    E=28;
elseif f>400e6 && f<2000e6
    E=1.375*sqrt(f/1e6);
elseif f>=2e9 && f<=300e9
    E=61;
else
    E=0;
end
```

III. Antenna design – Visual basic script for ANSYS HFSS

```
Dim oAnsoftApp
```

```
Dim oDesktop
```

```
Dim oProject
```

```
Dim oDesign
```

```
Dim oEditor
```

```
Dim oModule
```

```
Set oAnsoftApp = CreateObject("AnsoftHfss.HfssScriptInterface")
```

```
Set oDesktop = oAnsoftApp.GetAppDesktop()
```

```
oDesktop.RestoreWindow
```

```
Set oProject = oDesktop.GetActiveProject()
```

```
oProject.InsertDesign "HFSS", "HFSSDesign2", "DrivenModal", ""
```

```
Set oDesign = oProject.GetActiveDesign()
```

```
oDesign.ChangeProperty Array("NAME:AllTabs", Array("NAME:LocalVariableTab",  
Array("NAME:PropServers", _  
"LocalVariables"), Array("NAME:NewProps", Array("NAME:a", "PropType:=",  
"VariableProp", "UserDef:=", _  
true, "Value:=", "0.5mm"))))
```

```
oDesign.ChangeProperty Array("NAME:AllTabs", Array("NAME:LocalVariableTab",  
Array("NAME:PropServers", _  
"LocalVariables"), Array("NAME:NewProps", Array("NAME:b", "PropType:=",  
"VariableProp", "UserDef:=", _  
true, "Value:=", "a/20"))))
```

```
oDesign.ChangeProperty Array("NAME:AllTabs", Array("NAME:LocalVariableTab",  
Array("NAME:PropServers", _  
"LocalVariables"), Array("NAME:NewProps", Array("NAME:N", "PropType:=",  
"VariableProp", "UserDef:=", _  
true, "Value:=", "9"))))
```

```
oDesign.ChangeProperty Array("NAME:AllTabs", Array("NAME:LocalVariableTab",  
Array("NAME:PropServers", _  
"LocalVariables"), Array("NAME:NewProps", Array("NAME:c", "PropType:=",  
"VariableProp", "UserDef:=", _  
true, "Value:=", "2*a/N"))))
```

```
oDesign.ChangeProperty Array("NAME:AllTabs", Array("NAME:LocalVariableTab",  
Array("NAME:PropServers", _  
"LocalVariables"), Array("NAME:NewProps", Array("NAME:L", "PropType:=",  
"VariableProp", "UserDef:=", _  
true, "Value:=", "6*b"))))
```

```

oDesign.ChangeProperty Array("NAME:AllTabs", Array("NAME:LocalVariableTab",
Array("NAME:PropServers", _
    "LocalVariables"), Array("NAME:NewProps", Array("NAME:gap", "PropType:=",
"VariableProp", "UserDef:=", _
    true, "Value:=", "b"))))
Set oEditor = oDesign.SetActiveEditor("3D Modeler")
oEditor.CreateUserDefinedPart      Array("NAME:UserDefinedPrimitiveParameters",
"DllName:=", _
    "SegmentedHelix/PolygonHelix", "Version:=", "1.0", "NoOfParameters:=", 8,
"Library:=", _
    "syslib", Array("NAME:ParamVector", Array("NAME:Pair", "Name:=",
"PolygonSegments", "Value:=", _
    "4"), Array("NAME:Pair", "Name:=", "PolygonRadius", "Value:=", "b"),
Array("NAME:Pair", "Name:=", _
    "StartHelixRadius", "Value:=", "a"), Array("NAME:Pair", "Name:=", "RadiusChange",
"Value:=", _
    "0mm"), Array("NAME:Pair", "Name:=", "Pitch", "Value:=", "c"),
Array("NAME:Pair", "Name:=", _
    "Turns", "Value:=", "N"), Array("NAME:Pair", "Name:=", "SegmentsPerTurn",
"Value:=", _
    "100"), Array("NAME:Pair", "Name:=", "RightHanded", "Value:=", "1"))),
Array("NAME:Attributes", "Name:=", _
    "PolygonHelix1", "Flags:=", "", "Color:=", "(132 132 193)", "Transparency:=", _
0, "PartCoordinateSystem:=", "Global", "UDMId:=", "", "MaterialValue:=", _
    "" & Chr(34) & "copper" & Chr(34) & "", "SolveInside:=", false)

```

```

oEditor.CreateBox Array("NAME:BoxParameters", "XPosition:=", "a-b/sqrt(2)",
"YPosition:=", _
"0mm", "ZPosition:=", "c*N-b/sqrt(2)", "XSize:=", "L", "YSize:=", _
"-b*sqrt(2)", "ZSize:=", "b*sqrt(2)"), Array("NAME:Attributes", "Name:=", "Box1",
"Flags:=", _
"", "Color:=", "(132 132 193)", "Transparency:=", 0, "PartCoordinateSystem:=", _
"Global", "UDMId:=", "", "MaterialValue:=", "" & Chr(34) & "copper" & Chr(34) &
"", "SolveInside:=", _
false)

```

```

oEditor.CreateBox Array("NAME:BoxParameters", "XPosition:=", "a-b/sqrt(2)",
"YPosition:=", _
"0mm", "ZPosition:=", "-b/sqrt(2)", "XSize:=", "L", "YSize:=", _
"-b*sqrt(2)", "ZSize:=", "b*sqrt(2)"), Array("NAME:Attributes", "Name:=", "Box2",
"Flags:=", _
"", "Color:=", "(132 132 193)", "Transparency:=", 0, "PartCoordinateSystem:=", _
"Global", "UDMId:=", "", "MaterialValue:=", "" & Chr(34) & "copper" & Chr(34) &
"", "SolveInside:=", _
false)

```

```

oEditor.CreateBox Array("NAME:BoxParameters", "XPosition:=", "a-
b/sqrt(2)+b*sqrt(2)+L", "YPosition:=", _
"0mm", "ZPosition:=", "-b/sqrt(2)", "XSize:=", "-b*sqrt(2)", "YSize:=", _
"-b*sqrt(2)", "ZSize:=", "c*N+b*sqrt(2)"), Array("NAME:Attributes", "Name:=",
"Box3", "Flags:=", _
"", "Color:=", "(132 132 193)", "Transparency:=", 0, "PartCoordinateSystem:=", _
"Global", "UDMId:=", "", "MaterialValue:=", "" & Chr(34) & "copper" & Chr(34) &
"", "SolveInside:=", _

```

```

false)

oEditor.CreateBox Array("NAME:BoxParameters", "XPosition:=", "L+b*sqrt(2)+a-
b/sqrt(2)", "YPosition:=", _

"0mm", "ZPosition:=", "(c*N+b*sqrt(2))/2-b/sqrt(2)-gap/2", "XSize:=", "-b*sqrt(2)",
"YSize:=", "-b*sqrt(2)", "ZSize:=", _

"gap"), Array("NAME:Attributes", "Name:=", "Box4", "Flags:=", "", "Color:=", _

"(132 132 193)", "Transparency:=", 0, "PartCoordinateSystem:=", "Global",
"UDMId:=", _

"", "MaterialValue:=", "" & Chr(34) & "copper" & Chr(34) & "", "SolveInside:=", _

false)

oEditor.Subtract Array("NAME:Selections", "Blank Parts:=", "Box3", "Tool Parts:=", _

"Box4"), Array("NAME:SubtractParameters", "KeepOriginals:=", false)

oEditor.CreateRectangle Array("NAME:RectangleParameters", "IsCovered:=", true,
"XStart:=", _

"L+b*sqrt(2)+a-b*sqrt(2)", "YStart:=", "0mm", "ZStart:=", "(c*N+b*sqrt(2))/2-
b/sqrt(2)+gap/2", "Width:=", "-b*sqrt(2)", "Height:=", _

"-gap", "WhichAxis:=", "X"), Array("NAME:Attributes", "Name:=", _

"Rectangle1", "Flags:=", "", "Color:=", "(132 132 193)", "Transparency:=", 0,
"PartCoordinateSystem:=", _

"Global", "UDMId:=", "", "MaterialValue:=", "" & Chr(34) & "copper" & Chr(34) &
"", "SolveInside:=", _

false)

oEditor.Unite Array("NAME:Selections", "Selections:=",
"PolygonHelix1,Box3,Box2,Box1"), Array("NAME:UniteParameters",
"KeepOriginals:=", _

false)

```

```

oEditor.Move Array("NAME:Selections", "Selections:=", "PolygonHelix1,Rectangle1",
"NewPartsModelFlag:=", _
"Model"), Array("NAME:TranslateParameters", "TranslateVectorX:=", "0mm",
"TranslateVectorY:=", _
"0mm", "TranslateVectorZ:=", "-a")
oEditor.CreateRegion Array("NAME:RegionParameters", "+XPaddingType:=", _
"Absolute Offset", "+XPadding:=", "10mm", "-XPaddingType:=", "Absolute Offset", "-
XPadding:=", _
"10mm", "+YPaddingType:=", "Absolute Offset", "+YPadding:=", "10mm", "-
YPaddingType:=", _
"Absolute Offset", "-YPadding:=", "10mm", "+ZPaddingType:=", "Absolute Offset",
"+ZPadding:=", _
"10mm", "-ZPaddingType:=", "Absolute Offset", "-ZPadding:=", "10mm"),
Array("NAME:Attributes", "Name:=", _
"Region", "Flags:=", "Wireframe#", "Color:=", "(255 0 0)", "Transparency:=", 0,
"PartCoordinateSystem:=", _
"Global", "UDMId:=", "", "MaterialValue:=", "" & Chr(34) & "vacuum" & Chr(34) &
"", "SolveInside:=", _
true)
Set oModule = oDesign.GetModule("BoundarySetup")
oModule.AssignRadiation Array("NAME:Rad1", "Objects:=", Array("Region"),
"IsIncidentField:=", _
false, "IsEnforcedField:=", false, "IsFssReference:=", false, "IsForPML:=", _
false, "UseAdaptiveIE:=", false, "IncludeInPostproc:=", true)
oProject.Save

```


Referencies

- [1] Second Sight, "Second Sight Argus II," [Online]. Available: <https://www.secondsight.com/discover-argus/>. [Accessed 12 August 2019].
- [2] Medtronic, "Medtronic Synchroned II," [Online]. Available: <https://www.medtronic.com/it-it/operatori-sanitari/tddrelaunch/thank-you-for-contacting-us.html>. [Accessed 12 August 2019].
- [3] Medtronic, "Medtronic Reveal LINQ," [Online]. Available: https://www.medtronicacademy.com/sites/default/files/images/Reveal_LINQ_Front.png. [Accessed 12 August 2019].
- [4] Medtronic, "Medtronic Micra," [Online]. Available: http://www.medtronic.com/micraprtoolkit/img/hi-res/AdvisaSR_device.png. [Accessed 12 August 2019].
- [5] M. M. J. W. C. L. S. P. K. I. H. M. A. & A. D. Gray, "Implantable biosensors and their contribution to the future of precision medicine, 239, 21-29," *The Veterinary Journal*, vol. 239, pp. 21-29, 2018.
- [6] G. S. R. C. a. H. A. C. Rong, "In vivo biosensing: progress and perspectives," *ACS sensors*, vol. 3, no. 2, pp. 327-338, 2017.
- [7] Y.-T. Liao, H. Yao, A. Lingley, B. Parviz and B. P. Otis, "A 3- μ WCMOS Glucose Sensor for Wireless Contact-Lens Tear Glucose Monitoring," *IEEE Journal of Solid-State Circuits*, vol. 47, no. 1, pp. 335 - 344, 2012.
- [8] M. M. Ahmadi and G. A. Jullien, "A Wireless-Implantable Microsystem for Continuous Blood Glucose Monitoring," *IEEE Transactions on Biomedical Circuits and Systems*, vol. 3, no. 3, pp. 169-180, 2009.
- [9] S. O'Driscoll, S. Korhummel, P. Cong, Y. Zou, K. Sankaragomathi, J. Zhu, T. Deyle and A. Dastgheib, "A 200 μ m \times 200 μ m \times 100 μ m, 63nW, 2.4GHz injectable fully-monolithic wireless bio-sensing system," *IEEE Radio Frequency Integrated Circuits Symposium (RFIC)*, 2017.
- [10] FDA, "FDA approves first continuous glucose monitoring system with a fully implantable glucose sensor and compatible mobile app for adults with diabetes," [Online]. Available: <https://www.fda.gov/news-events/press-announcements/fda-approves-first-continuous-glucose-monitoring-system-fully-implantable-glucose-sensor-and>. [Accessed 12 August 2019].
- [11] D. D. F. F. A. Poscia, "A novel continuous subcutaneous lactate monitoring system," *Biosensors and Bioelectronics*, vol. 20, no. 11, pp. 2244-2250, 2005.

- [12] S. Milici, S. Amendola, A. Bianco and G. Marrocco, "Epidermal RFID passive sensor for body temperature measurements," *IEEE RFID Technology and Applications Conference (RFID-TA)*, 2014.
- [13] H. Jiang, X. Zhou, S. Kulkarni, M. Uranian and R. Seenivasan, "A Sub-1 μ W multiparameter injectable BioMote for continuous alcohol monitoring," *IEEE Custom Integrated Circuits Conference (CICC)*, 2018.
- [14] C. Boero, J. Olivo, S. Carrara and G. D. Micheli, "A Self-Contained System With CNTs-Based Biosensors for Cell Culture Monitoring," *IEEE Journal on Emerging and Selected Topics in Circuits and Systems*, vol. 2, no. 4, pp. 658 - 671, 2012.
- [15] P. G. Sandro Carrara, "Body Dust: Miniaturized Highly-integrated Low Power Sensing for Remotely Powered Drinkable CMOS Bioelectronics," *arXiv:1805.05840v1 [physics.app-ph]*, 2018.
- [16] Eversense, "The Eversense CGM system," [Online]. Available: <https://www.eversenseddiabetes.com/sensor>. [Accessed 12 August 2019].
- [17] H. B. D. G. F. V. T. R. E. K. G. H. C. S. a. P. D. Johannes Sperzel, "State of the art of leadless pacing," *Europace*, vol. 10, no. 17, p. 1508–1513, 2015.
- [18] I. B. F. a. B. B. Umay, "Localization and tracking of implantable biomedical sensors," *Sensors*, vol. 17, no. 3, p. 583, 2017.
- [19] S. K. e. a. Kelly, "A Hermetic Wireless Subretinal Neurostimulator for Vision Prostheses," *IEEE transactions on biomedical engineering*, vol. 58, no. 11, pp. 3197-3205, 2011.
- [20] G. M. A. G. a. P. S. G. Iddan, "Wireless capsule endoscopy," *Nature*, vol. 405, no. 6785, p. 417–417, 2000.
- [21] M. A. a. J.-M. Tarascon, "Building better batteries," *Nature*, vol. 451, no. 7179, p. 652–657, 2008.
- [22] R. C. R. D. D. W. L. E. C. G. M. N. A. M. & P. Y. Allon I. Hochbaum, "Enhanced thermoelectric performance of rough silicon nanowires," *Nature*, vol. 7175, no. 451, pp. 163-167, 2008.
- [23] S. B. J. H. a. Z. L. W. Xu, "Piezoelectric-nanowire-enabled power source for driving wireless microelectronics.," *Nature communications*, vol. 93, no. 1, 2010.
- [24] Z. L. a. W. W. Wang, "Nanotechnology-enabled energy harvesting for self-powered micro-/nanosystems," *Angewandte Chemie International Edition*, vol. 47, no. 51, pp. 11700-11721, 2012.
- [25] C. e. a. Dagdeviren, "Conformal piezoelectric energy harvesting and storage from motions of the heart, lung, and diaphragm," *Proceedings of the National Academy of Sciences*, vol. 5, no. 111, pp. 1927-1932, 2014.

- [26] P. P. L. A. C. B. S. C. A. P. & S. K. M. Mercier, "Energy extraction from the biologic battery in the inner ear," *Nature biotechnology*, vol. 12, no. 30, p. 1240, 2012.
- [27] S. K. a. D. R. L. Chaudhuri, "Electricity generation by direct oxidation of glucose in mediatorless microbial fuel cells," *Nature biotechnology*, vol. 10, no. 21, p. 1229, 2003.
- [28] B. I. J. T. K. a. R. S. Rapoport, "A glucose fuel cell for implantable brain-machine interfaces," *PloS one*, vol. 6, no. 7, 2012.
- [29] C. A. Balanis, *Antenna theory: analysis and design*, John Wiley & sons, 2016.
- [30] H. T. J. A. a. S. A. K. Ali, "Inductive link design for medical implants," *IEEE Symposium on Industrial Electronics & Applications*, vol. 2, 2009.
- [31] K. J. J. L. T. H. K. J. K. J. L. S. E. & K. S. J. Eom, "A wireless power transmission system for implantable devices in freely moving rodents," *Medical & biological engineering & computing*, vol. 8, no. 52, pp. 639-651, 2014.
- [32] K. a. B. W. F. Fotopoulou, "Wireless power transfer in loosely coupled links: Coil misalignment model," *IEEE Transactions on Magnetics*, vol. 2, no. 47, pp. 416-430, 2010.
- [33] S. P. C.-K. L. a. J. F. W. Aldhafer, "Electronic tuning of misaligned coils in wireless power transfer systems," *IEEE Transactions on Power Electronics*, vol. 11, no. 29, pp. 5975-5982, 2014.
- [34] S. a. D. S. Ozeri, "Ultrasonic transcutaneous energy transfer for powering implanted devices," *Ultrasonics*, vol. 6, no. 50, pp. 556-566, 2010.
- [35] K. J. R. G. Y. X. & T. N. V. Agarwal, "Wireless power transfer strategies for implantable bioelectronics," *IEEE reviews in biomedical engineering*, no. 10, pp. 136-161, 2017.
- [36] J. W. M. J. C. T. C. & A. A. Charthad, "A mm-sized implantable medical device (IMD) with ultrasonic power transfer and a hybrid bi-directional data link," *IEEE Journal of solid-state circuits*, vol. 8, no. 50, pp. 1741-1753, 2015.
- [37] S. L. R. W. & G. C. Gabriel, "The dielectric properties of biological tissues: III. Parametric models for the dielectric spectrum of tissues," *Physics in Medicine & Biology*, vol. 41, no. 11, p. 2271, 1996.
- [38] P. J. W. Debye, *Polar molecules*, Chemical Catalog Company, Incorporated, 1929.
- [39] K. S. & C. R. H. Cole, "Dispersion and absorption in dielectrics I. Alternating current characteristics," *The Journal of chemical physics*, vol. 9, no. 4, pp. 341-351, 1941.
- [40] R. C. D. Andreuccetti, "Calculation of the Dielectric Properties of Body Tissues in the frequency range 10 Hz - 100 GHz," ITALIAN NATIONAL RESEARCH COUNCIL - Institute for Applied Physics, 1997. [Online]. Available: <http://niremf.ifac.cnr.it/tissprop/htmlclie/htmlclie.php>.

- [41] N. E. G. M. K. A. K. N. Hasgall PA, "IT'IS Database for thermal and electromagnetic parameters of biological tissues," IT'IS, 30 July 2013. [Online]. Available: <https://itis.swiss/virtual-population/tissue-properties/database/dielectric-properties/>.
- [42] S. R. Best, "A discussion on the properties of electrically small self-resonant wire antennas," *IEEE Antennas and Propagation Magazine*, vol. 6, no. 46, pp. 9-22, 2004.
- [43] J. S. McLean, "A re-examination of the fundamental limits on the radiation Q of electrically small antennas," *IEEE Transactions on antennas and propagation*, vol. 44, no. 5, p. 672, 1996.
- [44] H. A. Wheeler, "Fundamental limitations of small antennas," *Proceedings of the IRE*, vol. 35, no. 12, pp. 1479-1484, 1947.
- [45] L. J. Chu, "Physical limitations of omni-directional antennas," *Journal of applied physics*, vol. 12, no. 19, pp. 1163-1175, 1948.
- [46] W. Geyi, "Physical limitations of antenna," *IEEE Transactions on Antennas and Propagation*, vol. 51, no. 8, pp. 2116-2123, 2003.
- [47] K. T. McDonald, "Reactance of small antennas," *Joseph Henry Laboratories, Princeton University, Princeton, NJ*, 2012.
- [48] R. Moore, "Effects of a surrounding conducting medium on antenna analysis," *IEEE Transactions on Antennas and Propagation*, vol. 11, no. 3, pp. 216-225, 1963.
- [49] A. K. B. M. & S. Z. Skrivervik, "Electrically small antenna design: from mobile phones to implanted sensors," *13th European Conference on Antennas and Propagation (EuCAP)*, pp. 1-5, 2019.
- [50] A. K. B. M. & S. Z. Skrivervik, "Fundamental Limits for Implanted Antennas: Maximum Power Density Reaching Free Space," *IEEE Transactions on Antennas and Propagation*, 2019.
- [51] A. e. a. Agarwal, "A 4 μ W, ADPLL-based implantable amperometric biosensor in 65nm CMOS," *Symposium on VLSI Circuits. IEEE*, 2017.
- [52] O. O. A. U. M. & K. M. Akkus, "Evaluation of skin and subcutaneous adipose tissue thickness for optimal insulin injection," *J Diabetes Metab*, vol. 3, no. 216, 2012.
- [53] I. C. N. I. R., Guidelines for limiting exposure to time-varying electric, magnetic, and electromagnetic fields (up to 300 GHz), vol. 74, 1998, pp. 494-522.
- [54] P. M. R. H. & R.-S. Y. Izdebski, "Conformal ingestible capsule antenna: A novel chandelier meandered design," *IEEE Transactions on Antennas and Propagation*, vol. 57, no. 4, pp. 900-909, 2009.

- [55] H. Z. P. C. P. Y. R. Y. L. X. F. M. .. & A. D. Huang, "RFID tag helix antenna sensors for wireless drug dosage monitoring," *IEEE journal of translational engineering in health and medicine*, vol. 2, pp. 1-8, 2014.
- [56] S. H. L. J. Y. Y. J. P. S. C. C. K. K. & N. S. Lee, "A wideband spiral antenna for ingestible capsule endoscope systems: Experimental results in a human phantom and a pig," *IEEE Transactions on Biomedical Engineering*, vol. 58, no. 6, p. 17, 2011.
- [57] E. Y. O. Y. B. B. C. W. J. & I. P. P. Chow, "Evaluation of cardiovascular stents as antennas for implantable wireless applications," *IEEE Transactions on Microwave Theory and Techniques*, vol. 57, no. 10, pp. 2523-2532, 2009.
- [58] A. H. C. V. A. D. J. D. & B. J. Vorobyov, "Folded loop antenna as a promising solution for a cochlear implant.," *8th European Conference on Antennas and Propagation*, pp. 1735-1738, 2014.
- [59] D. C. Z. F. Y. & R. E. T. Sirait, "A helical folded dipole antenna for medical implant communication applications," *2013 IEEE MTT-S International Microwave Workshop Series on RF and Wireless Technologies for Biomedical and Healthcare Applications (IMWS-BIO)*, pp. 1-3, 2013.
- [60] Y. L. X. L. J. & C. T. Fan, "A Miniaturized Circularly-Polarized Antenna for In-Body Wireless Communications," *Micromachines*, vol. 10, no. 1, p. 70, 2019.
- [61] X. Y. W. Z. T. F. Y. & T. E. M. Liu, "A miniaturized CSRR loaded wide-beamwidth circularly polarized implantable antenna for subcutaneous real-time glucose monitoring," *IEEE Antennas and Wireless Propagation Letters*, vol. 16, pp. 577-580, 2016.
- [62] X. Y. W. Z. T. F. Y. & T. E. M. Liu, "A miniaturized CSRR loaded wide-beamwidth circularly polarized implantable antenna for subcutaneous real-time glucose monitoring," *IEEE Antennas and Wireless Propagation Letters*, vol. 16, pp. 577-580, 2016.
- [63] H. Y. T. M. S. K. & I. K. Lin, "Performance of implantable folded dipole antenna for in-body wireless communication," *IEEE Transactions on Antennas and Propagation*, vol. 61, no. 3, pp. 1363-1370, 2012.
- [64] X. B. K. D. H. S. M. M. C. C. D. K. T. M. R. & R. A. Meng, "Dynamic evaluation of a digital wireless intracranial pressure sensor for the assessment of traumatic brain injury in a swine model.," *IEEE Transactions on Microwave Theory and Techniques*, vol. 61, no. 1, pp. 316-325, 2012.
- [65] S. & D. H. Manafi, "Design of a small modified Minkowski fractal antenna for passive deep brain stimulation implants," *International Journal of Antennas and Propagation*, 2014.
- [66] F. B. L. G. F. F. B. Z. J. F. B. Y. .. & S. A. K. Merli, "Example of data telemetry for biomedical applications: An in vivo experiment," *IEEE Antennas and Wireless Propagation Letters*, vol. 11, pp. 1650-1654, 2012.

- [67] Sigma-Aldrich, "Petri dishes, polystyrene," [Online]. Available: <https://www.sigmaaldrich.com/catalog/product/sigma/p5481?lang=it®ion=IT>. [Accessed 1 September 2019].
- [68] ThermoFisher, "Nunc Cell Culture / Petri Dishes," [Online]. Available: <https://www.thermofisher.com/order/catalog/product/150318>. [Accessed 1 September 2019].
- [69] V. A. M. N. & V. T. V. Tran, "Microwave complex permittivity measurement of biological medium for stem cell culture," *IEEE Instrumentation and Measurement Technology Conference*, pp. 319-322, 2009.
- [70] A. K. Skrivervik, "Implantable antennas: The challenge of efficiency," *7th European conference on antennas and propagation (EuCAP)*, pp. 3627-3631, 2013.
- [71] F. F. B. M. J. R. & S. A. K. Merli, "The effect of insulating layers on the performance of implanted antennas," *IEEE Transactions on Antennas and propagation*, vol. 59, no. 1, pp. 21-31, 2010.
- [72] J. M. C. D. K. Kapucu, "PRIME Conference in June 2013 and ICECS Conference in Dec. 2013".
- [73] O. M. F. J. N. M. F. & D. C. Kazanc, "Miniaturized antenna and integrated rectifier design for remote powering of wireless sensor systems," *IEEE Topical Conference on Biomedical Wireless Technologies Networks, and Sensing Systems (BioWireleSS)*, pp. 41-44, 2012.
- [74] O. M. F. & D. C. Kazanc, "High-Q adaptive matching network for remote powering of UHF RFIDs and wireless sensor systems," *IEEE Topical Conference on Wireless Sensors and Sensor Networks (WiSNet)*, pp. 10-12, 2013.